Experimental Study and Parametric Optimization of Tungsten Inert Gas (TIG) Welding of Stainless Steel AISI 316 Pipes

Lelisa Anbesa Debela

A Thesis Submitted to the Department of Mechanical Engineering

School of Mechanical, Chemical, and Materials Engineering

Presented in Partial Fulfillment of the Requirement for the Degree of Master's in Manufacturing Engineering

Office of Graduate Studies
Adama Science and Technology University

January, 2024
Adama, Ethiopia

Experimental Study and Parametric Optimization of Tungsten Inert Gas (TIG) Welding of Stainless Steel AISI 316 Pipes

Lelisa Anbesa Debela

Advisor:
Dr. Moera Gutu Jiru(Associate Professor)

A Thesis Submitted to the Department of Mechanical Engineering

School of Mechanical, Chemical, and Materials Engineering

Presented in Partial Fulfillment of the Requirement for the Degree of Master's in Manufacturing Engineering

Office of Graduate Studies
Adama Science and Technology University

January, 2024
Adama, Ethiopia

DECLARATION

I hereby declare that this Master Thesis entitled "**Experimental Study and Parametric Optimization of Tungsten Inert Gas (TIG) Welding of Stainless Steel AISI 316 Pipes**" is my original work. That is, it has not been submitted for the award of any academic degree, diploma or certificate in any other university. All sources of materials that are used for this thesis have been duly acknowledged through citation.

Lelisa Anbesa Debela	______________________	15/01/2024
Name of the students	Signature	Date

RECOMMENDATION

I, the major advisor of this thesis, hereby certify that I have read the revised version of the thesis entitled **"Experimental Study and Parametric Optimization of Tungsten Inert Gas (TIG) Welding of Stainless Steel AISI 316 Pipes"** prepared under my guidance by **Lelisa Anbesa Debela** Submitted in partial fulfilment of the requirements for the degree of Mater's of Science in Manufacturing Engineering.

Therefore, I recommend the submission of revised version of the thesis to the department following the applicable procedures.

Major Advisor	Signature	Date

APPROVAL SHEET

I, the advisors of the thesis entitled **"Experimental Study and Parametric Optimization of Tungsten Inert Gas (TIG) Welding of Stainless Steel AISI 316 Pipes"** and developed by **Lelisa Anbesa Debela** hereby certify that the recommendation and suggestions made by the board of examiners are appropriately incorporated into the final version of the thesis.

____________________	____________________	____________
Major Advisor	Signature	Date

We, the undersigned, members of the Board of Examiners of the thesis by **Lelisa Anbesa Debela** have read and evaluated the thesis entitled **"Experimental Study and Parametric Optimization of Tungsten Inert Gas (TIG) Welding of Stainless Steel AISI 316 Pipes"** and examined the candidate during open defense. This is, therefore, to certify that the thesis is accepted for partial fulfillment of the requirement of the degree of Master of Science in Manufacturing Engineering.

____________________	____________________	____________
Chairperson	Signature	Date
____________________	____________________	____________
Internal Examiner	Signature	Date
____________________	____________________	____________
External Examiner	Signature	Date

Finally, approval and acceptance of the thesis is contingent upon submission of its final copy to the Office of Postgraduate Studies (OPGS) through the Department Graduate Council (DGC) and School Graduate Committee (SGC)

____________________	____________________	____________
Department Head	Signature	Date
____________________	____________________	____________
School Dean	Signature	Date
____________________	____________________	____________
Office of Postgraduate Studies, Dean	Signature	Date

ACKNOWLEDGEMENTS

First and foremost, I want to thank Almighty God for giving me the strength and support I needed to complete this research study. I had like to express my profound gratitude to my Advisor, Dr. Moera Gutu, for giving critical guidance, encouragement, moral support, and on-going assistance throughout this project. Working and studying under your supervision was an incredible privilege and experience.I am incredibly appreciative for everything you have done for me.

I also owe a debt of gratitude to Mr. Birhane Asefa for his relentless advice, suggestion, and support during working at the Center of Welding Technology and Ethiopian Conformity Assessment Enterprise.

My heartfelt thanks and affection go out to my one and only Mrs. Aster Teshome. for her unwavering support and understanding. You have been my inspiration throughout this, and I'm confident you will be my pillar for the rest of my life. I am also grateful to my parents, sisters, and brothers for your love, prayers, and concern.

Finally, I had like to thank the Welding Training and Technology Center for providing partially funding for this research.

Thank you all

Table of Contents

LIST OF TABLES

LIST OF FIGURES

LIST OF ABBREVATIONS

A	Ampere
AC	Alternative Current
AISI	American Iron and Steel Institute
ANN	Artificial Neural Network
ANOVA	Analysis of Variance
Ar	Argon
ASTM	American Society for Testing Materials
BS	Bending Strength
CA	Constant Arc Mode
CS	Compressive Strength
DC	Direct Current
DCEN	Direct Current Electrode Negative
DCEP	Direct Current Electrode Positive
DoE	Design of Experiment
DP	Depth of Penetration
EPW	Pure Tungsten
FLM	Fuzzy Logic Method
FW	Fusion Welding
GA	Genetic Algorithm
GFR	Gas Flow Rate
GMAW	Gas Metal Arc Welding
GRA	Grey Relational Analysis

GRC	Grey Relation Coefficient
GRG	Grey Relation Grade
GRGi	Average Grey Relation Grade
GTAW	Gas Tungsten Arc Welding
H	Hydrogen
HAZ	Heat Affected Zone
He	Helium
HF	High Frequency
HV, HRC and HRB	Hardness Number Value
MPa	Mega Pascal
N	Nitrogen
OA	Orthogonal Array
PA	Pulse Arc Mode
PA	Horizontal Welding Positions
RG	Root Gap
RH	Rockwell Hardness
RSM	Response Surface Methodology
SS	Stainless Steel
SST	Scatter Search Technique
TGRA	Taguchi based Grey Relation Analysis
TIG	Tungsten Inner Gas
TM	Taguchi Method
UTM	Ultimate Tensile Strength
UTM	Universal Testing Machine
V	Volt
WB	Width of Bead
WC	Welding Current

YS	Yielding Strength
Zij	Normalized Value
Δ	Absolute Difference Coefficient
λ	Distinguishing Coefficient
%	Percentage
%E	Percentage of Elongation
%wt.	Weight Percentage
°C	Degree Celsius
µGRG	Predicted Mean Grey Relation Grade
304L	Low Carbon Content Than SS 304

ABSTRACT

Tungsten Inert Gas (TIG) welding is a form of arc welding that is utilized in a variety of sectors such as food, pharmaceuticals, chemical plants, marine, aerospace, medical devices, and implants. The procedure comprises various factors that the operator controls, which affect the microstructure and mechanical qualities of the joints. In this work, three TIG welding variables of welding current, root gap and shielding gas flow rate, were varied to three levels and their implications on hardness, ultimate tensile strength, compressive and bending strength were explored. Investigations were conducted out on a 2mm thick pipe of austenitic stainless steel AISI 316 grade using TIG welding equipment and were carried out using Taguchi-based Grey relation analysis L9 orthogonal array (OA). As a filler material, ER308L was employed. The results were examined using the signal to noise S/N ratio and analysis of variance. The optimum values of control variables in the AISI 316 grade control factors were welding current (WC) level 3 used 100A, gas flow rate (GRF) level 3 used 14 lit/min, and root gap (RG) 1.5mm. Welding current was the most important characteristic, contributing to 85.6% of Rockwell hardness, ultimate tensile strength, compressive and bending strength enhancement. The overall R^2 (adj) was 97.53%. Only 97.51% of the variance was explained by specified criteria, leaving 2.47% unaccounted. As a result, the validation experiment results demonstrated what was performed acceptable. The use of back gas purging devices improved stainless steel's ultimate tensile strength, bending strength, compressive strength, and Rockwell hardness substantially. Furthermore, the maximum Rockwell hardness, ultimate tensile strength, compressive strength, and bending strength 59.5 HRC improved by 1.7%, 912.5MPa advanced by 1.8%, 547.8MPa improved by 1.83%, and 1036MPa improved by 1.66%, respectively. The element performed has sound quality and good mechanical properties.

Keyword: TIG, AISI 316, Stainless steel, optimization, welding parameters

CHAPTER ONE
INTRODUCTION

1.1. Background of the Study

Welding is the permanent joining of two materials that, when pressure and heat are applied, coalesce at their contacting surfaces. Filler material might or might not be utilized for completing a weld connection [Khan, (2007); Jeffus., (2012)]. Welding is used in a variety of items, including farm equipment, mining equipment, construction equipment, railroad cars, automobiles, electronics, furnaces, boilers, and air conditioning systems. Large-scale welded constructions are becoming more common in shipbuilding, maritime engineering, and automobile production [Sharma et al., (2022); Xu et al., (2023)].

Nowadays, TIG welding, or tungsten inert gas welding, is a commonly used technique for welding difficult metals like titanium, magnesium, aluminum, and stainless steel, especially thin sections. It was needed minimum clean than other welding process, fumeless, spattering free and requires little to no finishing or only sporadic/intermittent finishing. In TIG welding, the stability and striking ease of the arc are enhanced by the use of a non-consumable tungsten electrode, which can be pure or blended with oxides [Karunakaran & Balasubramanian, (2011); Indira & Marpu, (2012)].

Fusion and solid-state welding processes are used in industrial applications, including Tungsten Inert Gas (TIG) welding for nuclear reactors, offshore constructions, pressure containers, and petrochemical equipment. Noble gas shielding, such as Ar, He, and combinations of Ar and He, is used in TIG welding to protect the tungsten electrode and weld pool from ambient gases. Welding unalloyed, low alloyed, and chrome steel material protected with argon gas during TIG welding produces a strong, reliable weld that satisfies the need for excellent mechanical qualities [Ye et al., (2021); Li et al., (2022); Yelamasetti et al., (2023)].

The TIG welding process technology uses two arc modes: constant arc mode (CA) and pulse arc mode (PA), which maintain arc stability and are used as significant and reliable procedures. TIG is a reliable, defect-free technology for welding joints connections. To manage heat inputs, welded structures get continuous current, whereas pulse current pulsates from peak to low.

High currents heat weld metals, facilitating fusion. When the current drops, the fusion zone cools the molten pool [Porchilamban & Amaladas, (2019); Sabzi et al., (2021); Yang et al., (2022)]. Constant current input throughout fusion welding causes novel phases within the metal morphology and micro segregation of the filler wire blending ingredients, resulting in undesirable welded structural properties. Because of the constant input of heat, the CA-TIG process has difficulty generating coarse-grained morphologies and a high Heat Affected Zone (HAZ) [Zhang et al., (2022); Yelamasetti et al., (2023)].

PA-TIG welding is commonly employed in Fusion Welding (FW) processes owing to its benefits over CA-TIG welding. It lowers micro segregation, pores, and residual strains while decreasing heat input. Elevated principal current during PC-TIG welding causes grain boundary enlargement and substructures [Yadav et al., (2023); Wang et al., (2022); Vemanaboina et al., (2023)]. In the fusion zones of continuous and pulsed current gas tungsten arc welding, the study found free defects welding. When compared to continuous current mode, pulsed current demonstrated a more refined microstructure and no micro segregation in the weld grain boundary. Grain refinement in the fusion zone is responsible for the improved mechanical properties observed with pulsed current as compared with continuous current mode. This implies that the mechanical properties of welds can be improved by the parameters of pulsed current [Srikanth & Manikandan,(2018)].

Gas tungsten arc welding (GTAW) is predominantly DCEN owing to its low-deposition method, which produces clean, tiny, and accurate welds. DCEN welding's workpiece-focused heat improves weld penetration and fusion, but it is rarely utilized because to the high heat concentration on the non-consumable electrode, which increases the danger of contamination and shortens the electrode's lifespan. TIG welding with DCEN provides excellent cleaning action because argon ions break up oxides on the workpiece. However, electrode oxidation is prevented due to adequate heat in the parent metal, which prevents impurities from being removed.This approach employs both AC and DC power sources, with the tungsten electrode polarized negatively. With straight polarity or DC electrode negative, the electrode becomes the cathode and the work piece becomes the anode [Norrish, (2006)]. This technique is capable of handling all welding positions, whereas others are only capable of handling one or two.

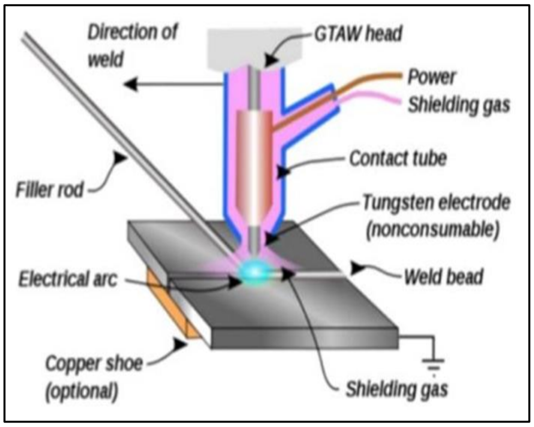

Figure 1.1. TIG Welding approach/method **[**Wahule & Wasankar,(2018)]

Figure 1.1 depicts a molten weld pool formed by an arc between a non-consumable tungsten electrode and base metal. For protection of the hot tungsten electrode against oxygen cross-contamination during TIG welding, an inert shielding gas is required [Jeffus & Baker, (2016)]. In the late 1930s and early 1940s, the aerospace industry developed Gas Tungsten Arc Welding (GTAW) methodology for welding magnesium. Riveting joints is a wasteful process that can result in stress concentrators, fractures, and fretting corrosion. Riveted plates may fail due to shearing, tearing, or crushing, as well as single or double shear shearing [Jeffus & Bower, (2009); Messele, (2019)].

Helium and DCEP welding currents were employed to shield a welding arc and molten weld pool in the 1920s, presenting difficulties in the adoption of GTAW welding technology. Understanding of gas composition and polarity increased process performance and decreased costs [Bhavsar & Patel, (2016)]. Welders regulate welding parameters such as material type, grinding size, filler metal type, welding joint, material size, ceramic gas cup size, torch orientation angle, travel speed, arc distance, inert gas type, gas flow rate, welding current, and polarity [Thakur & Chapgaon, (2016)].

Austenite stainless steel has been chosen by Ethiopia's government and business community for agriculture processing firms, beverage industries, food industries, soft drink facilities, and water facilities [Schmidt & Piotter, (2020); Deshwal & Panjagari, (2020)]. TIG welding was selected because of its higher weld quality, lack of noise, lack of flux, lack of smoke or fumes, suitability for welding very small components, and use of less filler metal. When the welding materials, joint arrangement, welding variables, and welding parameter level settings were incorrect, the weld bead did not achieve optimal weld strength and ductility. The

HAZ changed the internal composition crystalline phase and morphology of the metal, weakening it and lowering its mechanical strength [Linger & Bogale, (2023)]. Weld bead abandonment can be triggered for a loss of strength and hardness within the weld as an outcome of stress, friction, vibration, pressure, steam, and/or heat. Maintaining quality and accuracy is crucial to mitigate this impact developed in the pipe line and welding joint.

The most common are austenitic stainless steels with 16-25 wt.% chromium and 7-35 wt.% nickel. The austenitic stainless-steel grades 304, 304L, 304H, 316, and 316L have high thermal hardness and durability. They have been utilized through a wide range of manufacturing sectors due to their respective positions corrosion resistance, low temperature efficiency, and oxidation resistance due to these superior properties demanded within various application like: equipment, vessels, and pipelines in the chemical, food, power, oil, gas, pulp, and paper industries [Campbell, (1987); Linger & Bogale, (2023)].

The previous study considered the following major welding factors alone and in two compositions: welding current, gas flow rate, root gap, voltage, arc length, and travel speed. Primary controllable parameters influence bead width, bead height, penetration, arc stability, and mechanical property change during the welding process. Response surface methodology/RSM/, Taguchi technique, artificial neural network/ANN/, Genetic Algorithm (GA), scatter search technique, Grey Relational Analysis (GRA), and fuzzy logic method are some methods for optimizing process variables [Lugade & Deshmukh, (2015); Bopaliya, (2016); Ghosh et al., (2016); Wahule & Wasankar, (2018); Suraj et al., (2018); Messele, (2019); Linger & Bogale, (2023)].

The primary goal of this study was to experiment with mechanical properties of welding joint and optimize the settings of the TIG welding process on stainless steel 316 in order to maximize the weldment's hardness, tensile strength, and bending strength, as well as to investigate microstructural and mechanical characteristics.

1.2. Statement of the Problem

In Ethiopia there is agro-processing, beverage, food, and water plants used components made of austenitic stainless steel, notably SS-304, SS-316 and SS-304L, for corrosion resistance, low-temperature performance as well as oxidation resistance. TIG welding is subjected to weld stainless steel 316 major pipelines transmit massive amounts of crude oil, natural gas, and petroleum products, resulting in substantial losses in terms of individuals, financial resources, time and environmental damage. Internal weld discontinuities can be caused by weld discontinuities such as inadequate penetration, fusion, gas porosities, oxides, and fractures. New techniques have been created to increase weld quality, and current processes have been pushed to their limits. Manufacturers are looking for low-cost welding techniques with greater deposition rates, more comprehensive penetration, and more robust structures [Sidhu & Chatha, (2012)].

During the reconnaissance examination for plant faults, the Asella Malt plant factory company visited many factories and identified issues with welded seams that caused leaks and broke down. Weld beads fail due to a lack of strength, hardness, and ductility in the weld, particularly at Asela Malt Factory. Furthermore, poor welding material selection, joint geometry, welding variable selection, and acceptable welding parameter level settings contributed to weld bead failure. Because of these flaws in the welding components during overhaul and corrective maintenance, waste of raw and manufactured goods such as malt and input desired material for malt production such as ammonia and water easily flows and mixes with mad and dust, that demand additional costs with consume factor profit and decreasing factory profitability.

When the welding materials, joint configuration, welding variables, and welding parameter level settings are not suitable and appropriate, the weld bead does not achieve optimum weld strength and ductility, resulting in damage and breakdown of the welded joint when load or pressure is applied, as illustrated in Figure 1.2 below.

Figure 1.2. Weld bead specimens defect detected from the Asella Malt plant firm: (a) Weld bead crack and Base metal HAZ crack (from the industry).

Asella Malt Factory, a prominent Ethiopian malt maker, is facing reworking difficulties due to welding problems. The rework method costs the company extra money. To address this issue, the research concentrated on TIG welding parameters and the fundamental source of the problem. The use of root-cause research assisted in identifying causative variables and improving welding performance. As the cost of rework grows, so does the cost of failure, aggravating both malt quality, the final item product efficiency and customer satisfaction who consumed factory goods.

The most prevalent difficulties in a corporation are porosity and lack of fusion, which account for 75% of overall flaws. Poor welding quality reduces customer satisfaction, which leads to higher costs and a negative influence on the company's competitive market position. Internal failure costs have a higher impact on the organization than external failure costs since they are found during product or service manufacturing. To overcome this constraint and provide some insight, the TIG welding process parameters are modified on SS 316 using multi-objective optimization of Taguchi-based grey relation analysis to study the influence of welding variables on weld hardness values, tensile strength, and bending strength.

1.3. Objective

1.3.1. General Objective

The main objective of this research was to study the effect of welding parameters during TIG welding of 316 stainless steel pipes and parametric optimization of using Taguchi-based Grey Relational Analysis (TGRA) to determine the optimal levels settings of TIG welding process to improve mechanical properties.

1.3.2. Specific Objectives

1. To investigate the effect of welding parameters such as welding current, shielding gas flow and root gap on weld quality.
2. To optimize process parameters using Taguchi-based grey relation analysis.
3. To examine the impact of welding process parameters on mechanical properties such as tensile strength, hardness and bending strength.
4. To validate the outcomes by running confirmatory experiments.

1.4. Significance of the Study

When a high level of weld quality or a highly precise welding technique is required, TIG welding is essential for high-quality welds and precise welding operations. Grade 316 stainless steel is a versatile, corrosion-resistant alloy that is frequently used [Lugade and Deshmukh, (2015); Suraj et al., (2018)]. Inadequate welding variables and level setting selections cause weld bead failures. The thesis seeks to minimize welding flaws, reworking processes, and production duration, allowing the company to compete in welding quality while lowering maintenance costs. It provides welders with input data on welding defect reduction parameters and optimal joint penetration, guaranteeing high-quality and cost-effective repairs. The research provided beyond attempts to generate optimal TIG welding settings for Asella Malt manufacturing, therefore assisting other firms and providing critical information to researchers working on similar fields. The results may be a valuable resource for optimizing parameters in any firm with the objective of producing excellent products while minimizing quality costs such as rework and repair. This study will help researchers and industry understand how to determine optimal welding parameters and level settings.

- ANOVA and gray relational analysis are used as optimization approaches.
- The techniques to get quality qualities.

- Understanding the impact of process factors on welding quality. - Validating experimental results and identifying optimal parameters.

This thesis, undertaken at the Asella malt factory firm, provides welding enterprises with useful insights into selecting optimal parameters, acquiring quality characteristics, analyzing the influence of each parameter on welding quality, and validating findings from experiments for optimum process variables. for decreasing cost of maintenance and providing quality malt for customer satisfaction and enhance profitability of the company and workforce satisfaction.

1.5. Scope of the Study

This investigation of pipe welding techniques focused on three TIG welding parameters, each having three levels and one welding position. According to the selection criteria, the three key attributes had a higher impact on welding quality than the other welding parameters, and the single horizontal welding position was usually utilized on pipeline. The welding parameters chosen were welding current (80,90, and 100 amps), gas flow (10,12, and 14 lit/min) and root gap (1,1.5 and 2.5 mm). The following are the thesis scopes: The foundation metal for this optimization process is grade 316 stainless steel pipe with dimensions of diameter, length and thickness of SS-316 material pipe samples ϕ40mm X 200mm X 2mm, respectively. The Taguchi-based grey relational analysis approach is used in this experiment to investigate the optimization process factors. MINITAB 2023 software is used for the examination.

1.6. Limitation of the Study

The study focuses on the mechanical properties of 316 grade stainless steel materials with horizontal position and butt joint designs. Despite the fact that the research had achieved its objectives, there were certain inescapable limitations in the company's operations. Because this was a research investigation, each TIG welding variable had to be evaluated in order to optimize; however, there was insufficient equipment to investigate every welding variable. Arc length is necessary to address welding errors, and this exact gap may be monitored using a high-speed camera, which the company does not have this critical instrument.

1.7.Organization of the Study

The thesis is organized into five sections. The first chapter discusses the background of study, problem of the statements, objectives of study, scope of study, limitations, and significance of study. The next chapter is a review of the literature, which covers quality control tools, the purpose and consequences of each TIG welding parameter, welding techniques, welding processes, welding shapes, optimization tools and their applications, and welding parameter analysis tools. The third chapter discusses research procedures such as design of experiment (DOE), data validation strategies, and data collection methods. The third chapter addresses the data collection strategy, research design, data analysis procedure, data analysis tools. The fourth chapter summarizes the outcomes of the investigation as well as the experimental analysis and interpretation of the DOE data. Based on the data acquired, recommendations for remedies and their outcomes are also made. Finally, the conclusion and recommendations was done in fifth chapter.

CHAPTER TWO

LITERATURE REVIEW

2.1 Introduction

This chapter focuses on optimizing TIG welding method variables on stainless steel 316 grade, with a particular emphasis on weld bead form, mechanical features, process parameters, the Taguchi technique, mathematical modeling, and evolutionary algorithms. Research is examined and utilized to inspire and emulate previous findings.

2.2 Introduction to welding

The most prevalent method of connecting metals and metal alloys throughout structural applications is welding. The two primary types of welding techniques are solid-state welding methods and liquid-state welding techniques [Verma et al., (2023)]. Although solid-state welding has various benefits, such as friction stir welding, fusion welding technologies (liquid-state welding) have a wide range of usages within the manufacturing sector due to its capability to properly repair welds [Barnes & Pashby (2000)]. GTAW and GMAW welding are the majority of widely used fusion welding methods primarily because of their large-scale manufacturing capability and suitability for joining larger base metals [Sonsino et al., (1999)].

In fusion welding, high-quality welds are critical for greater mechanical properties strength . Weld bead shape, deposition rate, and hardness are measured using primary welding parameters such as current, electrode stick out, torch angle, voltage, and speed. Secondary characteristics include the torch angle, direction, nozzle distance, torch placement, free wire length, and shielding gas flow rate [Shih et al., (2011); Verma et al., (2023)].

2.3 Tungsten Inert Gas Welding

TIG welding is a critical arc welding process that uses a non-consumable tungsten electrode and inert gas to shield the arc. Using a noble gas shielding envelope such as argon, helium, or a mix of the two, this approach produces high-quality welds. The shielding gas protects the tungsten electrode and welding pool from ambient gases. Because of its high air tightness, TIG welding is commonly used to weld nonferrous metals like aluminium and magnesium [Huang et al., (2023)]. Throughout the welding formation process, there is good fluidity and minimal/fewer faults, such as dislocations [Trdan & Grum, (2012); Ryl et al., (2014); Dejun & Jinchun, (2015)].

2.4 Tungsten Electrode Classifications

Tungsten is created through the reduction of trioxide with hydrogen, refining it to 99.95% purity, squeezing it, and casting an ingot [Jeffus & Bower, (2009)]. The ingot is then heated to increase ductility, and electrodes of different lengths and diameters are formed [Jeffus, (2020)]. The aforementioned electrodes are available in sizes that range from 0.5 to 6.4 mm in diameter and 75 to 610 mm in length. A thick black oxide coating coats the tungsten electrode, which may be chemically cleaned or ground away [Jeffus & Bower, (2009)].

Tungsten is suitable for non-consumable electrodes due to its high melting temperature and strong electrical conductivity. Its arc temperature is 11,000°F (6000°C), however knowing the GTAW torch and electrode is critical [Jeffus, (2012)]. Small quantities of cerium, lanthanum, thorium, or zirconium are used to improve arc striking capability and endurance [Bower, (2010)]. Table 2.1 demonstrates the many types of tungsten electrodes and how to recognize them as well.

Table 2.1: Types of tungsten electrodes and their identification [Jeffus & Baker, (2016)**].**

No.	AWS Classification	Tungsten Compositions	TIP Color
1	EWP	Pure Tungsten	Green
2	EWTh-1	1% thorium added	yellow
3	EWZr	0.25% to 0.5% zirconium added	Brown
4	EWTh-2	2% thorium added	Red
5	EWG	Alloy not specified	Grey
6	EWCe-2	2% cerium added	Orange
7	EWLa-2	2% lanthanum added	Blue
8	EWL-1.5	1.5% lanthanum added	Gold
9	EWLa-1	1% lanthanum added	Black

Pure tungsten (EWP) electrodes are heat-resistant, erosive-resistant, and have high electron emission capabilities [Jeffus and Baker, (2016)]. Because of their high melting points, aluminum and magnesium are suitable for low-temperature AC welding, which may immediately shatter the oxide surface of these metals. They provide easy arc stability as well as balanced wave welding power. To get the highest arc stability, grind tungsten electrodes with the electrode axis perpendicular to the grinding wheel axis [O'Brien, (1991); Minnick, (1996); Lancaster, (1997)].

2.5 TIG welding parameters

Welders control factors such as electrode material, grinding shape, filler type, joint dimensions, base material, gas cup dimensions, torch orientation, travel speed, arc distance, inert gas type, gas flow rate, welding current, and polarity in TIG welding settings were discussed [Thakur & Chapgaon, (2016)].

2.6 **TIG Welding Apparatus**

TIG welding machines typically consist of a TIG torch, electrode, power supply, verious accessories and shielding gas delivery systems.

i. TIG torch

TIG torches, which give welding current and shielding gas to the weld, are either water-cooled or air-cooled. Figure 2.1 displays the air-cooled TIG welding torches. Air-cooled torches keep the welder cool while limiting the welding current to 200 amps. Water-cooled torches, represented in figure 2.2 [Minnick, (1996); O’Brien, (1991)], are designed for larger continuous welding currents than gas-cooled torches.

.

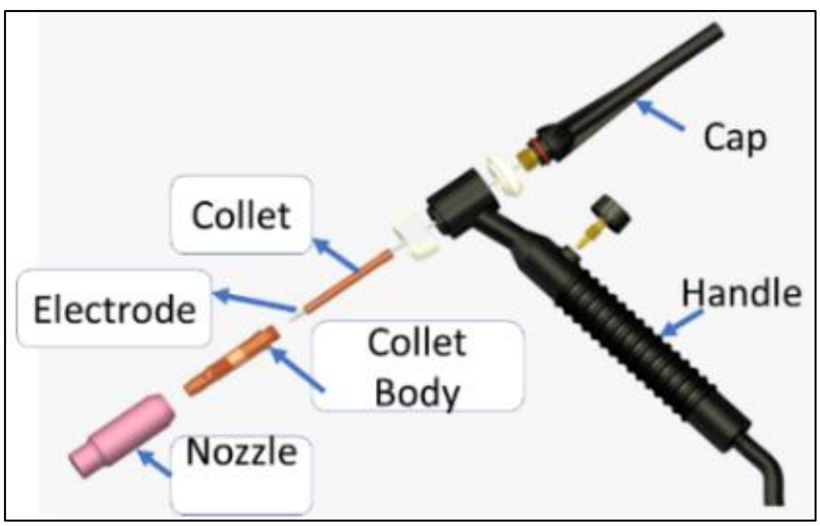

Figure 2.1. TIG welding process torch diagram [Rana et al., (2017)]

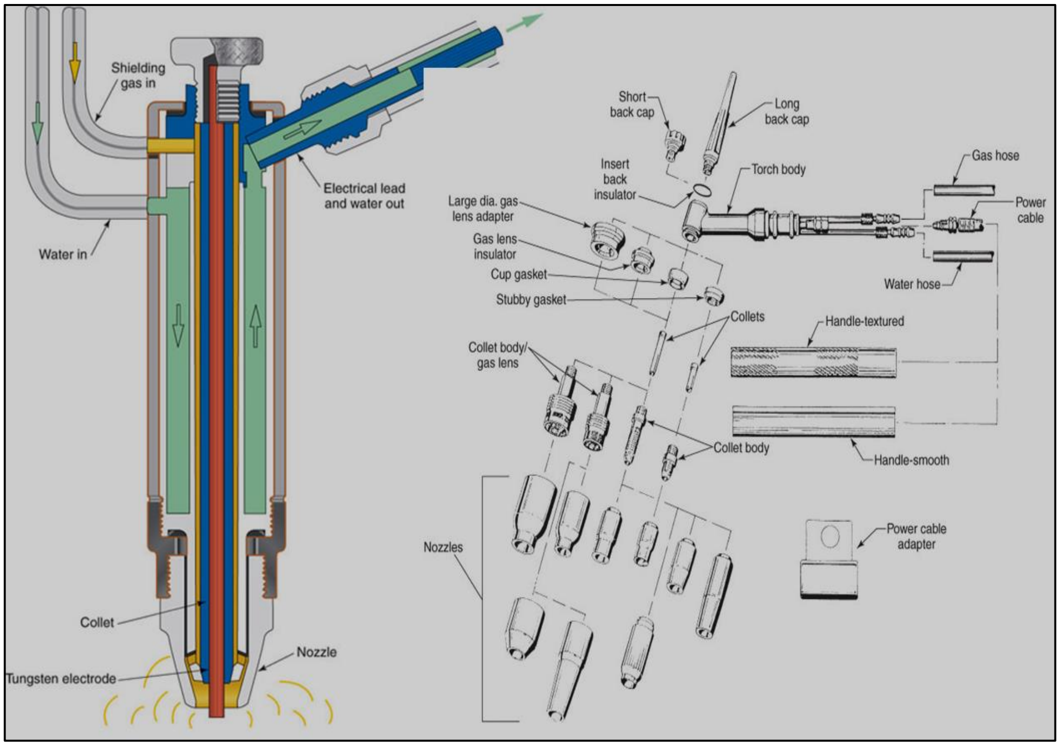

Figure 2.2. A cross-sectional image of a water-cooled torch **[**Minnick, (1996); O'Brien, (1991)**]**

ii. Power source

TIG welding requires a 70-80V open-circuit voltage power supply, whereas direct current welding requires a power source that rectifies alternating current from a 400V power supply and adjusts the intensity to the welder's desired level. Figure 2.3 depicts TIG welding heat dispersion using three distinct types of welding currents. Heat dispersion with the welding current method. DCEN produces deep penetration, DCEP produces broad welds with shallow penetration, and AC applies half of its heat to the work and the other half to the tungsten [Bower et al., 2010].

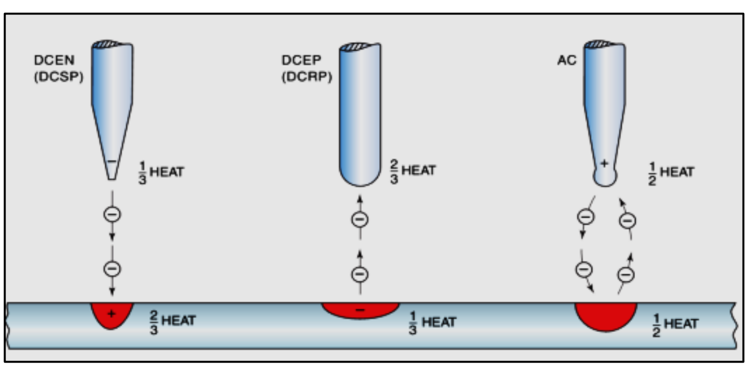

Figure 2.3.TIG welding Heat dispersion in the welding current method

iii. Shielding gas

Shielding gases shield the weld pool, electrode tip, and filler metal from air contamination during TIG welding. These are Ar, He, H, N, or mixtures of these elements. Working metals, as well as cost, temperature, arc stability, speed, spatter, electrode life, penetration depth, and corrosion resistance, all impact gas choices [Bhavsar & Patel, (2016); Jeffus and Baker, (2016)]. Shielding gas is required for TIG operations to maintain ionization environment, shield hot tungsten electrode, filler metal rod, melt pool, and electrode during cooling, and to use a cylinder with a pressure minimizing valve and flow meter [Parmar & Nair, (2019)]. Figure 2.4. Regulators below shown as the shielding gas regular used to control and manage the flow of shielding gas.

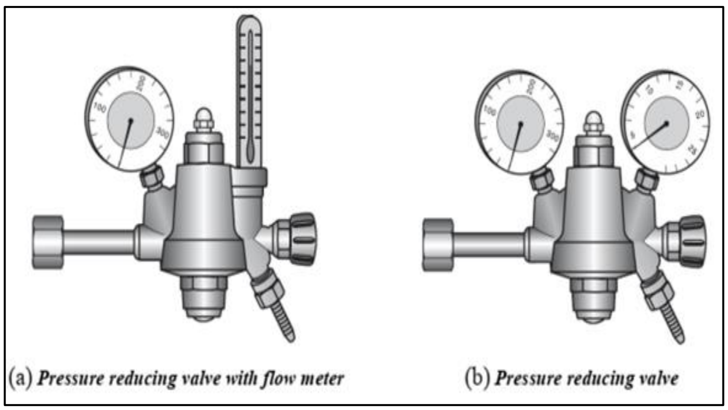

Figure 2.4. Regulators **[**Parmar & Nair, (2019)].

The pressure in steel cylinders ranges from 200 to 300 bar. Reduce the pressure of a gas cylinder to a safe operating pressure before using shielding gas. To lower pressure, a pressure-reducing valve can be utilized and the flowing gas can be controlled by nozzle size, weld pool size, and air velocity. Argon shielding gas flow rates are typically 7-16 L/min and nitrogen shielding gas flow rates are 14-24 L/min [O'Brien, (2004); Jeyaprakash et al., (2015)]. Figure 2.6 depicts pre-flow time, which happens when the gas flows for 3-5 seconds to remove air in nozzles or weld regions before the welding current is commenced.

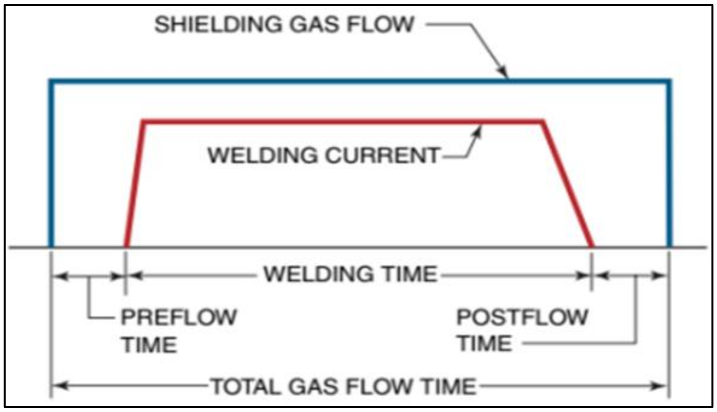

Figure 2.5. Welding time vs shielding flow of gas time [Bower et al., (2010)]

Subsequent flow duration is the amount of time that gas flows after the welding current terminates, protecting the molten weld pool, filler rod, and tungsten electrode from oxidation and contaminating. It is governed by welding current and electrode size [Bower et al., (2010)], as indicated in Table 2.2.

Table.2.2: Gas flow duration after welding

Electrode diameter within millimeters	Time for Gas Flow After Welding*
6	30 sec
5	25 sec
4	20 sec
3	15 sec
2.4	10 sec
2	8 sec
1	5 sec
0.5	5 sec
0.25	5 sec

TIG machines employ control systems to modify welding current, arc start, and shielding gas. Sophisticated boxes control shielding gas and postpone interruptions. High-frequency units raise voltage and frequency to produce a spark between the electrode tip and the workpiece surface by conveying an arc.

2.7 Stainless Steel Material

The American Iron and Steel Institute (AISI) classifies stainless steels into five types: austenitic, ferritic, martensitic, duplex, and precipitation-hardening [Richard, (1999)]. The majority of stainless steels used are austenitic stainless steels with 16-25 wt.% chromium and 7-35 wt.% nickel. The 300 series austenitic alloys are iron-chromium-nickel alloys, while the 200 series alloys also include manganese and nitrogen to substitute some of the nickel. Austenitic stainless steels are often utilized in the food, chemical, and petrochemical industries due to their better corrosion, low temperature performance and oxidation resistance. It is resistant to seawater, acids, and temperatures of up to 1100°C, assuring property degradation and ferrite resistance [Sharifitabar et al., (2011)].

According to [Anand & Mittal, (2017); O'Brien, (1991), TIG welding process provides advantages such as lower noise, better welds, minimal spatter or spater free, no flux addition, smoke, and odours. However, it has constraints such as slower transit speeds, lower metal deposition rates, harsher UV radiation, better hand-eye coordination, and higher equipment costs.

AISI SS 304 Stainless Steel Pipe is used to transport water, chemicals, low-pressure steam heat, waste disposal, ship plumbing, and structural elements. It is also used in high-pressure steam, radioactive materials, Alaskan pipeline, boilers, and refinery reactor lines, making it a valuable tool for designers and a highly demanded engineering material for applications [Bahrami & Taheri, (2019); Dak & Pandey, (2021); Sabzi et al., (2021)].

2.8 Applications Of TIG Welding Process

TIG welding is widely utilized in the aerospace, marine, and automotive industries for high-welding-requirement structural elements such as vehicle cylinder blocks and fuel tank welding [Szklarska-Smialowska, (1999); Hirschorn et al., (2010); Nguyen et al., (2018); Huang et al., (2023)]. Material phase shift occurs in a variety of metallic constructions, including buses, airplanes, reactors, and oil ducts. TIG welding joins workpieces by using a tungsten electrode shielded by inert gases such as argon, helium, nitrogen, hydrogen, or mixtures and a voltaic arc. This approach may be used to weld stainless steels and nonferrous metals [Goncalves et al., (2010); Nagesh & Datta, (2010)].

2.9 Welding Quality

Quality is an important feature of fabrication and welding since it is determined by the mechanical characteristics of the weld metal as well as the metallurgical qualities and chemical composition of the weld [Connor et al., (1987); American Welding Society, (1991)].

The investigator [Becker et al., (2002)], discovered that the dimensions of welded materials and the number of defects impact joint performance. These problems can be caused by deficiencies in product design, manufacturing procedures, material properties, or a combination of these. Other elements influencing weld quality include design, weld preparation, shielding, cleanliness, and procedure. Cracks are the most difficult defect kinds to repair owing to metallurgical behavior and welding circumstances.

Previous research [Yamauchi et al., (1983); Abrha, (2015)] classified DOE arc welding and other causes of welding defect as follows: unsatisfactory process conditions contribute for 45% of mistakes, human error accounts for 32%, inappropriate technique accounts for 10%, and unsuitable consumables account for 5% of unsatisfactory weld grooves. This result was obtained after investigating welding faults and their underlying causes.

2.10 Related research works on Welding Stainless Steel Material

2.10.1 Effect on hardness

This section's TIG welding technique with SS 316-based pipe metal-related components was evaluated to illustrate how welding variables impact the microhardness of the weld bead.

According to [Bhavsar and Patel, (2016)], authors investigated the effect of TIG welding process parameters on the mechanical properties of SS 316L welded joints. Researchers chose welding currents of 120, 150, and 180 amps, groove patterns of V, U, and V&U, and filler rods of ER304, ER308, and ER309 using a L9 orthogonal array. At 150A current U and V groove design and ER304 filler metal, the greatest hardness of 98 HRB was attained.

Researchers from [Saha & Dhami, (2018); Saha, (2020)] investigated the effect of TIG welding settings on 316L stainless steel pipe connections that were 4.75mm thick. In their Taguchi approach, researchers employed the L27 orthogonal array, the Taguchi algorithm, and four welding parameters: current, gas flow rate, welding speed, and filler rod diameter. The hardness values of gas flow rate (12 lit/hr.), current (150 amp) and filler rod diameter (3.2 mm) were then utilized by the investigators to find the optimal welding parameter combinations. Using the best welding conditions increased the hardness by 7.36 percent, from 92HV to 100 HV.

The research of [Sing et al., (2016)] investigated how welding process parameters affect the rate of deposition and hardness of SS 316L weld beads. Three input parameters were selected: current 110A, 120A, and 130A, gas flow rate 5lit/min, 10lit/min, and 15lit/min, and the number of weld passes 1, 2, and 3. The optimal parameter combination was discovered using the gray Taguchi technique and Minitab software. The greatest hardness value was 53 HRC, and gas flow rate was the most essential aspect parameters.

Lugade and Deshmukh (2015) examined optimizing process parameters for TIG welding SS 316L pipe with a thickness of 3mm and a filler wire thickness of 1.5mm. They calculated result variables such as hardness, tensile strength, and yield strength using input factors such as welding current, voltage, and gas flow rate. The experiment produced a maximum hardness of 205.56 BHN at optimal settings, with contribution percentages of 24%, 95.65%, and 51.9%, respectively.

According to [Chaudhari et al., (2019)] the parametric optimization of a TIG-welded 150 X 150 X 6mm SS 316L and mild steel pipe was explored. They employed Taguchi's technique with a L9 orthogonal array to achieve the highest Rockwell hardness score of 88.7HRB at an optimal variable configuration.

2.10.2 Tensile strength

This part analyzed the technique of TIG welding procedure using SS 316 pipe, which base metal-related articles to illustrate how welding variables impact the tensile strength of the weld bead. Scholars [Ghosh et al., (2016); Moi et al., (2018)] investigated TIG welding optimization by the use of welding procedure variables such as weld current, groove angle, and filler rods. They analyze the influence of these attributes under ideal conditions using the L9 orthogonal array-based Taguchi approach and ANOVA. The authors discovered that groove angle, filler metals, and weld current had the greatest influence on tensile strength. The authors investigate better tensile strength of 575.43MPa using optimal welding circumstances of 100A, groove angle, and filler material SS316L.

As [Lugde and Deshmukh, (2015)] improved the TIG welding process variables for SS304L pipe with a thickness of 3mm and a filler wire diameter of 1.5mm. The experiment was carried out with the procedure parameter selected according to L9 orthogonal array DOE with 140A current, 14 volts, and a gas flow rate of 25 liters per minute. Under optimum conditions, authors achieved 701.36 MPa ultimate tensile strength with 59% welding current, 44.5% voltage, and 44.5% gas flow rate of contribution percentage.

Scholar [Anand et al., (2017)], investigated the mechanical properties of weld joints in mild steel and 316L austenite steel. They used the Taguchi approach to optimize process variables, selecting Arc current (100,150,200A), voltage (18,22,26V), and shielding gas flow rate (10,12,14L/min) as the three control factors, each with three levels. The best welding configurations for current (100A), voltage (26V), and shielding gas flow rate (10L/min) resulted in the greatest tensile strength of 560.5 MPa, with percentage contributions of 47.50%, 24.55%, and 20.96%, respectively.

According to [Muluken, (2020)] investigated how various parameters influenced the joint's tensile strength, hardness, and percentage of elongation. They used the grey relational analysis technique and three welding factors (welding current, welding speed, and flux type) to optimize TIG welding parameters. The greatest tensile strength determined during testing was 542.78 KN/mm^2.

According to [Saha & Dhami, (2018); Saha, (2020)], experiments were conducted to explore the influence of TIG welding settings on the welded joints of 4.75mm thick SS 304L pipe. The current was the only variation in the optimum factor arrangements for ultimate tensile strength and hardness, with tensile strength increasing from 515MPa to 556MPa and hardness increasing from 92HV to 100HV.

2.10.3 Bending Strength

The current section inspected the process of TIG welding utilizing SS 304L pipe, which base metal-related items, to illustrate how welding variables impact the bending/flexural strength of the weld bead. As [Singh and Mittal (2017)], investigated the effect of welding process parameters on the mechanical and microstructural properties of dissimilar SS304-SS202 junctions welded with TIG. Using the Taguchi approach on the L9 orthogonal array, it was discovered that optimal welding settings such as 115A, 2.5mm/sec, and 12lit/min resulted in the maximum bending strength scores of 962.79N/mm^2.

According to [Kumar et al., (2017); Singh & Mittal,2017)], used TIG welding on SS 304L with three different thicknesses and E-308L filler metal in an experiment. The authors chose current, voltage, root gap, and gas flow rate as input welding parameters using Taguchi's L27 orthogonal array. The greatest bending strength was 106.33N/mm^2 at currents of 70A, voltages of 30V, and gas flow rates of 20lit/min.

2.11 Optimizations Techniques SS316 Pipe Welding

Primary controllable parameters influence bead width, bead height, penetration, arc stability, and mechanical property change during the welding operation. RSM, Taguchi technique, ANN, GA, scatter search technique (SST), GRM and fuzzy logic method (FLM) are some methods for optimizing process variables [Bopaliya, (2016); Ghosh et al., (2016); Wahule & Wasankar, (2018); Messele, (2019); Linger & Bogale, (2023)]. The major goal of this study was to optimize the welding procedure using TIG welding settings on SS 316 pipe in order to maximize the weldment's hardness, tensile strength and bending strength, as well as to investigate microstructural and mechanical properties.

Table 2.3: Parameters affect the optimization method, strength, hardness, and bending strength of TIG welding joints

No	Author and publication year	Process parameters								Methodology
		Travel speed	**welding current**	**Gas flow rate**	**Root Gap**	**Arc length**	**Pulse frequency**	**No of Passes**	**Groove angle**	
1	Nagesh & Datta, (2010)	18.1	4.56		65.32					Genetic Algorithm and ANN
2	Singh & Patel, (2014)	28.52	52.67						15.18	Taguchi Method
3	Lugade & Deshmukh, (2015)	44.87	28.14		20.85					Taguchi Method
4	Shaikh & Rao, (2015)	14	37		43					Taguchi Method and Grey Relational Analysis
4	Sing et al., (2016)		7.79	79.53				11.32		Grey Relational Analysis
5	Bachani & Ghetiya,(2018)	13.09	47.81				20.61			Grey Relational and Principal Component Analysis
6	Ahmad & Alam, (2018)	38.417	38.67			16.04				Taguchi Method and Grey Relational Analysis
7	Wahule & Wasankar, (2018)	58.73	27.94	8.21						Grey Relational Analysis
8	Hemnani et al., (2018).	18.1	1.65		74.56					Taguchi and ANOVA
9	Vora et al., (2021).	11.09	47.81				20.61			Response Surface Methodology (RSM)

To find welding factors, nine researchers evaluated their process factors, Wt.% of their contribution, and number of frequency cycles, as shown in table 2.3.

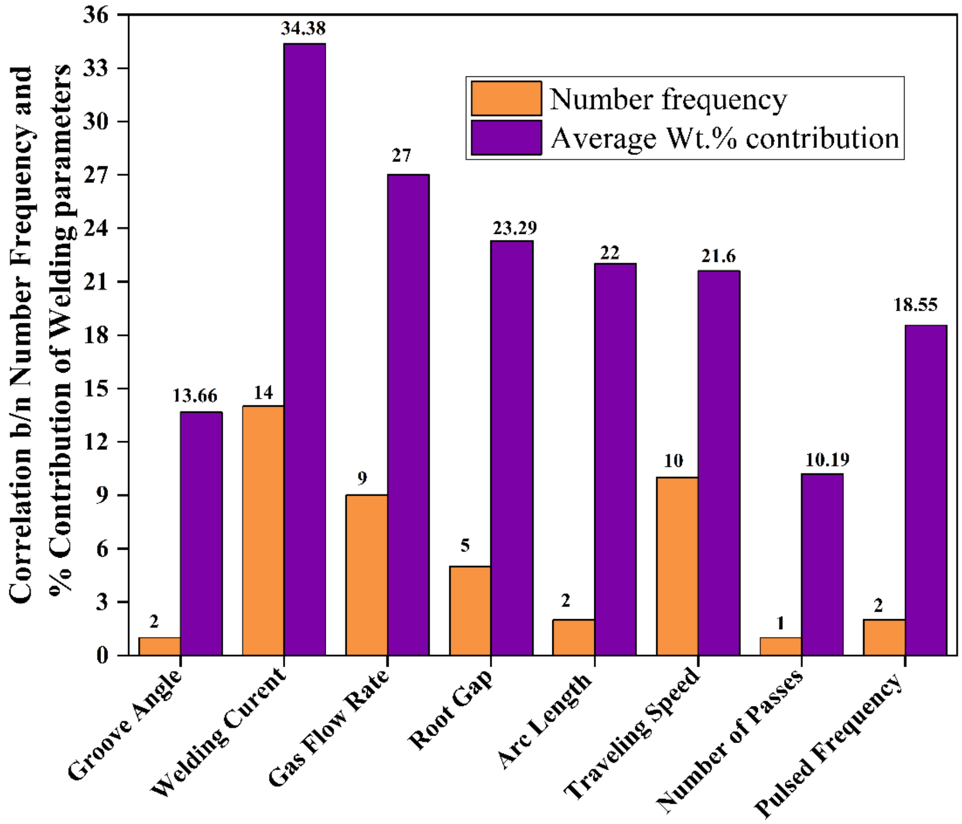

Figure 2.6. Correlation b/n number frequency and % contribution optimization method.

According to the Fig.2.6, this welding current has a total contribution proportion of 34.38% and operates at 15 Hz, with fourteen frequencies used. The second percentage for the contribution is 27% for the gas flow rate, and nine frequencies were chosen. The third contribution fraction of the root gap is 23.29%, and 5 frequencies were used. The fourth percent that contributes is 22% arc length, and two frequencies were used. The arc length utilizes 10 frequencies and contributes 21.6% of the fifth percentile. From the total of eight parameters, the first three variables (welding current, root gap, and gas flow rate) have 84.67% of the frequency ranges. As a result, the welding parameters were chosen based on their percentage contribution as well as the number of frequencies employed. Welding parameters or variables such as welding current, gas flow rate, travel speed, arc length, and root gap were investigated by several scholars, as shown in Table 2.3.

2.12 Orbital Stainless Steel AISI 316 Pipe Properties

Welding thick-walled pipes have become a critical procedure in a variety of industries, including offshore and onshore pipelines, vessel manufacturing, and nuclear power. Coil or pipe is used to make the majority of welded steel pipe. Choosing the right pipe for a certain work has an impact on the entire project by reducing the possibility of defects. The first and most important step is to choose a pipe material. Pipe wall thickness, outer diameter and cleanliness are all factors to consider when selecting an optimum pipe for a specific purpose. Pipe storage and handling are very vital in the welding industry, and pipes should be kept in good weather. Furthermore, inside the tube or pipe, dust, moisture, and grime make welding difficult and costly [Karataş, (2015)].

2.13 Stainless Steel AISI 316 Orbital Pipe TIG Welding

The term orbital pipe welding refers to an automated procedure that involves welding tubes and pipes in a fixed position with a track-mounted weld head. To make a weld, an orbital welding system's weld head revolves an electrode and electric arc around the weld joint. The orbital pipe welding approach could result in significant time, experienced welder and welding cost savings while also improving joint quality. TIG welding is commonly used to fabricate various materials such as aluminum, mild steel and stainless steel. Stainless steel is a ductile material that is simple to machine. Welding of Stainless-steel pipe is required to make numerous machine components with varying structural shapes. It has high machinability, as well as high strength, ductility and weld ability. It's most commonly utilized in a turned and polished or cold-drawn state. It resists induction hardening and flame hardening due to its low carbon concentration.

It will not respond to nitriding due to a lack of alloying elements. Carburization is possible to achieve case hardness more than RC65 for smaller sections; however, this hardness decreases as section size increases. The core strength will not change. Carbon nitriding, on the other hand, can be done and has several advantages over normal cycling**.** TIG welding is the most versatile and capable of producing high-quality welds. TIG welding delivers the high integrity necessary at the root of the weld, as well as weld speed. TIG welding machines are available with both high and low current ratings. TIG welding uses a current range of 150A to 350A, which is ideal for welding thick mild steel pipe [Latifi, (2012)].

2.13.1 Different Types of Welding Phases in Orbital Pipe Welding

Welding of pipe with a wall thickness of up to approximately larger pipe walls requires multi-pass welding the multi-pass method is often divided into three parts: root pass (open root), fill pass, and cap (final) pass, the number of phases is listed as four, with the hot pass counted as a separate phase. The first process creates a fine back inside the pipe, and the subsequent phases fill the groove. Welding processes in a sample of V grooves. The root pass weld is one of the most important pipe welds to ensure a defect-free weld. Pipe welding rules demand high-quality work that is fully penetrated and has a nice contour root pass. Welding parameters, joint geometry, welding positions, gravity, arc force, and gas flow all affect root pass welding. Precision fit-up, consistent gap throughout the entire joint, high operator expertise and tight fit-up tolerances are essential in root pass welding with orbital GMAW. After the root pass, the fill pass welding takes up the majority of the welding time. Fill welding normally consists of several layers, each of which is made up of many passes. Cap welding is a method of covering a welded junction and should be done in such a way that the joint has a good cosmetic look [Latifi, (2012)].

2.13.2 Welding Techniques Orbital Pipe Welding Groove Types

In comparison to hand pipe welding, automated pipe welding necessitates a high level of groove preparation and fit-up accuracy. Pipes with v girth-butt welds have also been widely employed in a variety of industries, including oil and gas pipelines, steam piping, and boiling water reactor piping systems. As a procedure approach, figure 2.7 depicts an orbital pipe welding groove.

Figure 2.7. Orbital pipe welding groove (Center of Excellence for Engineers image)

2.14 Summary of Literature Review

In the literature, welding parameters on Tungsten Inert Gas welding such as welding current, welding voltage, welding speed, arc length, angle of welding, air gap and welding position, stick length, shielding gas, work piece material weld-ability that affect the desired output such as strength, hardness, and micro-structure are discussed. However, the optimization of welding parameters and the characterization of AISI SS 316 Stainless Steel Pipe welded by Tungsten Inert Gas welding technique were not thoroughly investigated.

Researchers have experimented with process factors such as welding current, filer rod, and shielding gas flow rate in the gas tungsten arc welding process. Weak strength, low hardness, and low ductility of the weld result in weld bead failure. The causes of weld bead failure were suitable welding material selection, joint configuration, and welding parameter level settings. Welding parameters are the most typical cause of failure. These have occurred, but they do not explain the effect of these characteristics on weld joint strength. None of the studies have been done on AISI SS 316 Stainless Steel Pipe ϕ 40 mm x 200 mm x 2mm orbital pipes; they have only been done on aluminum, low carbon steel, and other stainless-steel pipes. Standard test specimen's materials, such as stainless-steel, were used as pipe.

As a result, research into the optimizations and characterization of welding settings for AISI SS 316 Stainless Steel Pipe is critical. Based on the literature review and main obstacles found in the literature, it was determined to study experimentally the following areas of welding process parameter optimizations in this thesis as a research gap.

Identifying the critical parameters (welding current, welding voltage, and welding speed) influencing the surface quality of the Tungsten Inert Gas welding process for AISI SS 316 Stainless Steel Pipe Φ40mm x 200mm x 2mm.The obstacles of welding AISI SS 316 Stainless Steel Pipe on Tungsten Inert Gas welding processes, and how to overcome them by selecting optimal welding settings.

In general, many researchers have a lot to say about the TIG welding process. Their work also has various input and output variables, and they may be optimized using a variety of approaches, tests, mathematical models, and other techniques. The purpose of this work is to evaluate and optimize the TIG welding process's welding parameters in relation to the mechanical properties of SS 316 weldments. The weld requirement's hardness and tensile strength are determined by the welding current. For optimizations, different researchers employ distinct approaches, tests, mathematical models, and other processes. The most significant challenges in welding stainless steel are: low heat conductivity and high electrical resistance, carbide precipitation, and cracking [Bopaliya, (2016)].

Reviewing the articles comprehensively may not cover the following topics;

- ✓ Previous research intended to optimize TIG welding process parameters on the mechanical characteristics of SS 316 weldments, concentrating on welding speed, current, and gas flow rate, with more investigation envisaged.
- ✓ Due to the scarcity of bending strength as an output response in Ethiopian TIG welding optimization studies, this research will make a substantial contribution.
- ✓ Ethiopia's limited research on TIG welding optimizations presents challenges in finding literature on root gap and bead combined analysis in SS 316 TIG welding pipes. This research aims to develop unique understanding and significantly impact the country's TIG welding optimizations.
- ✓ Many research investigations are limited to 100 amperes or above, as well as base material thicknesses of 3mm or greater. The investigation was conducted on existing base materials with a thickness is 2 mm and a working welding current effect and contributions of less than 100 amperes.

The investigation of microstructural alterations in AISI 316 SS weldments has been limited, necessitating the development of an appropriate welding parametric combination. The purpose of this study was to close this gap by using three distinct parametric combinations from the GTAW process to fabricate 2mm thick pipe 316 SS butt joints with the dimension of ϕ40 X 200m X 2mm. The goal was to investigate the quantitative and qualitative effects of welding current, gas flow rate and root gap on mechanical parameters such as tensile and impact, microstructure, and heat affecting zone. The welding heat inputs chosen were chosen to create a database that might benefit manufacturing operations in AISI 316 grade stainless steel welding processing. Theoretical analyses of complicated physical processes, such as TIG welding, sometimes adopt assumptions in order to simplify findings. Finding input-output correlations, on the other hand, might be difficult to determine. Theoretical studies look on the effects of variables including weld bead quality, shape, and mechanical properties. Most welding techniques aim to generate welded and weld beads that meet the required criteria, resulting in improved mechanical properties and a high-quality surface. Experiments and strategies for selecting factors that provide acceptable mechanical features are used.

CHAPTER THREE

MATERIALS AND METHODS

3.1 Introduction

This chapter contains in-depth information on the materials and procedures used in welding and sample analysis. It analyses a subject or situation using experimental analysis and a relevant research technique. The study's goal is to find significant information or concepts, pick the best design factors, and validate the improvement of robust and sound weld quality features utilizing the best parameters. Figure 3.1 depicts the work flow diagrams utilized in this inquiry.

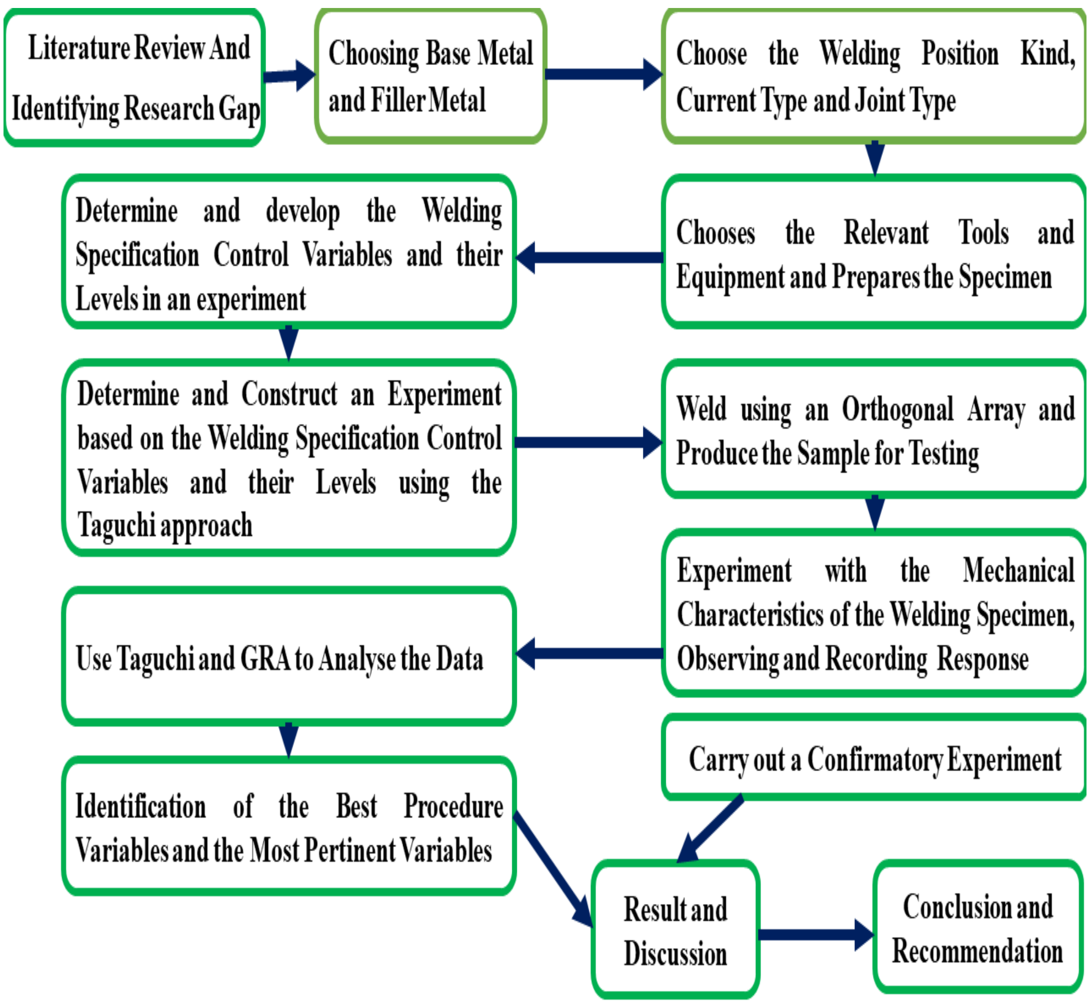

Figure 3.1. Workflow diagram

3.2 Materials and Equipment

The raw material in this study is 316 grade stainless steel pipes with dimensions of Φ40mm x 200mm x 2mm. The experiment is carried out using pipe welding on butt joint designs. Figure 3.2 depicts the butt weld arrangement. ER308L filler metals are indicated for the base metal of 316 stainless steel work pieces.

Figure 3.2. Welding joint design pipe welding

Design for a joint of the junction of work pieces or the edges of work pieces that are to be linked or have been attached as illustrated in figure 3.1 above. The type of joint is determined by the structural arrangement of the components that are joined to each other. Some welding connections may need edge preparation in order to weld or inspect and examinations the weld effectively.

3.2.1 Stainless Steels of AISI 316 Grade Stainless Steel Pipe Base Material

The chemical composition of austenitic stainless steels of AISI 316 grade Stainless Steel Pipe is potentially the most critical aspect pertaining to their weldability. Weld ability is defined by the American Welding Society (AWS) as a metal's ability to be welded under the fabrication circumstances imposed, into a specific, adequately designed structure, and to function well in the intended service. The chosen parent material 316 grade Stainless Steel Pipe austenitic stainless steels have outstanding weldability and can be welded instantaneously by all standard welding methods, with a good balance of toughness, strength, and ductility. Tables 3.1 show the chemical composition, mechanical, thermal, and physical characteristics of the test item, respectively. The chemical composition is the value of austenitic stainless-steel 316 grade, not the value of the test piece.

Table 3.1: The chemical composition of ER 308L filler material and SS 316 austenitic stainless steels is summarized for chosen base metals and filler materials (Bachani & Ghetiya, 2018).

No	Element	ER 308L	SS 316
1	Nickel	10	19.4
2	Chromium	18	19.7
3	Carbon	0.03	0.018
4	Copper	-	0.11
5	Phosphorus	0.045	0.024
6	Manganese	2	1.75
7	Silicon	0.75	0.31
8	Sulfur	0.3	0.015
9	Molybdenum	-	0.08
10	Nitrogen	0.1	-
11	Iron	Balance	Balance

Argon has been demonstrated to be the best gas for TIG welding stainless steel 316. It is an inert gas that is colorless and odorless, denser than air, non-hazardous and inflammable (Parmar & Nair, 2019). According to the company mark, argon gas with a purity of 99.99% is utilized for this investigation. Tables 3.2 and 3.3 summarize and analyze the physical and mechanical properties of SS 316 grade material according to ASTM and prior investigation publication [ASM, (1992); Zhong et al., (2019); Ghumman et al., (2022)].

Table 3.2: Physical characteristics for stainless steel 316 grade

Material	Melting point (ºC)	Thermal conductivity ($W.m^{-1}. K^{-1}$)	Specific heat capacity ($J. Kg^{-1}. k^{-1}$)	Thermal expansion ($mm.m^{-1}. K^{-1}$)	Density gm/cm^3
AISI 316	1375	15	490	16	8

Table 3.3: Mechanical characteristics for stainless steel 316 grade at ambient temperature

Material	Tensile strength (MPa)	Yield strength (MPa)	Elongation in 50mm (%)	Hardness (RHB)	Bending Strength (MPa)	Modulus of Elasticity (GPa)	Compressive Strength (MPa)
SS 316 or AISI 316	515	170	40	79	624	164	300

3.2.2 Equipment

Many tools and equipment are used in this work, as shown in table 3.4, including a meter, Vernier calipers, regulator, power saw, power supply, welding cable and tungsten electrodes. Material, equipment, machinery, and workshop infrastructure are crucial for this research. As a result, all of the necessary facilities are organized as part of the aforementioned endeavor.

Table 3.4: List of machinery, materials, and equipment

No	Machines	Materials	Tools and Equipment	Safety materials
1	TIG welding Machine (water cooled)	SS 316 stainless pipe	Regulator	Goggle
2	Universal Testing Machine	Argon gas	File	Apron
3	Bench type grinding machine	ER308L filler metal	argon gas cylinder	Helmet
4	Hydraulic press machine	Wire Polisher disk	Back purge device	Overall
5	Hacksaw	Grinding disc	Tong	Ear mask
6	Vickers hardness testing machine	Tungsten Electrode	Bench Vice	Gloves
7	Power hacksaw	Cutter disc	Adjustable wrench	Mouth mask
8	Portable grinder	Polisher disk	Wire brush	Safety shoe

This procedure makes use of a water-cooled TIG welding equipment. PROTIG- 315Di AC/DC welding equipment is employed in this investigation. This machine is equipped with a water-cooled welding torch and can generate up to 300 welding current for the wide range welding parameters and application.

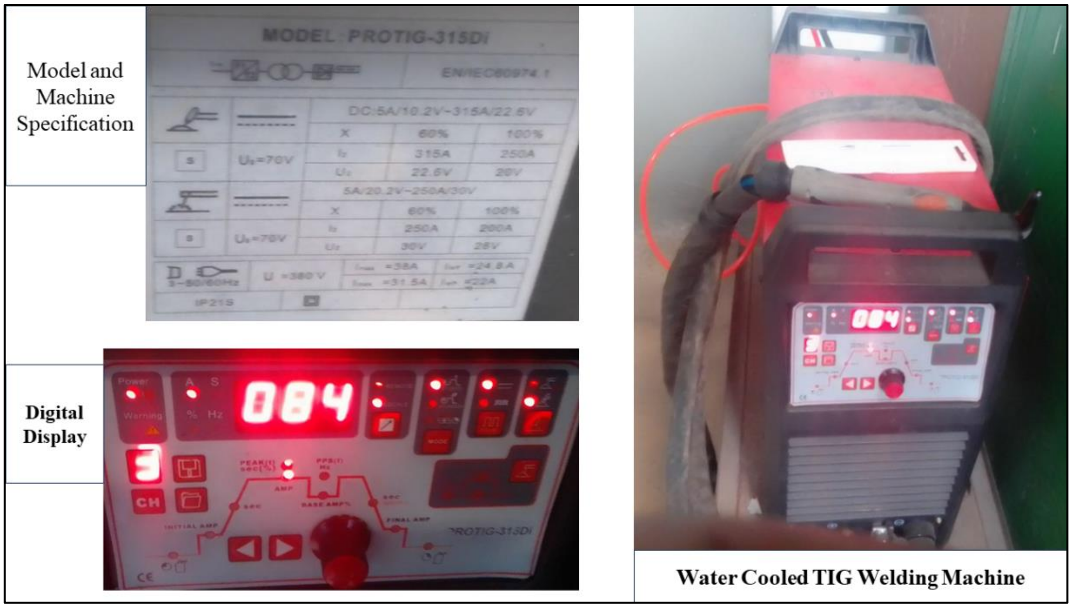

Figure 3.3. The TIG welding machine that was utilized to complete the experiment

The interior of the root pass weldment in stainless steel is exposed to air and may contaminate the weld. The air must be purged/shielded from the interior of the weldment for root pass welding. Backing purging gas can be used on the inside of the butt pipe weld and the adjacent base metal surfaces to keep the root weldment from oxidizing during welding [O'Brien, (2004)]. A backing gas is a device that performs a purpose in addition to keeping the welded components in excellent alignment. Argon gas is used as a purging gas in this investigation.

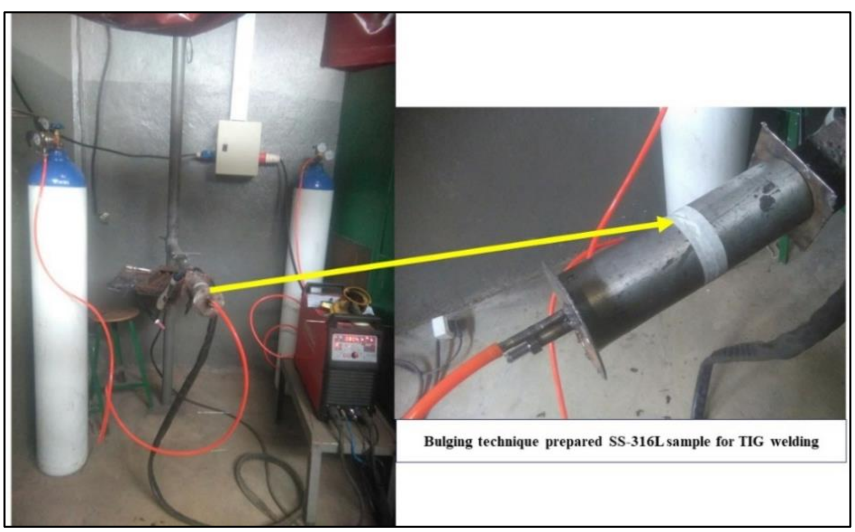

Figure 3.4. Gas purge backup mechanism

A Rockwell hardness tester type B and C, Beijing United testing equipment, was used for the hardness test shown in figure 3.5. The tensile test specimens were conducted using Figure 3.6, a universal tensile testing equipment with a maximum capacity of 600 KN. Tensile tests were performed. As indicated in Figure 3.6, the test samples were produced in accordance with the ASTM E8-04 sample geometrical guideline at the dowel time of 15 seconds. Compressive strength is defined as a material's capacity to withstand the direct pressure of applied compression force. On the same UTM was tested according to ASTM E9-09.

Figure 3.5. Rockwell hardness testing machine

Tensile and compressive testing was performed using a Bairoe computer controlled electro-hydraulic universal testing machine type HUT-600, as indicated in figure 3.5.

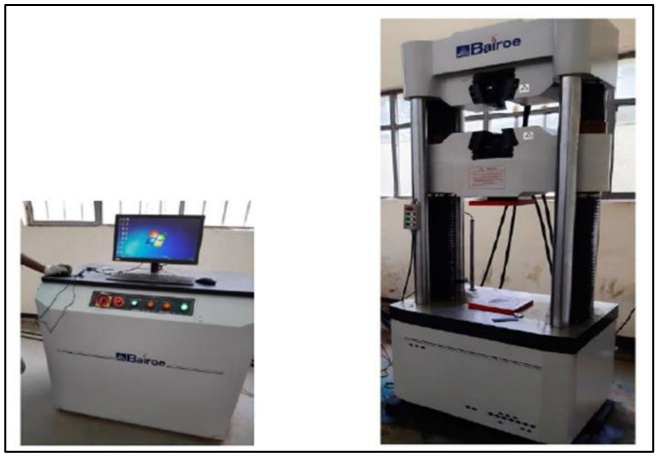

Figure 3.6. Universal testing Machine

ASTM E290 and EN 910 standard specifies the standards for bend testing to assess the ductility of metals. Bend testing provides a visual indicator of the material's ductility. The jig and fixture are readied to undergo the bend strength examination, that is installed on the universal testing machine. The span length of the bending jig and fixture is 54 mm and the internal length is 34 mm. and the servo-hydraulic testing machines are intended for carrying out tensile, compression, and bending tests on both metallic and non-metallic materials.as indicated in Figure 3.7.

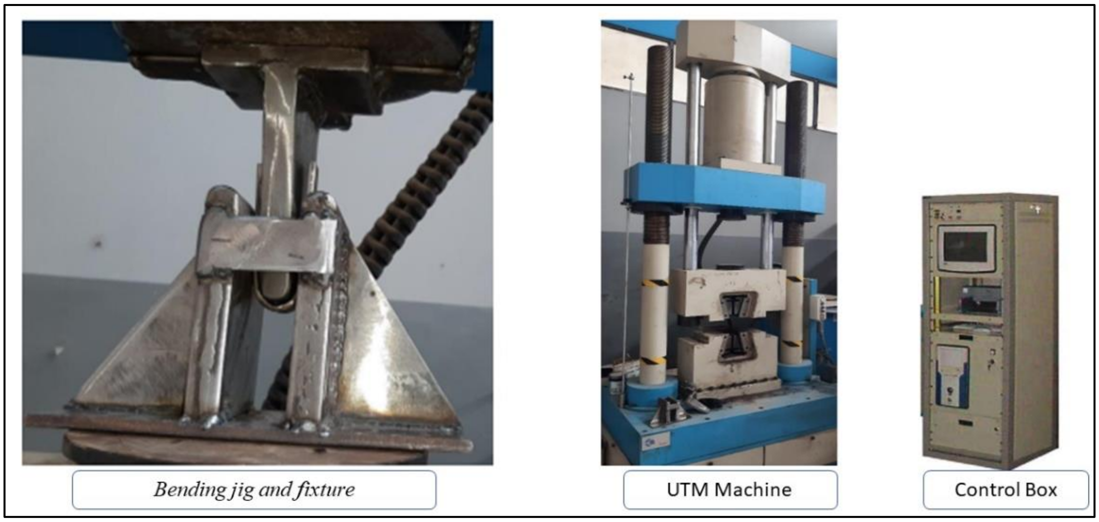

Figure 3.7. Bending testing using computerized universal testing devices

3.3 Methodology

A reliable and thoroughly reviewed source for the researcher to select the best approach and parameters for examining a variety of articles and papers produced by various authors for this thesis idea and concept. Researchers frequently use a range of optimizing strategies to achieve their goals. It may be summarized as follows: Taguchi based grey relation analysis utilizing with MINITAB 2023 software. The specifications of the SS 316 pipe base metal sample were ɸ40mm, 200mm length and 2mm thickness. Surfaces of workpieces were cleaned and prepared for welding, resulting in excellent robust and sound welds free of corrosion, scale, dirt, oil, and grease. A power hacksaw and grinder were used to prepare the samples edge.

The focus of the research is to look at how flat welding positions, especially butt joint and horizontal welding positions, are used to connect samples. This Position changes the welding position and rotation of workpieces and welders to make welding simpler, more efficient, and more rapidly performed welding speeds achieved. After gas purging and tack welding, TIG welding was employed to finish the initial joint arrangement. Depending on the welding conditions, the welding settings and circumstances were chosen.

3.4 Identifying the Parameter's Range of Operation

1.Welding current

Welding current is the most important controlled TIG welding factor, and it is determined by tungsten electrode diameter, gas type, and welding polarity. Lower current settings cause filler wire to stick, whereas fixed current settings change the voltage to maintain continuous arc current [Bhavsar & Patel, (2016); Thakur & Chapgaon, (2016)].

Table 3.4: Welding current optimization for figuring out current frequency

No	Author and publication year	Welding Current	Material type & thickness	Optimum response obtained
1	Bhavsar & Patel, (2016).	120, 150,180A	SS304L, 6mm	HV 150A, Impact strength 150A
2	Saha & Dhami, (2018)	90,150,180A	SS304,4.75mm	UTS 180A, HV 150A
3	Prajapati & Shah, (2016)	120,140,160A	SS304L, 6mm	Maximal penetration depth, weld width & distortion at 140A
4	Wahule & Wamankar, (2018)	80, 100,120A	SS-304 and Fe-410, 6 mm	UTS 120 A & Max. %E 120A
5	Shanmugasundar et al., (2019)	95, 120 ,140A	SS304, 3mm	HV 140, UTS 140 & YS at 140A
6	Bhadauria et al., (2018)	100, 115,130A	SS304, 3.5mm	Optimal Bead penetration, height & width at 123.703 A
7	Avinash et al., (2019)	160, 170,180A	SS-304 and Fe-410, 5mm	UTS 574.65MPA, 214VC Hardness &32.8% elongation at 120A
8	Sing et al., (2016)	100,115,120 A	AISI 316L, 3mm	ultimate tensile strength = 454.23 MPa
9	Ahmad & Alam, (2018)	140 150 ,160A	S30430, 3mm	Optimal UTS at 160A
10	Ogbonna et al., (2023)	120,150,180A	AISI 316& MS AISI 1008, 2.5mm	TS 559.25 MPa, YS 382.22 MPa, % elongation 33.34 % and hardness of 250.63 HV
11	Moi et al., (2018)	100, 125,150A	SS 316L, 3mm	UTS of 641.44MPa at 126.77A

According to Table 3.4, the welding current ranges from 80A to 180A, with a variation of 10 to 60A throughout a material thickness range of 2.5mm to 6mm.

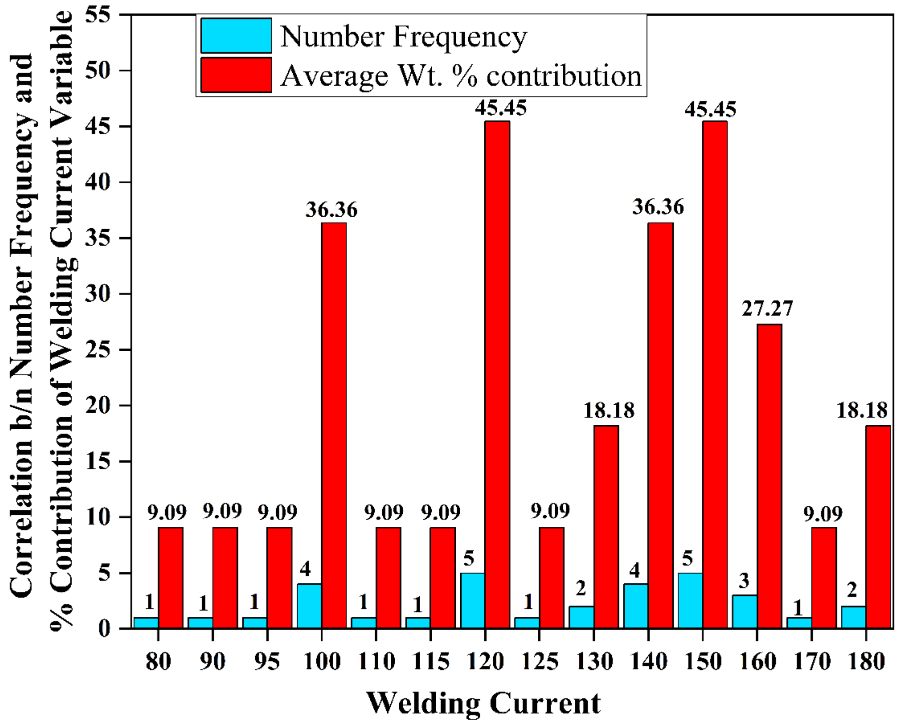

Figure 3.8. Correlation b/n number frequency and % contribution welding current

The welding current employed by the 11 academics assessed ranged from 80A to 180A, according to table 3.3. Figure 3.8 depicts the association between the frequency of b/n numbers and the percentage contribution of welding current in the scholar replication research publication. To identify the welding current variety, the maximum frequencies are 120A and 150A, 100A and 140A, and 160A, respectively. Because of the weld thicker base metal, several investigators choose this quantity to provide superior mechanical characteristics for the required engineering application. Because there have been few previous studies for 2mm thick stainless steel sheet metal rather than pipe, this investigation currently used the minimum welding current or 80A of the above scholar variation increments of 10 for three level design of experiments (80,90, and 100A) chosen to examine and optimize welding current to weld 2mm thick 316 grade stainless base metal pipe. Because changes in microstructural formation and heat input have a substantial impact on the efficiency of mechanical qualities of Austenite stainless steels in weldments, and it is highly strongly associated with the valuable mechanical achievement of AISI 316 grade stainless steel through GTAW.

2.Gas flow rate

The gas flow rate was chosen as a testing component because it can be easily changed using a gas flow meter. The use of a shielding gas impacts welding expenses, weld temperature, arc stability, weld speed, spatter, electrode lifespan, porousness, durability against corrosion, hardness, strength, and crack propagation of the weld material.

Table 3.5: Optimized gas flow rate for determining TIG welding process flow rate variation

No	**Author and publication year**	Material type & thickness	Gas flow rate	Optimum response obtained
1	Sing et al., (2016)	SS304, 5mm	5, 10 & 15 lit/min	Hv 15 lit/min, DR 15 lit/min
2	Wahule & Wasankar, (2018)	SS-304 and Fe-410,6mm	8, 12 & 16 lit/min	UTS 16 lit/min & Max. %E 16 lit/min
3	Singh et al., (2019)	304L ,5mm	9 & 15lit/min	UTS, %E & YS 9lit/min, Hardness WB, Hardness of HAZ & Toughness 15lit/min
4	Saha & Dhami, (2018).	SS304, 4.75 mm	10, 12 & 14	UTS 14, HV 12,
5	Moi et al., (2018)	316L, 3mm	6, 9 & 12 l/min	UTS 8.12 lit/min
6	Kumar et al., (2017).	SS304, 3mm	16, 18 & 20 lit/min	Hv 16 lit/min & Bend strength 20 lit/min
7	Ibrahim et al., (2017).	304L, 3mm	, 10, 12, 14 & 16 lit/min	PD 8 lit/min & BW 12 lit/min

The gas flow rate is mentioned from 7 various scholars in Table 3.5 to determine an average shielding gas flow rate, which ranges from 5 lit/min to 20 lit/min. Figure 3.9 displays the frequencies and rankings of the gas flow rate range used to determine the gas flow rate.

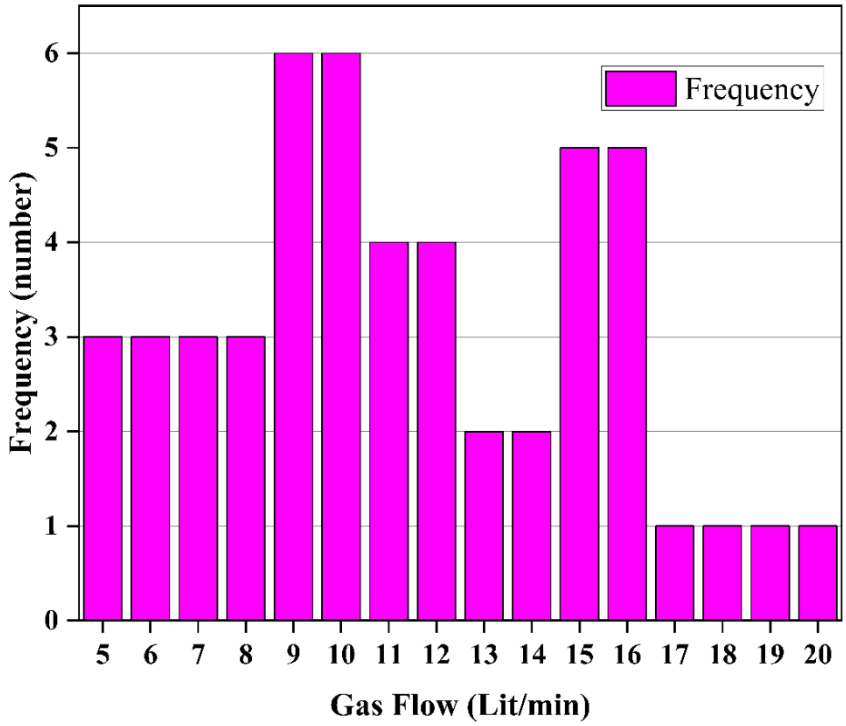

Figure 3.9. Designated gas flow frequency rate

The greatest frequencies observed in figure 3.9 depend on table 3.4 analyzed pervious research to compute the value of gas flow rate for this study are 9-10 lit/min, 15-16lit/min, 11-12 lit/min, and 5-8lit/min, ranked 1-4, respectively. The selection of variable ranges to achieve equal variation at each level. In this case, the fifth rank from 13-14lit/min and the sixth rank from 17-20lit/min is between 1 and 6 ranks; As a result, the level three design of experiment was used for the current examination of weld 2mm SS 316L pipe material using three levels of 10,12, and 14lit/min selected to analyses and optimize the mechanical qualities.

3.Root gap

The root gap is governed by elements such as electrode diameter, location, filler metal size, and current, which promotes weld penetration while limiting undercutting or extra material. Optimizing the root gap is essential for defining the gap range.

Table 3.6: Optimized root gap for gap ranging determination

No	Author and publication year	Material type & thickness	Root gap	Optimum response obtained
1	Gite & Pawar, (2016)	SS 304 ,3mm	0, 1.5 &2 mm	UTS and HV at root gap of 1.5mm
2	Wahule & Wasankar, (2018)	SS-304 and Fe-410, 6mm	0, 1 & 2 mm	UTS 2 mm & Max. %E 1mm
3	Bodkhe & Dolas, (2018).	SS 316L,5mm	1 & 2mm	Tensile Strength 1mm & distortion 2 mm
4	Kumar et al., (2017)	SS304,3mm	0.5 1 &1.5 mm	Optimal hardness and bend strength 0.5 mm root gap
5	Ahmad & Alam, (2018)	SS 0430,3mm	2, 2.5 & 3 mm	Bead Width, Depth of Penetration, Depth of HAZ &Width of HAZ 3mm

The root gap is mentioned from 5 distinct articles to pick the average gap, which ranges from 0 to 3 mm, as shown in table 3.6. Table 3.6 provides the frequencies and rankings of the gap range in order to select the gap between each level while taking other influencing elements into account.

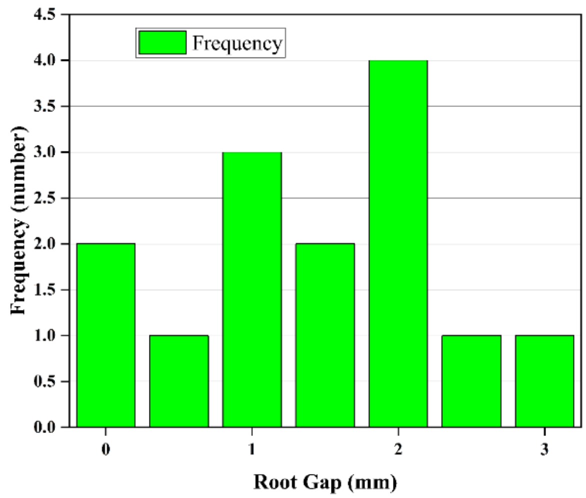

Figure 3.10. Designated root gap frequency rate

Table 3.5 and figure 3.10 contains the root gap values from the reviewed research study. The highest frequencies can be recognized at 2mm, whereas the second highest frequencies can be seen at 1mm. For this experiment, 1,1.5 and 2mm root gaps were used to test and optimize the optimal sound weld attributes.

3.5 Selection of welding process parameters

Welding procedural factors were those that influenced the welding process and the quality of the welds generated. There were three basic types of welding variables employed in this experiment. These factors were fixed or preselected, primary variable, and secondary configurable. The focus of the research is to look at how flat welding positions, especially butt joint and horizontal welding (PA) positions, are used to connect samples. This Position changes the welding position and rotation of workpieces and welders to make welding simpler, more efficient, and more rapidly performed welding speeds achieved. After gas purging and tack welding, TIG welding was employed to finish the initial joint arrangement. Depending on the welding conditions, the welding settings and circumstances were chosen.

Throughout the welding sample preparation and joint construction process, three process variables controlled the welding process and weld quality: fixed, primary, and secondary adjustable variables. The data was analyzed using the MINITAB18 software created by academics at Pennsylvania State University. Minitab and origin software executes computations and graph construction, freeing up users' time for analysis of data and comprehension.

Fixed or predetermined welding factors were those that were established prior the welding process actually started to performed the work. These included base metal type (SS 316), tungsten electrode type (WC20) and thickness, electrode size (2.4 mm diameter), filler metal type (ER308L), and current (DC) and polarity (DCEN), among other things. These factors cannot be modified after the welding process has begun.

Once the fixed variables were chosen, the key adjustable variables were the principal factors utilized to regulate the welding process. The key factors influence weld bead production by influencing bead width, bead height, penetration, arc stability, and so forth. The following welding factors were taken into account in this study: welding current, gas flow rate and root gap. These are simply adjustable and measurable, allowing them to be utilized to properly regulate the welding process. As a result, this study joins the sample by altering and adjusting the key changeable factors. These factors had a significant impact on the mechanical properties of the welded sample.

The minor adjustable factors utilized to manage the welding process were referred to as secondary adjustable variables. Typically, these characteristics were more difficult to quantify. Secondary adjustable factors explored in this work are the work angle and electrode travel angle. The electrode angles are referred to as the travel and work angles. The electrode's travel angle is the angle formed in the longitudinal plane by the joint and the electrode. The work angle is the angle formed between the electrode and the plane perpendicular to the travel direction. Variables associated with fixed welding conditions are shown in Table 3.7.

Table 3.7: Fixed welding circumstances variables (all examinations).

No	**Process Parameters**	**Details**
1	Electrode material	Lanthanide tungsten
2	Electrode diameter	2.4 mm
3	Electrode tip angle	45^0
4	Shielding gas	99.95% Ar
5	Back purging gas	99.95% Ar
6	Back purging gas flow rate	16 lit/min
7	Post flow shielding time	5 second
8	Filler metal diameter	1mm,1.6 mm & 2.6mm

Blue lanthanated tungsten is the most widely used and effective general-purpose electrode for DCEN and AC welding. It offers greatly improved arc starters, outstanding stability, and a broad amperage range. 2% lanthanated tungsten (colored blue) is at the top of the list. This is a real all-purpose electrode, with good arc starting properties and the capacity to carry large currents without spitting. It produces a steady arc at high and low current levels and works well on all metals.

The technique for selecting welding parameters summary, which was explored and created for the robust, new, and innovative welding engineering material joining, remains resilient throughout the experimental and optimization procedures used in the current study. The welding settings were chosen based on the most desirable conclusion from a previous investigation, the reputation of consistent mechanical qualities in many scholars' evaluated works, and the further enhancement of mechanical characteristics. Previous research discovered that welding parameters improved mechanical performance in the TIG welding process, which is consistent with the conclusions of many scholars' investigations. here were three variables in this study (welding current, gas flow rate, and root gap) with three levels for each according to table 3.8 selected TIG welding Parameters.

Table 3.8: displays the process parameters, as well as their levels

S/N	Process Parameters	Unit	Parameters designation	Level 1	Level 2	Level 3
1	Welding Current	Amps	WC	80	90	100
2	Gas Flow Rate	Lt/min	GFR	10	12	14
3	Root Gap	mm	RG	1	1.5	2

3.6 Multi objective Response Optimization

For novel initiatives, the welding engineer chooses welding settings considering existing experience or tests conducted experimentally. This procedure takes more time and money. There are other approaches for calculating process variables, however the methods presented here are suitable for optimizing TIG melting on SS 316 materials. These approaches are often used by researchers to optimize welding settings. This overview covers optimization methodologies in overall, with a concentration on engineering optimization applications. The goal of optimization methods is to identify variable values that optimize a multivariate objective function under a set of restrictions. Constraints define a search space, commonly referred to as a viable area, that must include the suitable response.

Table 3.9: Optimization technique paper review to determine optimum approach

No	Author and publication year	Input parameters	Material	Optimizing method	Output parameters
1	Wahule & Wasankar, 2018)	Current, Root gap and Gas Flow Rate	Fe-410 and SS 304	GRA	%E and UTS
2	Martins & Friday, (2022).	Current, Voltage, Gas flow rate	SS 304L	Taguchi	UTS
3	Saha et al., 2017)	Travel speed, Welding Current & Gas flow rate	M1020 carbon steel bar	Taguchi – GRA	HAZ width, BW, penetration Reinforcement
4	Bachani & Ghetiya, (2018).	Current, travel speed & flux	SS304L	GRA	Distortion, Penetration and Width
5	Bodkhe & Dolas, (2018)	Electrode gap, Travel speed	SS 304L	RSM	Depth of penetration
6	Avinash et al., (2019).	Welding Current, Travel speed & Flux type	SS 304	GRA	Tensile test, Hv & %Elongation
7	Rizvi & Tewari, (2018)	Wire feed rate, Arc voltage & Gas flow rate	SS 304	Taguchi GRA	UTS, Impact strength & Micro hardness
8	Singh et al., (2017).	Welding Current, Gas flow rate, Travel speed, gas flow rate	SS 304	Taguchi Method	weld width and weld penetration
9	Sutar & Jadhav, (2021).	welding current, gas flow rate and root gap	SS 304L	Taguchi Method	tensile strength, hardness and depth of penetration

10	Kumar et al., (2017)	Welding Current, Voltage, Root Gap & Gas flow rate,	SS 304	Taguchi Method & RSM	Hardness BHN Bending Strength
11	Lugade & Deshmukh, (2015)	Electrode gap, Travel speed, Welding Current, & Gas flow rate	304L	Taguchi Method	Tensile strength
12	Rizvi & Tewari, (2018).	Wire feed rate, Arc voltage & Gas flow rate	SS 304	Taguchi – GRA	UTS, Impact strength & Micro hardness
13	Gohel et al., (2016).	Gas flow rate, voltage, & current	SS304	Taguchi Method	Tensile test Hardness test
14	Ahmad & Alam, (2018)	Arc length, WeldingCurrent & Travel speed	304L	TaguchiMethod	BW, DP, Depthof HAZ, Width of HAZ
15	Vijayan & Rao, (2018)	Welding Current, Voltage, Welding Speed Gas flow rate,	AISI 4340	RSM & Genetic algorithm	Ultimate tensile strength
16	Saha et al., (2017)	Welding Current, Travel speed, & Gas flow rate	M1020 carbon steel bar	Taguchi – GRA	HAZ width, BW, Penetration Reinforcement

Based on the review summary of table 3.9, Six of the articles in the reviewed articles utilized the Taguchi method to optimally optimize their variables, four utilized a hybrid of Taguchi and GRA, three applied GRA, and one adopted Taguchi ANOVA, RSM, GA and RSM, Taguchi Method & RSM.

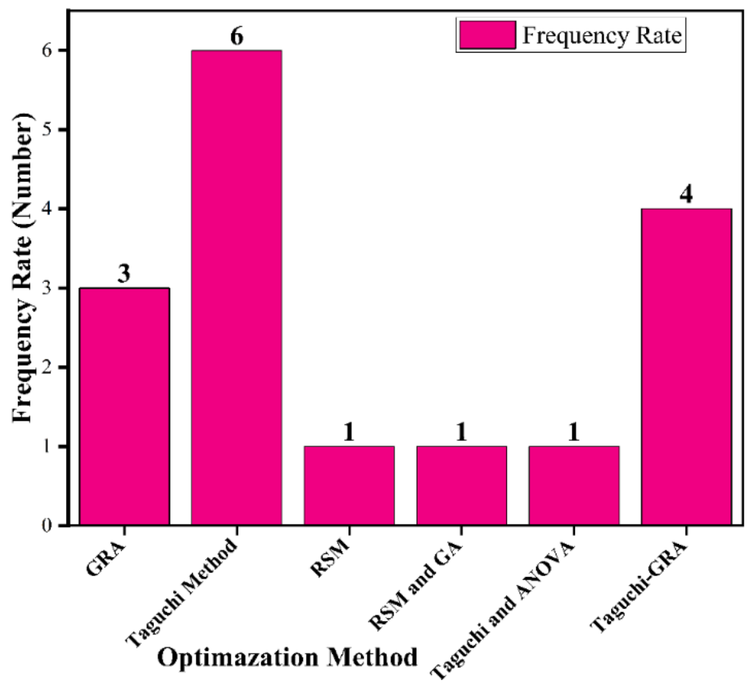

Figure 3.11. Designated optimization technique frequency rate

Figure 3.11 depicts the defined optimization technique frequency rate used to determine what scholars have done before and obtain consistent results that are feasible for the current research work inquiry to construct the optimization method methodology.

The Taguchi analysis assesses the influence of factors on a single performance index, whereas the grey relational based Taguchi analysis evaluates the influence of factors on a set of performance index parameters. Taguchi design of experiment is an effective approach for modelling and analyzing the impact of control elements on performance output. The decision-making process of control variables is the most crucial stage in this strategy. Taguchi resilient design was used to create the experimental approach, which was built on an orthogonal array with nine experiments (L9 orthogonal array). As a result, integrating Taguchi with grey relational analysis allows for simple and successful optimization depending on several aspects. The GRA technique based on Taguchi is a robust strategy for optimizing the specified welding parameters. The multi response optimization of TIG welding of SS 316 pipe base metal of ϕ40 X 2000 X 2mm was carried out in accordance with the approach illustrated in Figure 3.12.

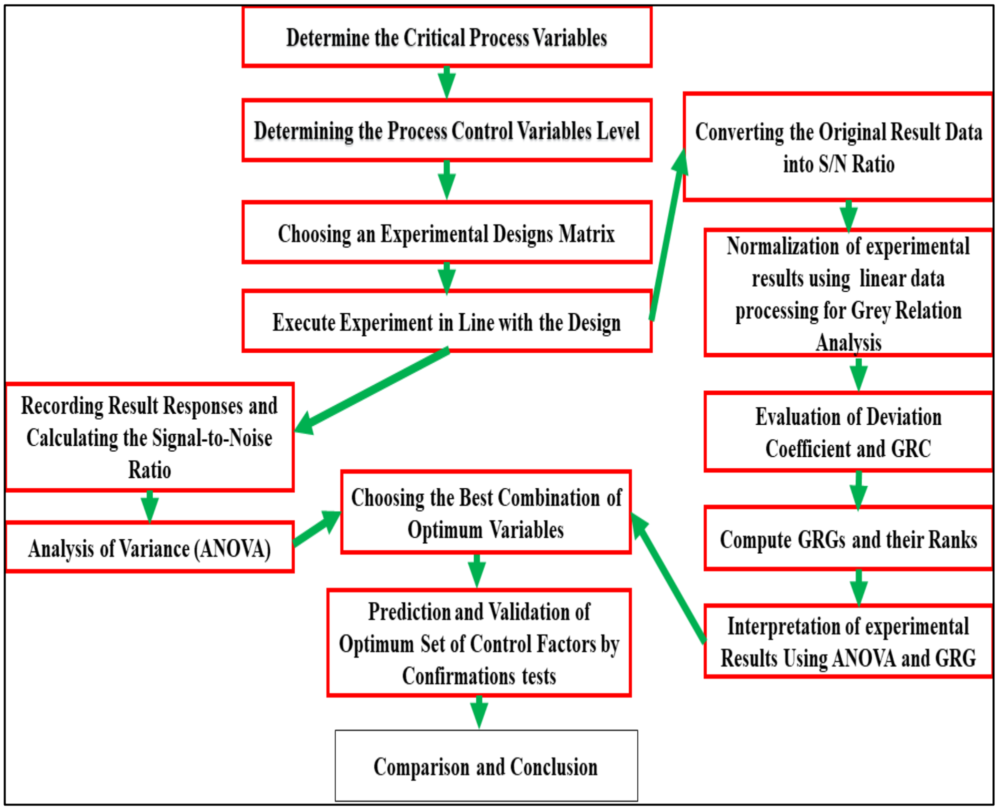

Figure 3.12. Taguchi based grey relation analysis flow diagram

3.6.1 Design of experiment using Taguchi method

To find the most suitable combination, the Taguchi method employs a fractional factorial Design of Experiment (DOE) technique and an orthogonal array library. It examines sample quality parameters and using ANOVA to discover process limits and optimal restrictions. This approach, low-cost approach compares outcomes with the least variation. This approach is simple to construct, utilize, and is affordable [Rajesh & Sumathi, (2020)].

The design of experiments (DOE) method is an experimental method for determining the influence of process variables on performance parameters. To maximize resource utilization, it entails organizing experiments, collecting data, and analyzing outcomes [Qazi et al., (2021)]. A fractional factorial matrix used for balanced comparisons is an orthogonal array (OA) [Haq et al., (2008)]. The Taguchi technique is an effective way for creating high-quality wending stainless steel pipe welding systems using L9 orthogonal array. This concept reduces iterations and gets the greatest outcomes in the shortest amount of time.

This thesis use optimization approaches such as the Taguchi methodology and grey relation analysis to examine articles using MINITAB analysis software. It specializes in welding 316 grade stainless steel with a focus on high-quality welds. The experiment includes three variables: welding process variables, conditions, and speed.

Degree of Freedom (DoF) is defined as the number of comparisons made between process parameters that are made to determine a better level. That is used to compute the minimum number of experiments that will be conducted to investigate the observed factors. The DoF value is given by equation below, and Table 3.10 shows the overall DoF of experimental factors in this investigation.

Degree of Freedom = number of levels - 1

Table 3.10: DoF of Experimental factors

Experimental Process Parameters	**DoF (Level – 1)**	**Sub Total**
WC	3	2
GRF	3	2
RG	3	2
Total		**6**

Table 3.8 shows an L9(3^3) OA, where, L3 is the maximum number of rows (experiments), 3 is the number of levels, and 3 is the number of columns (factors). Signal to noise (S/N) is a quality in the communication and engineering field, where is the ratio between the power of the signal (μ^2) and the power of the noise (σ^2) which expresses in decibels (dB) [Haq et al., (2008)]. S/N ratio has been used as the quality characteristic, which is available depending on the type of character such as smaller the better, larger the better, or nominal is the best.

Table 3.11: Types of problems and respective signal-to-ratio function

S/N function	S/N formula	Usage when the goal
Larger the better	$S/N = -10\log\left[\frac{1}{n}\sum_{i=1}^{n}\frac{1}{y_i^2}\right]$ Y = the observed data N = the number of observations	Maximize the response: for instance, in this study, maximizing the response of ➢ micro hardness, and ➢ Compressive, hardness, ultimate tensile and bending strength

The larger-the-better optimization strategy is employed in this research to obtain greater ultimate tensile strength, hardness values, and bending strength. A higher S/N Ratio refers to better quality regardless of the category of the quality parameter. Qualitative attribute. As a result, the best process parameter values were those with the highest S/N ratios [Saha, 2020].

3.6.2 Grey Relational Analysis

This study attempts to determine and optimize mechanical parameters with the following four goals in mind: to maximize the micro-Vickers hardness, compressive strength, bending strength and ultimate tensile strength of a new stainless-steel grade 316 material pipe welding through TIG. As a result, it's an instance of multi-response optimization, as opposed to single-performance characteristic optimization [Prakash et al., (2021)]. When one performance feature has a greater S/N ratio, another could have a lower S/N ratio. As a result, for the optimization of numerous performance aspects, an overall evaluation of the S/N ratio is necessary.

Grey Relational Analysis (GRA) is an efficient tool for such multi-response analysis. GRA is a measurement of the absolute value of the data difference between sequences, and it could be used to measure the approximate correlation between sequences. The GRA is a method of determining the absolute value of a data difference between two sequences, as well as an estimated correlation between them. It's a good way to look at the relationship between sequences with a small amount of data and it can look at a lot of different things.

Taguchi-based Grey relational analysis (TGRA) is familiar for treating problems having inter-functional relationships among multiple input parameters and response variables. The present investigation, which is further optimized using GRA, considers many input factors, including current, gas flow, and root gap, over nine separate sets of tests.

The responses considered during this study are bending strength, tensile strength, hardness, and compressive strength. These physic mechanical property performances were transformed into a single common dataset by estimating Grey Relational Grade (GRG). The highest value of GRG is assumed to be the most influential combination and is assigned with rank accordingly. GRG was estimated for all sets of data values and it is used to identify the most significant levels of input parameters at which improved results are obtained. The GRG is an average sum of the grey relational coefficient. The following diagram shows the major steps of GRA. Details of the GRA have been discussed in the result and discussion section by applying the response during optimization.

The experimental data, i.e., the measured aspects of quality attributes, are first normalized ranging from 0 to 1 in Grey relational analysis. The grey relational coefficient, based on normalized experimental data, is then produced to indicate the correlation between the desired and actual experimental data. The grey relational grade is then calculated by averaging the Grey relational coefficients for the selected replies.

The multiple answer procedure is evaluated overall using a grey relational grade. As a result, optimization of the intricate numerous process responses may be turned into optimization of a single grey relational grade using this technique. The optimal parametric combination with the greatest Grey relational grade is next assessed [Shaikh & Rao, (2015)]. The following stages are provided by GRA to analyze the system or process [Rudrapati et al., (2016)].

The Taguchi experimental design optimizes parameters using a L9 orthogonal array with 9 experiments, assuring trustworthy findings, considerable savings in experimental labor, and straightforward analysis. It takes into account the factors, levels, and constraints faced throughout the experiment. Table 3.12 describes the experimental combinations in full, including orthogonal array matrices designed with the MINITAB 23 software, as well as how the experiment was carried out using the specified variables. The Taguchi technique is a prominent quality optimization strategy that seeks to eliminate variance and flaws in a product or process. It is founded on the notion of resilient design, which involves creating a product or process that can operate effectively in a variety of environments while minimizing the influence of external factors.

Table 3.12: list of experiments

No	Welding Current	Gas Flow	Root Gap
1	80	10	1
2	80	12	1.5
3	80	14	2
4	90	10	1.5
5	90	12	2
6	90	14	1
7	100	10	2
8	100	12	1
9	100	14	1.5

The entire investigation was carried out in accordance with the specifications and mechanical parameters such as tensile strength, weld hardness, and bending strength were tested by obtaining a sample from the weld products. An orthogonal array is a set of variables (input parameters) over the parameters of the output that provides the best configuration of process control variables.

CHAPTER FOUR
RESULTS AND DISCUSSION

4.1 Experimental Works

All pipe was cleaned with a polisher disc before to welding to remove any pollutants such as rust, dust, or oil, and the edge was prepared according to the design using a stainless-steel grinding disc. The welding experiment was carried out with the orthogonal array shown in Table 3.12. Figure 4.1 shown Welding experimentation of welded specimen according DOE of orthogonal array experiment list.

Figure 4.1. Welding experimentation of welded specimen

4.2 Visual inspection of TIG-welded samples

Based on EN 970 standard visual inspection, the weld surface is observed with the naked eye throughout to detect surface flaws of the weldment. Table 4.1 shows the visual inspection findings; specimens 4 through 9 exhibit no defects. Other welding flaws observed included no spatter due to TIG welding's spatter-free nature, an uneven weld bead, and excessive deposition. The aforementioned welding defects have the following causes: An uneven welding bead seen after visual examination in sample 2 might be caused by a poorly held electrode/filler rod and a faster arc transit speed, During visual inspection, the overwhelming deposition seen in samples 1 and 3 might be produced by additional weld metal on the back side of the joint, excessive filler metal addition, and low arc travel speed, all due to a very narrow root gap.

In general, the impact of welding specimen of weld root observed deep penetration observed due to this reason significantly enhanced sound penetration during this assessment, thereby improving the mechanical properties of the weld joint.

Table 4.1: Detected visual examination of weld samples

No	Welding Current	Gas Flow	Root Gap	Result of Visual Inspection
1	80	10	1	Incessant deposition with no spatter
2	80	12	1.5	Uneven bead and no spatter
3	80	14	2	Overwhelming deposition with no spatter
4	90	10	1.5	No defects
5	90	12	2	No Spatter and uneven weld bead
6	90	14	1	No defects
7	100	10	2	No Spatter and uneven weld bead
8	100	12	1	No defects
9	100	14	1.5	no flaws or spattering

4.3 Validation of the SS 316 Base Metal Composition

Spectroscopy is a fundamental analytical tool in chemistry for detecting, determining, or quantifying a specimen's molecular and structural composition. It examines how light of a given wavelength interactions in a specimen, thereby enabling for the precise determination of elements in materials with undetermined chemical composition or position.

Figure 4.2. Composition analysis of SS 316 through spectroscopy

The AISI 316 stainless steel composition was validated by burning it in an argon atmosphere to determine the major element of the welded work piece in the spectroscopic testing equipment for verification of the ingredient in the welded base material. The composition of the selected base metal AISI 316, as shown in Figure 4.3, agrees with the laboratory composition analysis of the spectroscopic examination result.

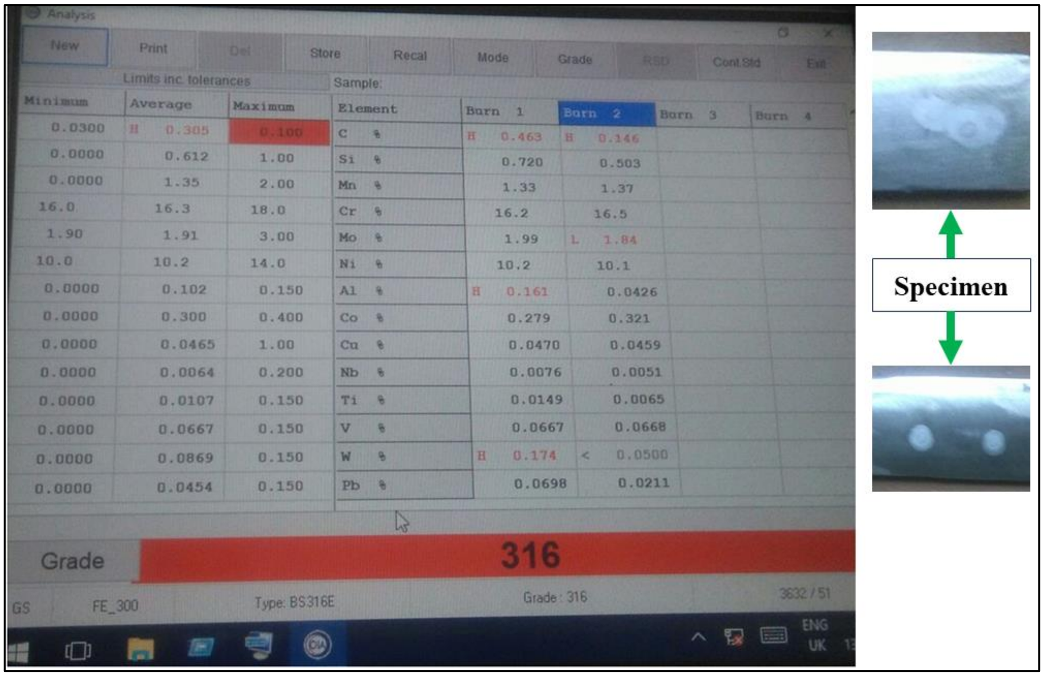

Figure 4.3. Result of the chemical composition of weld base metal of AISI 316 stainless steel

4.4 Micro hardness Analysis

The term "hardness" is used within a variety of sectors, including the metals sector, metallurgist, lubrication engineer, design, mineralogist, and machining method. Durability to deformations, penetration of the body, wear, stress from flow, scratching, and machining are numerous instances of it (Parthasarathy1, Ganesh, & Chellamuthu, 2018). Brinell, Rockwell, and Vickers scales are typically used in welding examinations for hardness assessment, with direct reading equipment used for differential depth determination measurement (Committee, 2000). Rockwell Hardness is a widely employed and independent determination of hardness technique that measures the permanent depth of impression generated by a force/load on an indenter [Saha, (2020)]. It employs steel ball and diamond cone indenters, with the B scale employing hardened steel balls with a main load of 90kg. Hardened steel ball indenters with 1/16 diameters are used to test softer materials such as completely annealed steels, cast irons, and nonferrous metals.

A ball indenter is used to provide a preliminary test force to a sample, lowering surface polish. To achieve the complete test load, a substantial load is applied, and the ultimate position is measured. The difference in distance between before and after the load is turned into a hardness number. The specimen is prepared with a 25mm width and polished using 400,800, and 1200 grade sandpaper to eliminate impurities. Figure 4.4 displays a Hardness specimen for testing in accordance with the ASTM E8-04 standard manufactured samples. Table 4.2 displays the experimental weld bead Rockwell hardness result value.

Figure 4.4. Hardness specimen for testing prepared before testing and after testing

Table 4.2: The experimental Rockwell hardness value

S. N	Weld Bead Hardness Type "B" in HRB value			Average Hardness in HRB value
	trial-1	trial-2	trial-3	
1	99.6	98.5	98.8	**98.9**
2	99.5	100.6	99.3	**99.8**
3	100.3	99.5	100.2	**100**
4	101.3	103.6	101.4	**102.1**
5	103	102.5	102	**102.5**
6	101.2	99.8	118.6	**106.5**
7	103.2	112.7	120.3	**112.1**
8	113.8	120	109.2	**114.3**
9	115.8	107	127.9	**116.9**

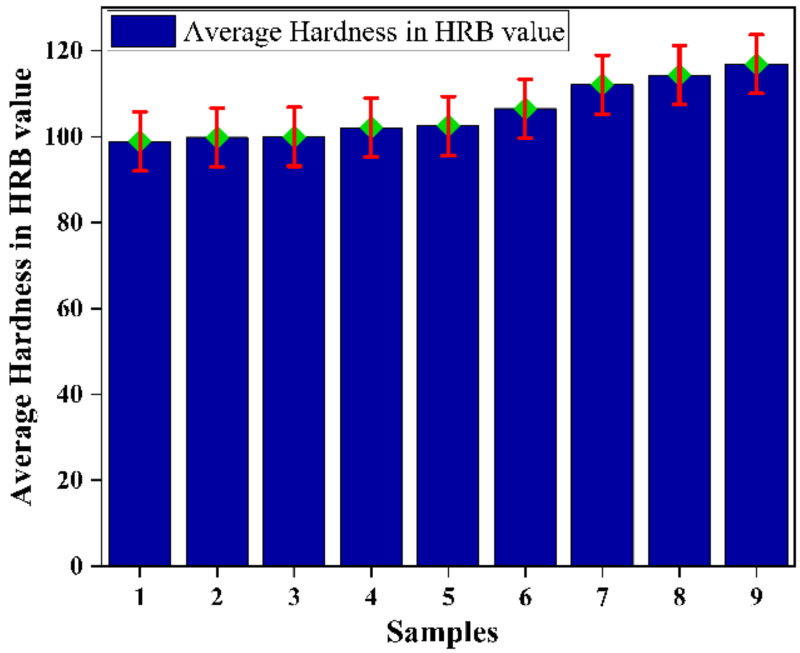

Figure 4.5. Graph hardness specimen for testing

The hardness test was repeated three times on each experiment's weld bead. The greatest hardness value was 116.9 HRB with a 100A welding current, 14 lit/min flow of gas rate, and 1.5mm root spacing. Similarly, the lowest hardness value for 80A welding current, 10 lit/min gas flow rate, and 1mm root spacing was 98.9HRB. HRB Indenter US 100kgf hardness test result based on ASTM Rockwell testing experiment. Maximum hardness is recorded in the graph of figure 4.5 with greater gas flow rate and higher welding current. Because the quantity of heat generated during welding affects the hardness value of the weld bead. This experimental investigation coincided and agreed with the findings of previously published studies [Bhavsar and Patel, (2016); Sing et al., (2016); Chaudhari et al., (2019), Linger & Bogale, (2023)]. As a result, the micro hardness at 100A welding current achieved 116.9 HRB, an improvement of 1.48% over the Rockwell hardness type "B" of ASTM data for AISI 316.

4.5 Tensile Strength

Tensile tests are critical for assessing the behavior and design parameters of engineered materials. They quantify Young's stress and offer data concerning strength and ductility under uniaxial loads, which aids in material examinations, alloy growth and development, control of quality, and design [Joseph et al., (2016)]. Tensile samples were manufactured utilizing an

ASTM-compliant band saw and grinder. The geometric design for ASTM E8-04 standards is shown in Figure 4.6.

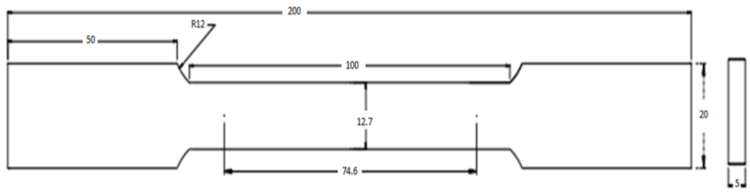

Figure 4.6. Drawing of tensile test sample manufactured in compliance with ASTM-E8-04

Figure 4.6 depicts a tensile examination sample with larger grasping ends. Deformation and failures need a smaller section with a small cross-sectional region.

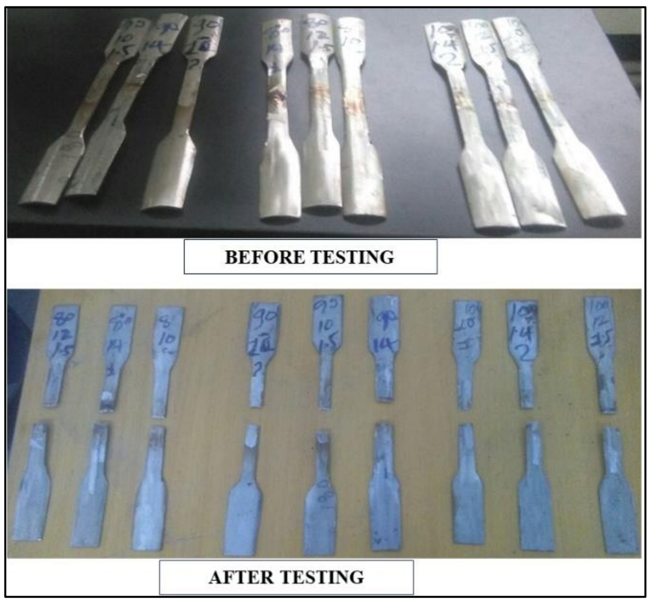

Figure 4.7. Tensile examination samples prepared before testing and after testing

Tensile testing involves inserting a sample into a machine and applying tension to it. As the gauge length rises, so does the force. As shown in figure 4.7, two specimens were fabricated transverse to the weld bead, and the tests were performed twice. As shown in table 4.3, the average result is attained.

Table 4.3: Tensile examination outcomes

S. N	Trial -1	Initial dimensions			Fm	UTS	Trial-2	Initial dimensions			Fm	UTS	Average UTS
		W	T	L	KN	MPa		W	T	L	KN	MPa	MPa
1	1	12	5	200	44.6	**742.8**	1	12	5	200	46.9	**733.8**	**738.3**
2	2	12	5	200	39.2	**746.4**	2	12	5	200	47.1	**745.1**	**745.8**
3	3	12	5	200	48.2	**769.8**	3	12	5	200	43.2	**785.4**	**777.6**
4	4	12	5	200	54.7	**810**	4	12	5	200	50.8	**789**	**799.5**
5	5	12	5	200	55.1	**815**	5	12	5	200	39.8	**796.8**	**805.9**
6	6	12	5	200	50.3	**811.2**	6	12	5	200	51.2	**802.8**	**807**
7	7	12	5	200	52.3	**836.4**	7	12	5	200	50.4	**806.4**	**821.4**
8	8	12	5	200	47.6	**828.6**	8	12	5	200	48.8	**813**	**820.8**
9	9	12	5	200	47.7	**885**	9	12	5	200	53.2	**850.8**	**867.9**

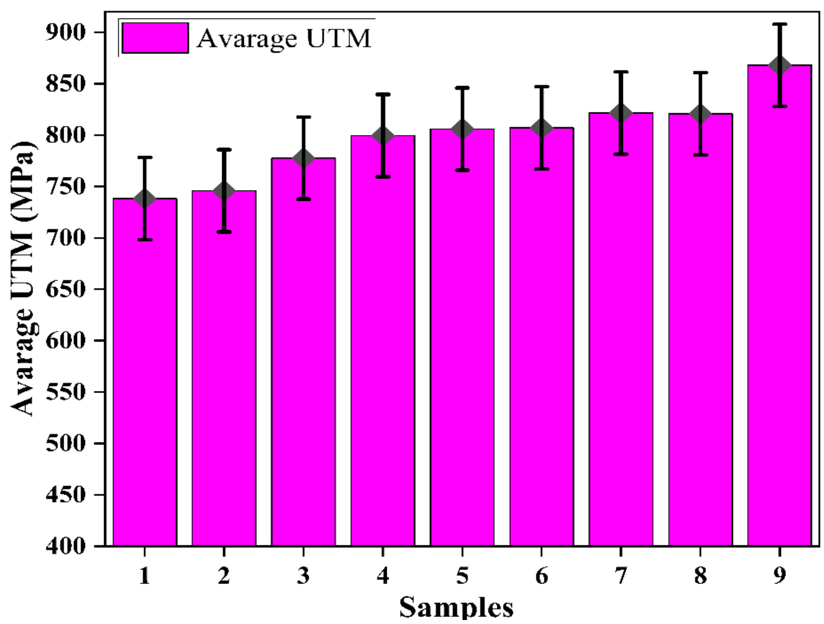

Figure 4.8. Graph Average Tensile Strength specimen for testing

A single experiment yielded two tensile inspection specimens, as shown in figure 4.8, with average results. The ultimate strength of a material is the maximum stress that it can withstand when subjected to pulling or stretching before fracture or breakdown. The experiment was carried out at room temperature. After 9 experiments with an ultimate welding current of 100

A, a gas flow rate of 14lit/min, and a root spacing of 1.5mm, the maximum attainable tensile strength was 885 MPa.

Conversely, the lowest tensile strength measured at 742.8MPa was reached in first attempt experiments with a lowest welding current of 80A, a highest gas flow rate of 10lit/min, and a root gap of 1mm. The outcomes reveal that when welding current and gas flow rate rise, so does the tensile strength. The tensile strength of a material is determined by its chemical composition, structure, and manufacturing background. This study of experimentation coincided with the conclusions of earlier scholars [Ghosh et al., (2016); Moi et al., (2018); Lugde and Deshmukh, (2015); Anand et al., (2017); Muluken, (2020); Linger & Bogale, (2023)]. Furthermore, the highest ultimate tensile strength was obtained for the sample that was welded with the highest current. Throughout the electrical current range used in this study, tensile strength is linked to welding current. As a result, with greater current, desirable optimum ultimate tensile strength was obtained [Ramakrishnan et al., (2021)]. As a consequence, the tensile strength was 885MPa at 100A welding current and 14lit/min shielding gas flow rate, an enhancement of 1.72% higher than the tensile strength of ASTM data for AISI 316.

4.5.1 Bending Strength

Bend testing determines the ductility and strength of a material by bending it over a radius. It assesses weld plastic deformation as well as flaws such as sidewall fusion, root fusion, and joint penetration. Bend testing is an important method for evaluating the modulus of elasticity and bending strength of a material. Two face bend samples have been bent 180° in welding investigations using a 20 mm (4T) mandrel diameter ASME section IX mandrel [Joseph et al., (2016)] as shown in figure 4.10. The samples are gently and gradually bent from the center in a circle of a given radius as shown in figure 4.9. Due to strain during bending, certain samples develop exterior surface cracks, rendering them undesirable for use in technical applications. High bend strength is permitted if there are no apparent cracks on the exterior surface [Kumar et al., (2017)].

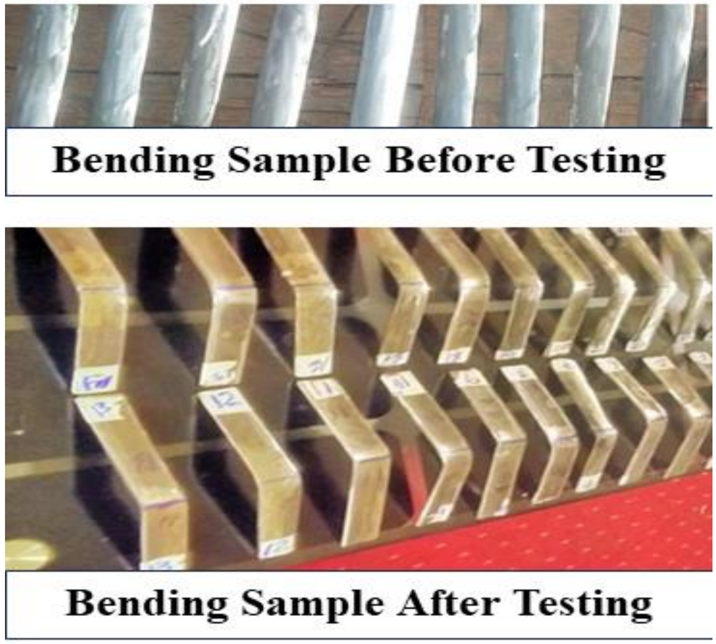

Figure 4.9. Bending examination samples prepared before testing and after testing

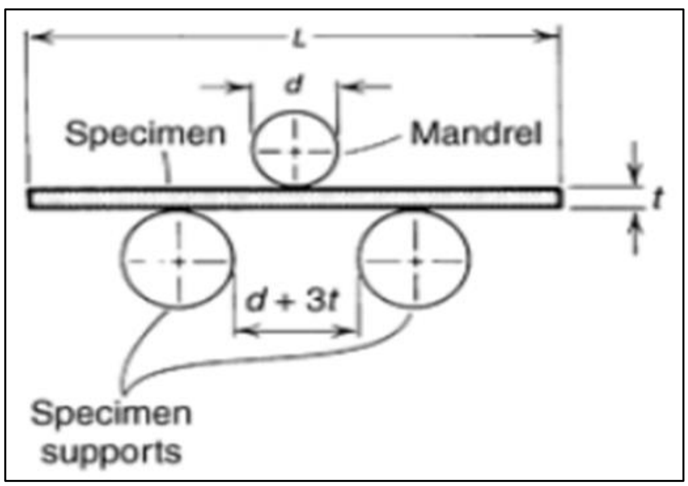

Figure 4.10. Mandrel diameter vs length of span

Table 4.4: Bending examination outcomes

Trial 1	W (mm)	T (mm)	L (mm)	F (KN)	BS (MPa)	Trial 2	W (mm)	T (mm)	L (mm)	F (KN)	BS (MPa)	Average Bending Strength (MPa)
1	19.4	4.4	53.9	4.19	**889**	1	21.4	4.5	53.9	4.72	**889.79**	**889.5**
2	20.4	4.6	53.9	4.7	**891.8**	2	21.2	4.4	53.9	4.5	**897.78**	**894.79**
3	20.5	4.5	53.9	4.68	**901.85**	3	21.7	4.5	53.9	4.94	**904.9**	**903.5**
4	20.2	4.4	53.9	4.39	**912.65**	4	19.4	4.3	53.9	4.24	**912.4**	**912.52**
5	19.4	4.7	53.9	4.24	**912.4**	5	18.4	4.4	53.9	3.98	**913.28**	**912.84**
6	18.4	4.4	53.9	3.99	**914.78**	6	18.4	4.5	53.9	3.98	**914.28**	**914.53**
7	19.5	4.3	53.9	4.14	**934**	7	20.2	4.4	53.9	4.33	**932.84**	**933.42**
8	20.3	4.3	53.9	4.33	**936.7**	8	21.2	4.4	53.9	4.56	**961.25**	**948.98**
9	21.6	4.5	53.9	4.71	**969.99**	9	19.7	4.5	53.9	4.54	**1000.76**	**985.5**

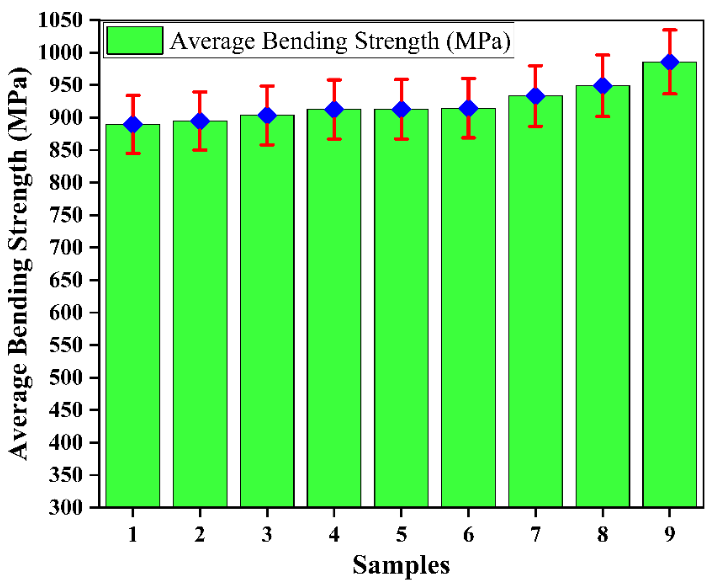

Figure 4.11. Graph Average bending strength specimen for testing

Bending strength is the ability of a material to withstand bending under force. It is critical in the design of structures and components because as deformation rises, the material's crystalline structure strengthens and slippage decreases, resulting in increased bending strength. Bend testing determines a material's ductility and strength by bending it around a circle of radius as shown in figure 4.9. Two examination specimens were prepared from each experiment workpiece item and the result outcome reaction was averaged as shown table 4.4. and figure 4.11.

The highest achievable bending strength reached 1000.76MPa ninth experiments parameters with a maximum welding current of 100A, a gas flow rate of 14lit/min, and a root gap of 1.5 mm. Similarly, a minimal bending strength measured to be 889MPa was observed using the first trial settings parameters of 80A welding current, 10 lit/min gas flow rate, and 1mm root gap. This experimental inquiry aligned with the findings of prior scholar investigations [Kumar et al., (2017); Singh & Mittal,2017); Linger & Bogale, (2023)]. As a result, the bending strength was 1000.76MPa at 100A welding current and 14 lit/min shielding gas flow rate, an improvement of 1.6% greater than the ASTM values for AISI 316.

4.5.2 Compressive Strength Analysis

The compressive strength of the specimens under investigation was evaluated using a universal testing machine (UTM) model Bairo electro computer-controlled -hydraulic universal testing machine type HUT-600 from Beijing United Tester Co., LTD, Beijing, China with a load capacity of 600KN was applied to the specimen. Due to the considerably elevated hardness of the weld joint, all samples were squeezed uniformly with 100KN to obtain the desired result and optimal parameter assessment.

Table 4.5: Compressive strength of examination outcomes

S. N	**Trial -1**	**Compressive Strength** MPa	**Trial-2**	**Compressive Strength** MPa	**Average Compressive Strength** MPa
1	1	371.4	1	440.8	443
2	2	447.8	2	447.7	447.5
3	3	461.9	3	471.4	466.6
4	4	486	4	473.4	479.7
5	5	489	5	478.8	483.5
6	6	486.7	6	487.7	484.2
7	7	501.8	7	483.8	492.8
8	8	497.6	8	487.8	492.5
9	9	531	9	510.9	520.7

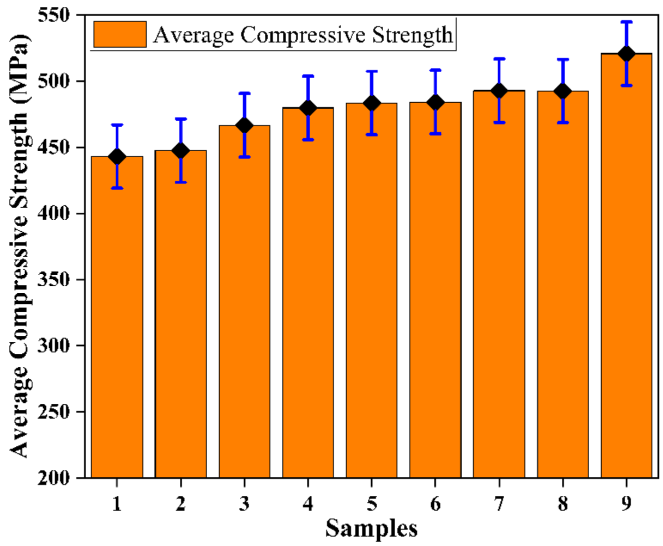

Figure 4.12. Graph Average compressive strength specimen for testing

Two examination specimens were prepared from each experiment workpiece item and the result outcome reaction was averaged as shown Table 4.5 and Figure 4.12. The highest achievable bending strength reached 531MPa nineth experiments parameters with a maximum welding current of 100A, a gas flow rate of 14lit/min, and a root gap of 1.5 mm. Similarly, a minimal bending strength measured to be 371.4MPa was observed using the first trial settings parameters of 80A welding current, 10 lit/min gas flow rate, and 1mm root gap.

As a consequence, the compressive strength at 100A welding current reached 531MPa, an improvement with 1.77% when compared to the maximum compressive strength of ASTM of AISI 316 data.

4.6 Taguchi-based Grey Relational Analysis (TGRA)

Grey Relational Analysis (GRA) is used in this work to measure the S/N ratio of attributes of performance and examine links across sequences with minimal data. The Taguchi-based GRA deals with problems that include multiple input variables and response factors. A single dataset contains nine sets of testing, including hardness, compressive strength, bending strength, and ultimate tensile strength. An arrangement with the greatest GRG value is regarded as powerful. For better results, GRG is calculated for every collection of data. The TGRA was applied to coincide the principles of the multi-response optimized performance technique [Ashebir et al., (2022)].

4.5.1. Comparison of Experimental Results

Throughout multi-response optimization process, Taguchi-based Grey Relational Analysis (TGRA) has utilized for discover known as most effective combinations occurring into process variables [Kasman, (2013), Jayaraman, (2014), Joshi et al., (2019)]. Taguchi was utilized for the design of the experiment and execution, whereas GRA was performed to analyses matrix outcomes of the experiment [Jayaraman , (2014)]. The Taguchi technique was used to collect information on responses for each and every one of the SS 316 material welded by TIG welding examined with the approach developed by Taguchi. Table 4.6 displays the results of observed responses statistics with larger better-quality characteristics, which include Ultimate tensile strength, bending strength, compressive strength and Rockwell hardness respectively, where the desirable quality features must be increased in order to improve advancement and the S/N must increase in order to improve performance. This strategy was utilized to enhance the design of the product, the method of production process and the mechanism/system effectiveness performances.

Table 4.6: Data from Measured Experimental Results Larger is the higher-quality distinguishing characteristic

S.	Microhardness (RH) (HRB)			Ultimate Tensile Strength (UTS) (MPa)		Compressive Strength (CS) (MPa)		Bending Strength (BS) (MPa)	
N	**H-1**	**H-2**	**H-3**	**UTS-1**	**UTS-2**	**CS-1**	**CS-2**	**BS-1**	**BS-2**
1	99.6	98.5	98.8	742.8	733.8	371.4	440.8	889	889.8
2	99.5	100.6	99.3	746.4	745.1	447.8	447.7	891.8	897.8
3	100.3	99.5	100.2	769.8	785.4	461.9	471.4	901.85	904.9
4	101.3	103.6	101.4	810	789	486	473.4	912.65	912.4
5	103	102.5	102	815	796.8	489	478.8	912.4	913.3
6	101.2	99.8	118.6	811.2	802.8	486.7	487.7	914.78	914.3
7	103.2	112.7	120.3	836.4	806.4	501.8	483.8	934	932.8
8	113.8	120	109.2	828.6	813	497.6	487.8	936.7	961.3
9	115.8	107	127.9	885	850.8	531	510.9	969.99	1001

Whereas, Microhardness: H-1, H-2, H-3; Ultimate Tensile Strength: UTS -1, UTS -2; Compressive Strength: CS-1, CS-2; Bending Strength: BS-1, BS-2

4.6.1 Analysis based on the Taguchi technique

The Taguchi methodology was considered to be one of the absolute most potent and efficient methods for generating high-quality AISI 316 materials welded by TIG welding methods employing L9 OAs [Ghumman et al., (2022)]. L9 (or 3^3) orthogonal arrays confirm that there currently are three variables which include welding current, shielding gas flow rate, and root gap, in addition to there are three levels for each of the three components, which produces 9 trials (table 3.12). Taguchi's method of experimentation concentrates on reducing the total amount of repetitions. It also provides for the best outcomes in the shortest amount of period. This sophisticated tool analyses were carried out utilizing the Minitab Statistical Software (version 2023) to replicate trials of experimentation.

The Degree of Freedom (DoF) determines the minimum number of contrasts between parameters associated with the process by measuring the total number of experimentations required to study the variables that were observed. The study computes signal-to-noise ratios for RH, UTS, CS, and BS, which is used to determine improved welding performance. For calculating the S/N ratio, utilize Equation (4.1). TIG welding process factor and mechanical Properties bending strength, Hardness, Compressive strength, and Ultimate tensile strength relationship are evaluated. NOISE symbolizes detrimental scores, whereas SIGNAL represents favorable ones.

4.6.2 Multi-Response Optimized Performance within GRA

Taguchi's method is used to determine the best process parameter configurations for a particular answer characteristic. For several replies with varying quality aspects, multi-response optimization using GRA is recommended [Achuthamenon et al., (2018)]. GRG combines many goals into a single goal [Jayaraman, (2014)]. The study sought to identify the optimal process parameter combination for reducing wear rate, porosity, and increasing Rockwell microhardness type "C" and compressive strength experimental result obtained. This approach generates a GRG for analyzing the association degree of numerous replies [Jailan et al., (2009)]. In this study, multiple performance criteria are combined into a single grey relationship grade [Haq et al., 2008]. The following stages are investigated for GRA.

Stage 1: The conversion of results from experiments into S/N ratios (η) using quality characteristics formulae, with bigger ratios indicating higher quality. For this inquiry, reproduce compression strength, ultimate tensile strength, and bending strength twice, and Rockwell hardness type "B" tests three times.

$$\frac{S}{N}(\eta) = -10Log\left[\frac{1}{z}\sum_{i=1}^{z}\frac{1}{Yi^2}\right] \qquad (4.1)$$

whereas z is the number of replication test was performed and Yi had a response that was values that were measured.

Table 4.7: The ratio S/N (η) for the determined values

Larger is better

S. N	Ratio of S/N of (H)	Ratio of S/N of (UTS)	Ratio of S/N of (CS)	Ratio of S/N of (BS)
1	39.91	57.36	50.08	58.98
2	39.98	57.45	51.26	59.03
3	39.99	57.81	51.59	59.12
4	40.18	58.05	51.89	59.2
5	40.21	58.12	51.96	59.21
6	40.47	58.13	51.99	59.22
7	40.94	58.27	52.14	59.4
8	41.14	58.28	52.12	59.54
9	41.29	58.76	52.63	59.87

Stage 2: Using equations (4.1) and (4.2), normalize ij as Zij (0 Zij 1) to decrease variation and prevent using different units. Taguchi's technique generates normalized S/N ratios between 0 and 1 using a grey relational generating mechanism [Jailani et al., (2009); Meignanamoorthy et al., (2022)]. Greater values maximize compression strength, ultimate tensile strength, and bending strength of normalization of the S/N ratio, with larger being preferable. Normalization of the S/N ratio is accomplished using equation (4.2), with bigger being better.

$$Zij = \frac{nij - \mathrm{Min}(nij)}{Max(nij) - \mathrm{Min}(nij)} \qquad (4.2)$$

where Zij is the normalized value for the i^{th} experiment for the j^{th} dependent factor/response, ηij is the S/N ratio to be normalized, and max (ηij) and min(ηij) are the maximum and minimum values of ηij, correspondingly. Based on [Julong, (1989)], larger normalized results equate to higher achievement, and the optimal normalized outcome should equal one. The GRC is then calculated to indicate the relationship between ideal (best) and actual examination outcomes. Table 6 figured out normalized S/N ratios of determined results computed from table 6, calculated data utilized the above-mentioned formulae (4.2).

Table 4.8: Computed Normalized S/N ratios of determined results

S. N	S/N ratios normalized (η) for higher is better			
	Ratio of S/N of (H)	**Ratio of S/N of (UTS)**	**Ratio of S/N of (CS)**	**Ratio of S/N of (BS)**
1	0	0	0	0
2	0.050724638	0.022838215	0.462745098	0.056179775
3	0.057971014	0.321428571	0.592156863	0.157303371
4	0.195652174	0.492857143	0.709803922	0.247191011
5	0.217391304	0.542857143	0.737254902	0.258426966
6	0.405797101	0.55	0.749019608	0.269662921
7	0.746376812	0.65	0.65	0.471910112
8	0.891304348	0.657142857	0.8	0.629213483
9	1	1	1	1

Stage 3. The computation of the deviation sequences ((Δ_{ij}) in both quality characteristics is identical, and the equation is as follows; Δ= absolute difference between Zij^0 and Zij, which is a variation from the desired level and may be considered a quality loss. Table 4.9 shows the Deviation sequence for the various normalized S/N ratios (η).

$$\Delta_{ij} = Z_{ij}^{0} - Z_{ij} \tag{4.3}$$

whereas Δij denotes the deviation series and Zij^0 is typically equal to one ($Zij^0 = 1$).

Stage 4: Computation of GRCs calculation: The following equation is used to calculate the GRC for normalized S/N ratio data.

$$\mathbf{Zij} = \frac{\Delta\mathrm{Min} + \lambda\Delta\mathrm{Max}}{\Delta\mathrm{ij} + \lambda\Delta\mathrm{Max}} \quad \begin{cases} i = 1, 2, 3 \ldots 27 \\ j, = 1, 2, 3, 4 \end{cases} \tag{4.4}$$

λ is the distinguishing coefficient, specified in the range 0 ≤λ ≤1 (its value can be adjusted based on the system's real requirements). is also known as the identification coefficient, and it ranges between 0 and 1. According to [Naqiuddin et al., (2018);Ikubanni et al., (2021); Acır et al., (2017)], λ = 0.5 is typically used since choosing 0 or 1 has no influence on the value of the parameter rankings sequence. The GRC values derived from equation (4.4) are shown in Table 912. Stage 5: Determine the GRGi: After determining the GRCij, the GRGi may be calculated as follows;

$$\boldsymbol{GRGi} = \frac{1}{m}\sum GRCij \qquad (4.5)$$

whereas m denotes the total number of responses (or achievement attributes) and equals 4 due to the four responses (H, UTS, CS, and BS). Table 8 shows the GRCs and GRGs for all experimentations that were calculated in the similar way.

Table 4.9: Deviation Series progression for normalized S/N ratios (η)

S. N	**Deviation Series (Δij have the exact same equation expression)**			
	ΔH	**ΔUTS**	**ΔCS**	**ΔBS**
1	1	1	1	1
2	0.949275362	0.977161785	0.537254902	0.943820225
3	0.942028986	0.678571429	0.407843137	0.842696629
4	0.804347826	0.507142857	0.290196078	0.752808989
5	0.782608696	0.457142857	0.262745098	0.741573034
6	0.594202899	0.45	0.250980392	0.730337079
7	0.253623188	0.35	0.35	0.528089888
8	0.108695652	0.342857143	0.2	0.370786517
9	0	0	0	0

Table 4.10: Grey relational grades (GRGs) and Grey relational coefficients (GRCs)

S. N	**Grey Relational Coefficients (GRCs)**				**Grey Relational Grades (GRGs)**
	H	UTS	CS	BS	
1	1	1	1	1	1
2	0.513011152	0.505775505	0.650510204	0.514450867	0.545936932
3	0.514925373	0.595744681	0.710306407	0.542682927	0.590914847
4	0.554216867	0.663507109	0.775075988	0.570512821	0.640828196
5	0.56097561	0.68627451	0.791925466	0.574193548	0.653342283
6	0.627272727	0.689655172	0.799373041	0.577922078	0.673555755
7	0.797687861	0.740740741	0.740740741	0.654411765	0.733395277
8	0.901960784	0.744680851	0.833333333	0.729508197	0.802370791
9	1	1	1	1	1
Average mean of GRG					**0.737816**

Stage 6: Select the most optimally suited variable and level configurations. The higher the grey relationship grade, the higher the product degree of excellence attribute; hence, the variable influence may be investigated, and the optimal amount level satisfies every single one may be determined.

The GRG was stated according to [Haq et al., 2008] can be used to identify controllable components. This may be accomplished in two methods: (1) utilizing Minitab software to determine the ideal parameter configurations, or (2) manually calculating the average of the GRG scores. The procedure for finding the average GRG [Bodunrin et al., (2015)] is as follows:(1) The GRGs are grouped by variable level for each of the columns in the OA;(2) Taking the average of GRGs;(3) Computation of grade scores for every single L9 OA examination according to DOE.

For the purpose of quantifying the influence of variable i, for instance, an overall mean of grade ratings (AvgG) for each level j is found, which is written as AGVij, and its impact, Ei, may be defined as follows:

$$Ei = Max\ (AGVij) - Min\ (AGVij) \tag{4.6}$$

If the variable i can be controlled, the optimal level j* is calculated by (4.6)

Table 4.11: Average GRG response table

S. N	Factor of Control	GRG Averages by Parameter Levels			Max-Min (*Ei*)	Rank
		L1	**L2**	**L3**		
1	Welding Current (WC)	1.977652407	2.186765128	**2.673555755**	0.695903347	1
2	Gas Flow Rate (GRF)	2.136851779	1.967726234	**2.535766068**	0.568039834	2
3	Root Gap (RG)	2.199279216	**2.374223473**	2.264470601	0.174944258	3

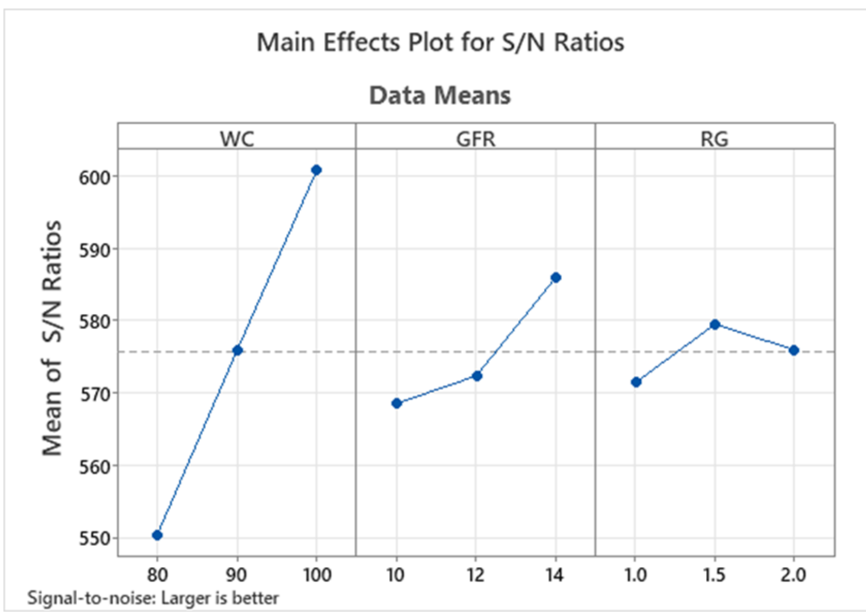

Figure 4.13. Main Effect graph for S/N Ratios

The results of the GRA of GRGs and the Taguchi S/N ratios analysis are similar and agree in this particular investigation, as shown in Figure 4.13 and Table 4.11.According to the response table in table 8 and the response graph in figure 4.13 of the GRG in table 9, the optimal levels' settings of TIG welding control parameters in the synthesis of AISI 316 control factors were welding current (WC) level 3 used 100A, gas flow rate (GRF) level 3 used 14 lit/min, and root gap (RG) 1.5mm. It can also be generated as WC3, GFR3 and RG2.

4.7 Perform Analysis of Variance (ANOVA)

ANOVA is used to determine the importance and contribution of every procedure variable to the grey relational grade value. The goal of the ANOVA is to determine which process factors have a substantial impact on performance metrics [Naik & Reddy, (2018)]. To execute an ANOVA utilizing investigation [Sanjay Kumara, (2020)] shown in table 19.

Table 4.12: ANOVA Analysis of Variables

Source	DoF	Adj SS	Adj MS	F calculated	P value	% of contribution	Remark
Welding current (WC)	2	0.4247208	0.1415736	88.36	0.0001	85.6	Significance
Gas flow rate (GFR)	2	0.0500997	0.0167003	10.42	0.0003	9.2	Significance
Root gap (RG)	2	0.0272685	0.0272685	17.02	0.0001	5.2	Significance
Error	2	0.0026093	0.0013041				
Error pooled	2	0.0128205	0.0016023				
Total	10	0.5149085				100	

To establish the relevance of each variable, it is required to know the crucial P-value and compare it to the estimated P-value. If the estimated P-value is less than or equal to the 0.05 crucial P-value, the variable is significant. According to this study analysis ANOVA table 19, all three characteristics (Welding Current (WC), Gas Flow rate (GFR), and Root gap (GR)) are significant.

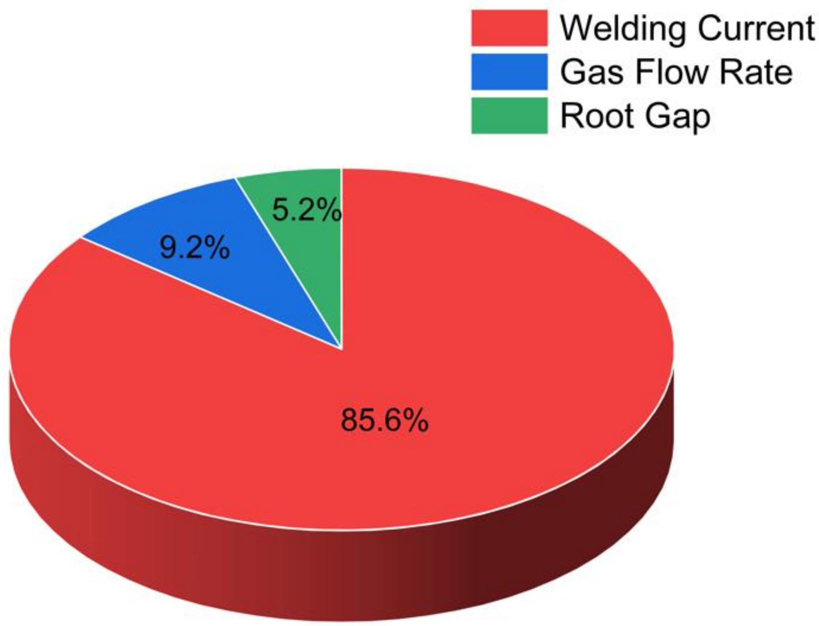

Figure 4.14. Contribution percentage input process factor

According to the ANOVA outcomes, three variables, namely Welding Current (WC) with 85.6% contribution, Gas Flow Rate (GFR) with 9.2% contribution and Root Gap with 5.2% contribution as shown figure 4.14 Contribution percentage, constitute significant factors considering their determined P-values are less than the threshold for significance ($P \leq 0.05$).

4.8 Interval Confidence and Prediction of Mean Values

4.8.1 Prediction of Mean Values

Table 9 and Figure 4.13 depict the best and most important variables, which include WC3, GFR3, and RG2. The best potential grey relational grade (GRG) is predicted at the optimal configuration of the process variables. According to (Surinder Kumar, 2019) determines the response value characteristic's predicted mean. The Taguchi MINITAB software computed and determined the Prediction Mean (µGRG) to be 0.624209 or µGRG= 0.624209.

Whereas TGRG is the comprehensive mean of grey relationship grade =**0.737816**

µGRG= 0.624209. The projected mean of the grey relational grade is **0.624209**, which is utilized for comparison and determine on the confirmation test's ultimate outcome. Whether or not it fits inside the ideal condition of the confidence interval of expected mean values.

4.8.2 Confidence Interval

A range of confidence is a set of values whereby a population-unknown variable (e.g., mean, variance, etc.) may be found. The anticipated mean of GRG on confirmatory examination is determined applying the subsequent formula (Surinder Kumar, 2019).

$$\mathbf{CI} = \sqrt{\mathbf{F}\alpha\,(\mathbf{1}, \boldsymbol{f_e}) * \mathbf{Ve}\left(\frac{\mathbf{1}}{\boldsymbol{n_{eff}}} + \frac{\mathbf{1}}{\mathbf{R}}\right)}$$

Where $F\alpha\ (1, f_e) = P_{0.05}(1,2) = 2.92$

α = risk= 0.05

f_e = error pooled of DF= 2 (P-Table in the Appendices 1)

Ve =variance= pooled Error for adjacent mean square =0.0016023

R= the number of confirmation tests = 3

n_{eff} = 0.818

The no of effective number of replications (n_{eff}) is calculated

n_{eff}

$$\boldsymbol{n_{eff}} = \frac{\boldsymbol{Te}}{\mathbf{1+}\boldsymbol{Ts}} = \frac{\mathbf{9}}{\mathbf{1+10}} = \mathbf{0.818}$$

Where

n_{eff} is expressed mathematically

Te= total number of experiments

Ts = the sum of the DF used to estimate the factor of average value= DF of pooled error =2

Therefore the calculated CI

$$\mathbf{CI} = \sqrt{\mathbf{2.92} * 0.0016023\left(\frac{\mathbf{1}}{\mathbf{0.818}} + \frac{\mathbf{1}}{\mathbf{3}}\right)} = \mathbf{0.085}$$

Comparing µGRG with CI

$\mu\mathrm{GRG} - \mathrm{CI} < \mu GRG < \mu GRG + CI$

<u>**0.709209**-0.085 < µGRG < **0.709209**+0.085</u>

<u>**0.624209**< µGRG < **0.794209**</u>

The verification experimental work of GRG value must be between 0.624209 and 0.794209 at a level of confidence of 95%.

4.9 Verification Experimentation

Confirmation experiments validate findings by validating the validity of the optimization approach and performance enhancement with projected maximum desired setting, assuring the highest level of or optimum performance. Validation experiments are performed with 100A welding current, 14 lit/min gas flow rate, and 1.5mm root gap at the optimal level of process factors. WC level 3, GFR3, and RG2 are the best TIG welding parameters for controlling for welding AISI 316 base metal control variables with three replications. As a result of the confirmation experiment, every variability is reduced, and the optimum results obtained are acceptable, as shown in Table 4.13.

Table 4.13 Validation outcomes tests of three samples replication for all outcomes using the best parameters

S. N	Microhardness (H) (HRC)				Ultimate Tensile Strength (UTS) (MPa)			Compressive Strength (CS) (MPa)			Bending Strength (BS) (MPa)		
	Trial-1	**Trial-2**	**Trial-3**	**Avg.**	**Trial-1**	**Trial-2**	**Avg.**	**Trial-1**	**Trial-2**	**Avg.**	**Trial-1**	**Trial-2**	**Avg.**
1	67.1	35.8	67.7	**56.9**	866	957	**911.5**	519	574	**546.5**	983	1087	**1035**
2	44	66.8	63.8	**58.2**	867	959	**913**	520	575	**547.5**	984	1088	**1036**
3	67.8	67.9	54.4	**63.4**	868	960	**914**	522	577	**549.5**	986	1090	**1038**

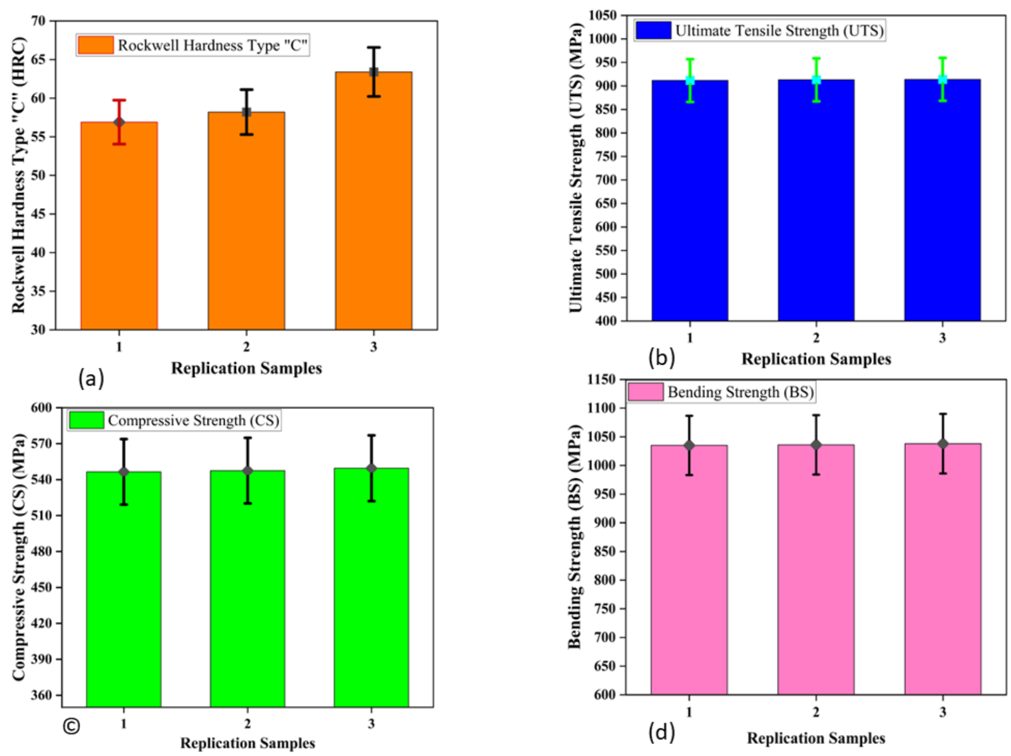

Figure 4.15. Result of the Optimized Validation Analysis: (a) Rockwell hardness type "C", (b) UTM, (c) Compressive strength and (d) Bending strength

Low welding currents prevent the welded joint from properly fusing together due to an inadequate heat input. On the other hand, sufficient heat input is provided as welding current rises, resulting in correct fusion developed in the weldment. The proper fusion that results from the current increase promotes deep penetration between joined specimens and increases the microhardness, Ultimate Tensile Strength, Compressive Strength and Bending Strength characteristics of the specimens. Extremely high principal current during TIG welding results in substructures and grain boundary enlargement, which do not meet the World Welding Society's ISO welding position guidelines for material thickness. This result was consistent and in agreement with the earlier investigation. [Srikanth & Manikandan, (2018); Porchilamban & Amaladas, (2019); Sabzi et al., (2021); Wang et al., (2022); Yang et al., (2022); Zhang et al., (2022); Yelamasetti et al., (2023);Yadav et al., (2023); Vemanaboina et al., (2023)].

Table 4.14: Validation results are evaluated using average Mean GRG parameters

S. N	**Data Transformation within S/N Ratios**				**Normalization of S/N Figures**				**Δ Absolute Difference Values**				**GRC**			
	RH	UTS	CS	BS	RH	UTS	CS	BS	ΔRH	ΔUTS	ΔCS	ΔBS	RH	UTS	CS	BS
1	33.9	59.11	54.72	60.26	0	0	0	0	1	1	1	1	0.5	0.5	0.5	0.5
2	34.8	59.17	54.73	60.27	0.45	0.8571	0.2	0.3333	0.55	0.1429	0.8	0.6667	0.6452	0.875	0.5556	0.6
3	35.9	59.18	54.77	60.29	1	1	1	1	0	0	0	0	1	1	1	1
Average Mean of GRG																

The validation examination outcome's mean GRG of 0.7229 falls between 0.624209 and 0.794209. The efficacy of the optimal situation may be ensured if the expected values of the various performance factors are close to each other. The grey relationship grade for the experiment outcome is 0.7229, which is in the middle of the confidence range. As a result, the validation experiment assessment results show that the experiment is compressively acceptable.

The confirmation experiment yielded a hardness of 59.5 HRC, an ultimate tensile strength of 912.5MPa, a compressive strength of 547.8MPa, and a bending strength of 1036MPa, as shown in table 4.15 and figure 15. This conclusion was confirmed by the experiment [Linger & Bogale, (2023)], which claimed that when current was increased, mechanical characteristics improved significantly.

Table 4.15: Validation examination conclusion

	Optimal Parameters	
	Prediction	**Experiment**
Setting Levels	WC3, GFR3 and RG2	WC3, GFR3 and RG2
Hardness		59.5 HRC
Ultimate Tensile Strength		912.5MPa
Compressive Strength		547.8MPa
Bend Strength		1036MPa
GRG	**0.6242**	**0.7229**

According to the inquiry of this research, substantially increased mechanical characteristics of SS 316L pipe welded by TIG welding procedure and past scholar agree with these results. Minimal heat input joints have good tensile strength and ductility, but extremely large heat input joints have low ductility and strength, hence the researcher chose a lower welding current from the evaluated paper's used parameters this conclusion agree with the investigation prior publication [Mohammed et al. (2017); Kumar & Shahi, (2014)].

CHAPTER FIVE

CONCLUSION AND RECOMMENDATION

5.1. Conclusion

The stainless-steel weldment failure owing to incorrect variable level setup and the lack of backup purge gas in the process of TIG welding. The current research used a grey-based Taguchi optimization technique to optimize the method of TIG welding on 316 stainless steel material. The investigation included nine trials in which back weld bead contamination was controlled using gas purging devices attached to the workpiece and welding torch. The researchers investigated the implications of welding current, gas flow rate, and root gap on Rockwell hardness, ultimate tensile strength, compressive and bending strength on SS 316 materials using a grey-coupled-with-Taguchi technique of butt joint weldment.

The optimum values of TIG welding control variables in the AISI 316 control factors were welding current (WC) level 3 used 100A, gas flow rate (GRF) level 3 used 14 lit/min, and root gap (RG) 1.5mm. ANOVA revealed that the F-values of welding current, gas flow rate, and root gap were more than the crucial F values. Furthermore, their P-values were less than 0.05, indicating that they were significant for all input parameters. Welding current was the most important characteristic, contributing to 85.6% of Rockwell hardness, ultimate tensile strength, compressive and bending strength enhancement. The overall R2 (adj) is 97.53%. Only 97.51% of the variance is explained by specified criteria, leaving 2.47% unaccounted for. This component of the measurement error was minor and acceptable at the 95% confidence level.

The validation investigation was carried out with the optimal variable level values. According to validation, the average GRG of 0.7229 was discovered between the 95% confidence range of 0.7229 falls between 0.624209 and 0.794209. As a result, the validation experiment examination results demonstrated that what was performed was acceptable. The ultimate tensile strength, bending strength, compressive strength, and Rockwell hardness of stainless steel were increased by employing well-prepared back gas purging devices. Furthermore, the maximum Rockwell hardness, ultimate tensile strength, compressive strength, and bending strength were 59.5 HRC with 1.7% improvement, 912.5MPa with 1.8% advancement, 547.8MPa with 1.83% enhanced effectiveness, and 1036MPa with 1.66% enhanced efficiency, respectively. In the manual TIG welding procedure, the weldment also performed its specified tasks for a predetermined amount of time.

4.10 Recommendation

The goal of this research is to optimize TIG welding process parameters such as welding current, gas flow rate, and root gap. Other welding aspects, such as filler metal type, filler metal thickness, filler metal deposition rate, joint design, electrode angle, and so on, require more investigation. This thesis is limited to the usage of 316 stainless steel tubing as a basic material; however, the study may be broadened to incorporate other types of materials. On the specimen, only the mechanical properties of the weld on hardness, tensile strength, compressive strength, and bending strength are tested and inspected; it can also be studied for other non-destructive test methods such as impact strength, radiographic testing, and ultrasonic testing for better joint analysis.

REFERENCE

Abrha, H. (2015). Analysis and Optimization of MAG welding Parameters Using Genetic Algorithm (Doctoral dissertation, M. Sc. Thesis, Ethiopian Institute of Technology–Mekelle (EiT-M), School of Mechanical and Industrial Engineering, Mekelle University, Mekelle, Ethiopia).

Achuthamenon Sylajakumari, P., Ramakrishnasamy, R., & Palaniappan, G. (2018). Taguchi grey relational analysis for multi-response optimization of wear in co-continuous composite. Materials, 11(9), 1743.

Acır, A., Canlı, M. E., Ata, İ., & Çakıroglu, R. (2017). Parametric optimization of energy and exergy analyses of a novel solar air heater with grey relational analysis. Applied Thermal Engineering, 122, 330-338.

Ahmad, A., & Alam, S. (2018, August). Grey based Taguchi method for optimization of TIG process parameter in improving tensile strength of S30430 stainless steel. In IOP Conference Series: Materials Science and Engineering (Vol. 404, No. 1, p. 012003). IOP Publishing.

Anand, K. R., & Mittal, V. (2017). Review on the parametric optimization of tig welding. Int. Res. J. Eng. Technol. (IRJET), 4(01), 2395-0056.

Avinash, S., Balram, Y., Babu, B. S., & Venkatramana, G. (2019). Multi-response optimization of pulse TIG welding process parameters of welds AISI 304 and Monel 400 using grey relational analysis. Materials today: proceedings, 19, 296-301.

Bachani, S. I., & Ghetiya, N. D. (2018). Multi-objective optimization of process parameter in Activated Tungsten Inert Gas (A-TIG) Welding. Nirma University Journal of Engineering and Technology (NUJET), 6(1), 13-20.

Bachani, S. I., & Ghetiya, N. D. (2018). Multi-objective optimization of process parameter in Activated Tungsten Inert Gas (A-TIG) Welding. Nirma University Journal of Engineering and Technology (NUJET), 6(1), 13-20.

Bahrami, A., & Taheri, P. (2019). A study on the failure of AISI 304 stainless steel tubes in a gas heater unit. Metals, 9(9), 969.

Barnes, T. A., & Pashby, I. R. (2000). Joining techniques for aluminium spaceframes used in automobiles: Part II—adhesive bonding and mechanical fasteners. Journal of materials processing technology, 99(1-3), 72-79.

Bhadauria, N., Vashishtha, P., & Mishra, S. (2018). Optimization of parameters of GTAW for surfacing of AISI 304. International Journal of Applied Engineering Research, 13(6), 238-240.

Bhavsar, A. N., & Patel, V. A. (2016). Influence of process parameters of TIG welding process on mechanical properties of SS304L welded joint. International Research Journal of Engineering and Technology (IRJET), vol3, pp-977-984, 3(05).

Bodkhe, S. C., & Dolas, D. R. (2018). Optimization of activated tungsten inert gas welding of 304L austenitic stainless steel. Procedia Manufacturing, 20, 277-282.

Becker, W. T., Shipley, R. J., Lampman, S., Sanders, B. R., Henry, S. D., Anton, G. J., ... & Terman, C. (Eds.). (2002). ASM handbook: failure analysis and prevention. ASM International.

Bodunrin, M. O., Alaneme, K. K., & Chown, L. H. (2015). Aluminium matrix hybrid composites: a review of reinforcement philosophies; mechanical, corrosion and tribological characteristics. Journal of materials research and technology, 4(4), 434-445.

Bopaliya, H. M. (2016). Optimization of Process Parameters in TIG Welding on Dissimilar Metals SS-304 and SA 515 (Grade-60) (Doctoral dissertation).

Bower, L., Jeffus, L. F., & Roy, D. (2010). Welding skills, processes and practices for entry-level welders. Book 1.

Campbell, R. D. (1987). An investigation into the physical metallurgy, welding metallurgy, hot-cracking and weld pool shape of ferritic stainless steels. Rensselaer Polytechnic Institute.

Chaudhari, V., Bodkhe, V., Deokate, S., Mali, B., & Mahale, R. (2019). Parametric optimization of TIG welding on SS 304 and MS using Taguchi approach. Int. Res. J. Eng. Technol, 6(5), 880-885.

Connor, L. P., O'Brien, R. L., & Oates, W. R. (Eds.). (1987). Welding handbook: welding processes (Vol. 2). Amer Welding Society.

Dak, G., & Pandey, C. (2021). Experimental investigation on microstructure, mechanical properties, and residual stresses of dissimilar welded joint of martensitic P92 and AISI 304L austenitic stainless steel. International Journal of Pressure Vessels and Piping, 194, 104536.

Dejun, K., & Jinchun, W. (2015). Salt spray corrosion and electrochemical corrosion properties of anodic oxide film on 7475 aluminum alloy. Journal of Alloys and Compounds, 632, 286-290.

Deshwal, G. K., & Panjagari, N. R. (2020). Review on metal packaging: Materials, forms, food applications, safety and recyclability. *Journal of food science and technology*, *57*(7), 2377-2392.

Ghosh, N., Pal, P. K., & Nandi, G. (2016). Parametric optimization of MIG welding on 316L austenitic stainless steel by Grey-Based Taguchi method. Procedia Technology, 25, 1038-1048.

Ghumman, K. Z., Ali, S., Din, E. U., Mubashar, A., Khan, N. B., & Ahmed, S. W. (2022). Experimental investigation of effect of welding parameters on surface roughness, micro-hardness and tensile strength of AISI 316L stainless steel welded joints using 308L filler material by TIG welding. Journal of Materials Research and Technology, 21, 220-236.

Gite, K. A., & Pawar, R. S. (2016). Effect of Welding Geometry Parameter on Hardness for Aisi304 Tig. IJARIIE-ISSN (O)-2395-4396, 2(4), 735-744.

Gohel, V., Makwana, J., & Ranjan, R. (2016). Thermo-Mechanical analysis in TIG welding of SS 304. International Journal of Engineering Development and Research, 4(2), 1704-10.

Goncalves, C. V., Carvalho, S. R., & Guimarães, G. (2010). Application of optimization techniques and the enthalpy method to solve a 3D-inverse problem during a TIG welding process. Applied Thermal Engineering, 30(16), 2396-2402.

Handbook of structural welding: processes, materials and methods used in the welding of major structures, pipelines and process plant. Elsevier.

Haq, A. N., Marimuthu, P., & Jeyapaul, R. (2008). Multi response optimization of machining parameters of drilling Al/SiC metal matrix composite using grey relational analysis in the Taguchi method. The International Journal of Advanced Manufacturing Technology, 37, 250-255.

Hemnani, M., Mittal, P., & Goyal, S. (2018). Optimization of Tungsten Inert Gas welding using taguchi and ANOVA. International Journal for Research in Applied Science & Engineering Technology, 6(5).

Hirschorn, B., Orazem, M. E., Tribollet, B., Vivier, V., Frateur, I., & Musiani, M. (2010).

Determination of effective capacitance and film thickness from constant-phase-element parameters. Electrochimica acta, 55(21), 6218-6227.

Huang, Y., Wang, B., Guo, J., Fan, D., & Yu, S. (2023). Investigation of the Mechanism of Powder Pool Coupled Activating TIG Welding. Metals, 13(5), 830.

Ibrahim, M., Maqsood, S., Khan, R., Amjad, M., & Jaan, S. (2017). Optimization of gas tungsten arc welding parameters on penetration depth and bead width using Taguchi method. Journal of Engineering and Applied Sciences (JEAS), 35(2).

Ikubanni, P. P., Oki, M., Adeleke, A. A., & Agboola, O. O. (2021). Optimization of the tribological properties of hybrid reinforced aluminum matrix composites using Taguchi and Grey's relational analysis. Scientific African, 12, e00839.

Indira Rani, M., & Marpu, R. N. (2012). Effect of pulsed current TIG welding parameters on mechanical properties of J-joint strength of Aa6351. The International Journal of Engineering and Science (IJES), 1(1), 1-5.

Jailani, H. S., Rajadurai, A., Mohan, B., Kumar, A. S., & Sornakumar, T. (2009). Multi-response optimization of sintering parameters of Al–Si alloy/fly ash composite using Taguchi method and grey relational analysis. The International Journal of Advanced Manufacturing Technology, 45, 362-369.

Jayaraman, P. (2014). Multi-response optimization of machining parameters of turning AA6063 T6 aluminum alloy using grey relational analysis in Taguchi method. Procedia Engineering, 97, 197-204.

Jeffus, L. (2012). Welding Principles and Applications Cengage Learning.

Jeffus, L. (2020). Welding: Principles and Applications: Cengage Learning

Jeffus, L., & Baker, B. (2016). Pipe Welding. Cengage Learning.

Jeffus, L., & Bower, L. (2009). Welding skills, processes and practices for entry-level welders: book 1. Cengage Learning.

Jeffus., L. (2012). Welding Principles and Applications. Canada: Delmar, Cengage Learning.

Jeyaprakash, N., Haile, A., & Arunprasath, M. (2015). The parameters and equipment used in TIG welding: A review. The International Journal of Engineering and Science (IJES), 4(2), 11-20.

Joseph, G. B., Mageshwaran, G., Kumar, R. A., Raj, R. D., Jeevahan, J., & Kunjan, M. (2016). characteristics studies of stainless steel (AISI type 304l) welded by ER310L filler using tig welding. International Journal of Chemical Sciences, 14(4), 2527-2534.

Joshi, M. P., Singh, J., Prakash, C., & Singh, S. (2019, October). On the multi-parametric optimization of quality characteristics of the hybrid Al-6061 composites fabricated through powder metallurgy. In IOP Conference Series: Materials Science and Engineering (Vol. 561, No. 1, p. 012053). IOP Publishing.

Julong, D. (1989). Introduction to grey system theory. The Journal of grey system, 1(1), 1-24.

Kasman, S. (2013). Multi-response optimization using the Taguchi-based grey relational analysis: a case study for dissimilar friction stirs butt welding of AA6082-T6/AA5754-H111. The international journal of Advanced manufacturing technology, 68, 795-804.

Khan, M. I. (2007). Welding science and technology. New Age International.

Karunakaran, N., & Balasubramanian, V. (2011). Effect of pulsed current on temperature distribution, weld bead profiles and characteristics of gas tungsten arc welded aluminum alloy joints. Transactions of Nonferrous Metals Society of China (English Edition), 21(2), 278–286. https://doi.org/10.1016/S1003-6326(11)60710-3

Kumar, S., & Shahi, A. S. (2014). On the influence of welding stainless steel on microstructural development and mechanical performance. Materials and Manufacturing Processes, 29(8), 894-902.

Kumar, S., Narayan, A., Bhardwaj, A. K., & Kumari, L. (2020). Optimization of Aisi 304 Weld Joint Characteristics Using Taguchi Technique: International Conference on Recent Trends in Artificial Intelligence, IoT, Smart Cities & Applications. Amit kumar and Bhardwaj, Abhijeet Kumar and Diwakar, Shivendar kumar and Kumari, Lalita, Optimization of AISI, 304.

Kumar, S., Singh, P., Patel, D., & Prasad, S. B. (2017). Optimization of TIG welding process parameters using Taguchi's analysis and response surface methodology. International Journal of Mechanical Engineering and Technology, 8(11), 932-941.

Latifi Jr, H. (2012). Advanced orbital pipe welding.

Li, L., Du, Z., Sheng, X., Zhao, M., Song, L., Han, B., & Li, X. (2022). Comparative analysis of GTAW+ SMAW and GTAW welded joints of duplex stainless steel 2205 pipe. International Journal of Pressure Vessels and Piping, 199, 104748.

Linger, M. A., & Bogale, T. M. (2023). Parameters optimization of tungsten inert gas welding process on 304L stainless steel using grey based Taguchi method. Engineering Research

Express, 5(1), 015013

Lugade, P. S., & Deshmukh, M. J. (2015). Optimization of process parameters of activated tungsten inert gas (A-TIG) welding for stainless steel 304L using Taguchi method. International Journal of Engineering Research and General Science, 3(3), 854-860.

Martins, A. A., & Friday, I. D. (2022). Parametric Optimization of Gas Tungsten Arc Welding (GTAW) on the Tensile Strength of AISI 316l Austenitic Stainless Steel Using Taguchi Method. Journal of Materials Engineering, Structures and Computation, 1.

Meignanamoorthy, M., Vinayagam, M., Ravichandran, M., Raja, T., Gacem, A., Mezni, A., ... & Ganesan, M. (2022). Evaluation on powder metallurgy process parameters of ball-milled AA8079-B4C nanostructured composites via taguchi grey relational analysis. Journal of Nanomaterials, 2022.

Messele, E. (2019). Multi-Objective Process Parameters Optimization of Friction Stir Welding on 6061 Aluminum Alloy using Taguchi and Grey Relational Analysis (Doctoral dissertation).

Minnick, W. H. (1996). Gas tungsten arc welding handbook.

Mohammed, G. R., Ishak, M., Aqida, S. N., & Abdulhadi, H. A. (2017). Effects of heat input on microstructure, corrosion and mechanical characteristics of welded austenitic and duplex stainless steels: A review. Metals, 7(2), 39.

Moi, S. C., Pal, P. K., Bandyopadhyay, A., & Rudrapati, R. (2018). Determination of tungsten inert gas welding input parameters to attain maximum tensile strength of 316L austenitic stainless steel. Strojnícky časopis-Journal of Mechanical Engineering, 68(3), 231-248.

Muluken, A. L. (2020). Multi-Objective Optimization of Tungsten Inert Gas Welding Process Parameters on 304L Stainless Steel Using Taguchi-Based Grey Relational Analysis (Doctoral dissertation).

Nagesh, D. S., & Datta, G. L. (2010). Genetic algorithm for optimization of welding variables for height to width ratio and application of ANN for prediction of bead geometry for TIG welding process. Applied soft computing, 10(3), 897-907.

Naik, A. B., & Reddy, A. C. (2018). Optimization of tensile strength in TIG welding using the Taguchi method and analysis of variance (ANOVA). Thermal Science and Engineering Progress, 8, 327-339.

Naqiuddin, N. H., Saw, L. H., Yew, M. C., Yusof, F., Poon, H. M., Cai, Z., & San Thiam, H.

(2018). Numerical investigation for optimizing segmented micro-channel heat sink by Taguchi-Grey method. Applied Energy, 222, 437-450.

Nguyen, V. N., Nguyen, Q. M., & Huang, S. C. (2018). Microstructure and mechanical properties of butt joints between stainless steel SUS304L and aluminum alloy A6061-T6 by TIG welding. Materials, 11(7), 1136.

Norrish, J. (2006). High-energy density processes. Advanced Welding Processes, J. Norrish, Ed. Elsevier, 136-164.

O'Brien, A. (2004). AWS Welding Handbook. Volume, 2, 52.

O'Brien, R. L. (1991). Welding Handbook. Volume 2: Welding Processes. (Retroactive Coverage). American Welding Society, 1991, 955.

Ogbonna, O. S., Akinlabi, S. A., Madushele, N., Fatoba, O. S., & Akinlabi, E. T. (2023). Grey-based taguchi method for multi-weld quality optimization of gas metal arc dissimilar joining of mild steel and 316 stainless steels. Results in Engineering, 17, 100963.

Parmar, H., & Nair, V. (2019). Review on investigate the TIG welding of Aluminum by controlling parameter. International Research Journal of Engineering and Technology, 6(3), 349-354.

Parthasarathy[1], S., Ganesh, N., & Chellamuthu, K. Experimental investigation of hardness of al6061 with graphine and molybdenum metal matrix composite.

Porchilamban, S., & Amaladas, J. R. (2019). Structural relationships of metallurgical and mechanical properties influenced by Ni-based fillers on Gas Tungsten Arc Welded Ferritic/Austenitic SS dissimilar joints. Journal of Advanced Mechanical Design, Systems, and Manufacturing, 13(1), JAMDSM0023-JAMDSM0023.

Prajapati, S., & Shah, K. (2016). Experimental study on activated tungsten inert gas welding-a review paper. Int. J. Advance Research and Innovative Ideas in Education, 2, 2555-2559.

Prakash, J. U., Rubi, C. S., Rajkumar, C., & Juliyana, S. J. (2021). Multi-objective drilling parameter optimization of hybrid metal matrix composites using grey relational analysis. Materials Today: Proceedings, 39, 1345-1350.

Qazi, M. I., Abas, M., Khan, R., Saleem, W., Pruncu, C. I., & Omair, M. (2021). Experimental investigation and multi-response optimization of machinability of AA5005H34 using composite desirability coupled with PCA. Metals, 11(2), 235.

Rajesh, R., & Sumathi, S. (2020). Certain performance investigation on hybrid TiO2/Al2O3/MoS2 nanofiller coated 3Ø induction motor: a Taguchi and RSM based approach. Energy Reports, 6, 1638-1647.

Ramakrishnan, A., Rameshkumar, T., Rajamurugan, G., Sundarraju, G., & Selvamuthukumaran, D. (2021). Experimental investigation on mechanical properties of TIG welded dissimilar AISI 304 and AISI 316 stainless steel using 308 filler rod. Materials Today: Proceedings, 45, 8207-8211.

Rana, P., Singh, B., & Singh, J. (2017). Parametric study of dissimilar material on gas tungsten arc welding. International Journal of Engineering Sciences, 25, 60-67.

Richard D. Campbell, P. E. (1999). Welding of stainless steels. Florida, United States of America: American Welding Society

Rizvi, S. A., & Tewari, S. P. (2018). Optimization of gas metal arcwelding parameters of SS304 austenitic steel by Taguchi–Grey relational analysis. Journal of Computational & Applied Research in Mechanical Engineering (JCARME), 7(2), 189-198.

Rudrapati, R., Chowdhury, N., & Bandyopadhyay, A. (2016). Parametric optimization of TIG welding process in butt joining of mild steel and stainless steel. International Journal of Current Engineering and Technology, 6, 144-149.

Ryl, J., Wysocka, J., Jarzynka, M., Zielinski, A., Orlikowski, J., & Darowicki, K. (2014). Effect of native air-formed oxidation on the corrosion behavior of AA 7075 aluminum alloys. Corrosion science, 87, 150-155.

Sabzi, M., Anijdan, S. M., Eivani, A. R., Park, N., & Jafarian, H. R. (2021). The effect of pulse current changes in PCGTAW on microstructural evolution, drastic improvement in mechanical properties, and fracture mode of dissimilar welded joint of AISI 316L-AISI 310S stainless steels. Materials Science and Engineering: A, 823, 141700.

Schmidt, R. H., & Piotter, H. M. (2020). The hygienic/sanitary design of food and beverage processing equipment. *Food safety engineering*, 267-332.

Saha, D., Sushma, S., & Jalageri, M. (2017, March). Parametric optimization of Tig welding for M1020 using Taguchi-grey relation-based design method. In Proceedings of the International Conference on Emerging Trends in Science, Engineering and Management, Hyderabad, India (pp. 17-18).

Saha, M. (2020). Effect of welding parameter of welded joint of stainless steel 304 by TIG welding. Available at SSRN 3643709.

Saha, M., & Dhami, S. S. (2018). Effect of TIG welding parameter of welded joint of stainless steel SS304 by TIG welding. Trends in mechanical engineering & technology, 8(3), 18-27.

Shaikh, I. A., & Rao, M. V. (2015). A Review on optimizing process parameters for TIG welding using Taguchi method & grey relational analysis. Int. J. Sci. Res., 4(6), 2449-2452.

Shanmugasundar, G., Karthikeyan, B., Ponvell, P. S., & Vignesh, V. (2019). Optimization of process parameters in TIG welded joints of AISI 304L-austenitic stainless steel using Taguchi's experimental design method. Materials today: proceedings, 16, 1188-1195.

Sharifitabar, M., Halvaee, A., & Khorshahian, S. (2011). Microstructure and mechanical properties of resistance upset butt welded 304 austenitic stainless-steel joints. Materials & Design, 32(7), 3854-3864.

Sharma, P., Chattopadhyaya, S., Singh, N. K., Kumar, A., Sharma, S., Li, C., ... & Krolczysk, G. (2022). Recent developments in the design, development, and analysis of the influence of external magnetic-field on gas-metal arc welding of non-ferrous alloys: review on optimization of arc-structure to enhance the morphology, and mechanical properties of welded joints for automotive applications. Heliyon, e11812.

Shih, J. S., Tzeng, Y. F., & Yang, J. B. (2011). Principal component analysis for multiple quality characteristics optimization of metal inert gas welding aluminum foam plate. Materials & Design, 32(3), 1253-1261.

Sidhu, G. S., & Chatha, S. S. (2012). Role of shielded metal arc welding consumables on pipe weld joint. International journal of emerging technology and advanced engineering, 2(12), 746-750.

Sing, S., Sing, M., & Kumar, V. (2016). Experimental Analysis of TIG Welding of Stainless Steel 304 using Grey Taguchi Method. International Journal of Technical Research (IJTR), 5(1), 51-55.

Singh, A. K., Debnath, T., Dey, V., & Rai, R. N. (2017). An approach to maximize weld penetration during TIG welding of P91 steel plates by utilizing image processing and Taguchi orthogonal array. Journal of The Institution of Engineers (India): Series C, 98, 541-551.

Singh, A., & Mittal, R. (2017). Experimental analysis on TIG welding process parameters of dissimilar metals SS304-SS202 using Taguchi Method. International Journal of Engineering and Manufacturing Science, 7(2), 248-249.

Singh, B., Singhal, P., & Saxena, K. K. (2019). Investigation of thermal efficiency and depth of penetration during GTAW process. Materials Today: Proceedings, 18, 2962-2969.

Singh, V., & Patel, V. (2014). Experimental investigation of GTAW for austenitic stainless steel using DOE. International Journal for Technological Research in Engineering, 1(9), 991-995.

Sonsino, C. M. (1999). Overview of the State of the Art on Multiaxial Fatigue of Welds. European Structural Integrity Society, 25, 195-217.

Srikanth, A., & Manikandan, M. (2018, February). Investigation on Microstructure and Mechanical Properties of Continuous and Pulsed Current Gas Tungsten Arc Welded alloy 600. In IOP Conference Series: Materials Science and Engineering (Vol. 310, No. 1, p. 012073). IOP Publishing.

Suraj, M., Tripathy, S., & Senapati, N. P. (2018). Optimization of Process Parameters during TIG Welding of 304L Stainless Steel with and without Flux. International Journal of Engineering & Technology, 7(4.39), 308-313.

Sutar, V. J., & Jadhav, B. R. (2021). Implementation of TOPSIS optimization technique in comparative analysis of conventional TIG and activated TIG welding of stainless steel 304L. International Journal of Materials Engineering Innovation, 12(3), 188-206.

Szklarska-Smialowska, Z. (1999). Pitting corrosion of aluminum. Corrosion science, 41(9), 1743-1767.

Thakur, P. P., & Chapgaon, A. N. (2016). A review on effects of GTAW process parameters on weld. IJRASET, 4, 136-140.

Trdan, U., & Grum, J. (2012). Evaluation of corrosion resistance of AA6082-T651 aluminum alloy after laser shock peening by means of cyclic polarization and ElS methods. Corrosion Science, 59, 324-333.

Vemanaboina, H., Babu, M. M., Prerana, I. C., Edison, G., Yelamasetti, B., Saxena, K. K., ... & Agrawal, M. K. (2023). Evaluation of residual stresses in CO2 laser beam welding of SS316L weldments using FEA. Materials Research Express.

Verma, R. P., Pandey, K. N., András, K., Khargotra, R., & Singh, T. (2023). Difficulties and redressal in joining of aluminium alloys by GMA and GTA welding: A review. Journal of Materials Research and Technology.

Vijayan, D., & Rao, V. S. (2018, July). Process parameter optimization in TIG welding of AISI 4340 low alloy steel welds by genetic algorithm. In IOP Conference Series: Materials Science and Engineering (Vol. 390, No. 1, p. 012066). IOP Publishing.

Vora, J., Patel, V. K., Srinivasan, S., Chaudhari, R., Pimenov, D. Y., Giasin, K., & Sharma, S. (2021). Optimization of activated tungsten inert gas welding process parameters using heat transfer search algorithm: with experimental validation using case studies. Metals, 11(6), 981.

Wahule, A., & Wasankar, K. (2018). Multi-response optimization of process parameters of TIG welding for dissimilar metals (SS-304 and Fe-410) using grey relational analysis. Int. Res. J. Eng. Technol, 5(6), 986-993.

Wang, B., Qiu, F., Chen, L., Zhou, Q., Dong, B., Yang, H., ... & Hu, M. (2022). Microstructure and shearing strength of stainless steel/low carbon steel joints produced by resistance spot welding. Journal of Materials Research and Technology, 20, 2668-2679.

Welding, G. T. A. (1991). American Welding Society. Welding Handbook, 8th.

Xu, F., Hou, Z., Xiao, R., Xu, Y., Wang, Q., & Zhang, H. (2023). A novel welding path generation method for robotic multi-layer multi-pass welding based on weld seam feature point. Measurement, 112910.

Yadav, A. K., Agrawal, M. K., Saxena, K. K., & Yelamasetti, B. (2023). Numerical simulation and experimental residual stress analyses of dissimilar GTA weldments of AA 5083 and AA 6082. International Journal on Interactive Design and Manufacturing (IJIDeM), 1-11.

Yamauchi, N., Inaba, Y., & Taka, T. (1983). Formation mechanism of lack of fusion in MAG welding. Transactions of the Japan Welding Society, 14(1), 76.

Yang, T., Xiao, Y., Zhuang, Y., Liu, J., Li, H., & Wang, Y. (2022). Effect of microstructural heterogeneity on corrosion fatigue crack growth behavior of 60-mm thick-plate TC4 titanium alloy NG-GTAW welded joint. International Journal of Fatigue, 163, 107030.

Ye, C., Zhai, W., Lu, G., Liu, Q., Ni, L., Ye, L., & Fang, X. (2021). Microstructural evolution and mechanical integrity relationship of dissimilar metal welding between 2205 duplex stainless steel and composite bimetallic plates. Proceedings of the Institution of Mechanical Engineers, Part C: Journal of Mechanical Engineering Science, 235(23), 7033-7044.

Yelamasetti, B., Adithya, G. S., Ramadevi, R. S., Sonia, P., Saxena, K. K., Kumar, N., ... & Al-kafaji, F. H. K. (2023). Metallurgical, mechanical and corrosion behavior of pulsed and constant current TIG dissimilar welds of AISI 430 and Inconel 718. Journal of Materials Research and Technology.

Zhang, Q., Zhuo, Z., Zhou, H., & Wang, J. (2022). Microstructure analysis and hardness prediction based on microstructure evolution theory in multi-pass welded joint. Proceedings of the Institution of Mechanical Engineers, Part C: Journal of Mechanical Engineering Science, 236(13), 7246-7258.

APPENDIX

Appendix -I F- Table Value

	DF1	α = 0.05																	
DF2	1	2	3	4	5	6	7	8	9	10	12	15	20	24	30	40	60	120	Inf
1	161.45	199.5	215.71	224.58	230.16	233.99	236.77	238.88	240.54	241.88	243.91	245.95	248.01	249.05	250.1	251.14	252.2	253.25	254.31
2	18.513	19	19.164	19.247	19.296	19.33	19.353	19.371	19.385	19.396	19.413	19.429	19.446	19.454	19.462	19.471	19.479	19.487	19.496
3	10.128	9.5521	9.2766	9.1172	9.0135	8.9406	8.8867	8.8452	8.8123	8.7855	8.7446	8.7029	8.6602	8.6385	8.6166	8.5944	8.572	8.5494	8.5264
4	7.7086	6.9443	6.5914	6.3882	6.2561	6.1631	6.0942	6.041	5.9988	5.9644	5.9117	5.8578	5.8025	5.7744	5.7459	5.717	5.6877	5.6581	5.6281
5	6.6079	5.7861	5.4095	5.1922	5.0503	4.9503	4.8759	4.8183	4.7725	4.7351	4.6777	4.6188	4.5581	4.5272	4.4957	4.4638	4.4314	4.3985	4.365
6	5.9874	5.1433	4.7571	4.5337	4.3874	4.2839	4.2067	4.1468	4.099	4.06	3.9999	3.9381	3.8742	3.8415	3.8082	3.7743	3.7398	3.7047	3.6689
7	5.5914	4.7374	4.3468	4.1203	3.9715	3.866	3.787	3.7257	3.6767	3.6365	3.5747	3.5107	3.4445	3.4105	3.3758	3.3404	3.3043	3.2674	3.2298
8	5.3177	4.459	4.0662	3.8379	3.6875	3.5806	3.5005	3.4381	3.3881	3.3472	3.2839	3.2184	3.1503	3.1152	3.0794	3.0428	3.0053	2.9669	2.9276
9	5.1174	4.2565	3.8625	3.6331	3.4817	3.3738	3.2927	3.2296	3.1789	3.1373	3.0729	3.0061	2.9365	2.9005	2.8637	2.8259	2.7872	2.7475	2.7067
10	4.9646	4.1028	3.7083	3.478	3.3258	3.2172	3.1355	3.0717	3.0204	2.9782	2.913	2.845	2.774	2.7372	2.6996	2.6609	2.6211	2.5801	2.5379
11	4.8443	3.9823	3.5874	3.3567	3.2039	3.0946	3.0123	2.948	2.8962	2.8536	2.7876	2.7186	2.6464	2.609	2.5705	2.5309	2.4901	2.448	2.4045
12	4.7472	3.8853	3.4903	3.2592	3.1059	2.9961	2.9134	2.8486	2.7964	2.7534	2.6866	2.6169	2.5436	2.5055	2.4663	2.4259	2.3842	2.341	2.2962
13	4.6672	3.8056	3.4105	3.1791	3.0254	2.9153	2.8321	2.7669	2.7144	2.671	2.6037	2.5331	2.4589	2.4202	2.3803	2.3392	2.2966	2.2524	2.2064
14	4.6001	3.7389	3.3439	3.1122	2.9582	2.8477	2.7642	2.6987	2.6458	2.6022	2.5342	2.463	2.3879	2.3487	2.3082	2.2664	2.2229	2.1778	2.1307
15	4.5431	3.6823	3.2874	3.0556	2.9013	2.7905	2.7066	2.6408	2.5876	2.5437	2.4753	2.4034	2.3275	2.2878	2.2468	2.2043	2.1601	2.1141	2.0658
16	4.494	3.6337	3.2389	3.0069	2.8524	2.7413	2.6572	2.5911	2.5377	2.4935	2.4247	2.3522	2.2756	2.2354	2.1938	2.1507	2.1058	2.0589	2.0096
17	4.4513	3.5915	3.1968	2.9647	2.81	2.6987	2.6143	2.548	2.4943	2.4499	2.3807	2.3077	2.2304	2.1898	2.1477	2.104	2.0584	2.0107	1.9604
18	4.4139	3.5546	3.1599	2.9277	2.7729	2.6613	2.5767	2.5102	2.4563	2.4117	2.3421	2.2686	2.1906	2.1497	2.1071	2.0629	2.0166	1.9681	1.9168
19	4.3807	3.5219	3.1274	2.8951	2.7401	2.6283	2.5435	2.4768	2.4227	2.3779	2.308	2.2341	2.1555	2.1141	2.0712	2.0264	1.9795	1.9302	1.878
20	4.3512	3.4928	3.0984	2.8661	2.7109	2.599	2.514	2.4471	2.3928	2.3479	2.2776	2.2033	2.1242	2.0825	2.0391	1.9938	1.9464	1.8963	1.8432
21	4.3248	3.4668	3.0725	2.8401	2.6848	2.5727	2.4876	2.4205	2.366	2.321	2.2504	2.1757	2.096	2.054	2.0102	1.9645	1.9165	1.8657	1.8117
22	4.3009	3.4434	3.0491	2.8167	2.6613	2.5491	2.4638	2.3965	2.3419	2.2967	2.2258	2.1508	2.0707	2.0283	1.9842	1.938	1.8894	1.838	1.7831
23	4.2793	3.4221	3.028	2.7955	2.64	2.5277	2.4422	2.3748	2.3201	2.2747	2.2036	2.1282	2.0476	2.005	1.9605	1.9139	1.8648	1.8128	1.757
24	4.2597	3.4028	3.0088	2.7763	2.6207	2.5082	2.4226	2.3551	2.3002	2.2547	2.1834	2.1077	2.0267	1.9838	1.939	1.892	1.8424	1.7896	1.733
25	4.2417	3.3852	2.9912	2.7587	2.603	2.4904	2.4047	2.3371	2.2821	2.2365	2.1649	2.0889	2.0075	1.9643	1.9192	1.8718	1.8217	1.7684	1.711
26	4.2252	3.369	2.9752	2.7426	2.5868	2.4741	2.3883	2.3205	2.2655	2.2197	2.1479	2.0716	1.9898	1.9464	1.901	1.8533	1.8027	1.7488	1.6906
27	4.21	3.3541	2.9604	2.7278	2.5719	2.4591	2.3732	2.3053	2.2501	2.2043	2.1323	2.0558	1.9736	1.9299	1.8842	1.8361	1.7851	1.7306	1.6717
28	4.196	3.3404	2.9467	2.7141	2.5581	2.4453	2.3593	2.2913	2.236	2.19	2.1179	2.0411	1.9586	1.9147	1.8687	1.8203	1.7689	1.7138	1.6541
29	4.183	3.3277	2.934	2.7014	2.5454	2.4324	2.3463	2.2783	2.2229	2.1768	2.1045	2.0275	1.9446	1.9005	1.8543	1.8055	1.7537	1.6981	1.6376
30	4.1709	3.3158	2.9223	2.6896	2.5336	2.4205	2.3343	2.2662	2.2107	2.1646	2.0921	2.0148	1.9317	1.8874	1.8409	1.7918	1.7396	1.6835	1.6223
40	4.0847	3.2317	2.8387	2.606	2.4495	2.3359	2.249	2.1802	2.124	2.0772	2.0035	1.9245	1.8389	1.7929	1.7444	1.6928	1.6373	1.5766	1.5089
60	4.0012	3.1504	2.7581	2.5252	2.3683	2.2541	2.1665	2.097	2.0401	1.9926	1.9174	1.8364	1.748	1.7001	1.6491	1.5943	1.5343	1.4673	1.3893
120	3.9201	3.0718	2.6802	2.4472	2.2899	2.175	2.0868	2.0164	1.9588	1.9105	1.8337	1.7505	1.6587	1.6084	1.5543	1.4952	1.429	1.3519	1.2539
Inf	3.8415	2.9957	2.6049	2.3719	2.2141	2.0986	2.0096	1.9384	1.8799	1.8307	1.7522	1.6664	1.5705	1.5173	1.4591	1.394	1.318	1.2214	1

Appendix -II P-Table Value

P-value- definition, formula, table, finding p-value, significance

P-Value

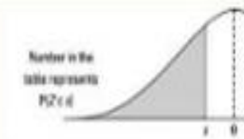

Percentage Points of the Chi-Square Distribution

Degrees of Freedom	Probability of a larger value of x^2								
	0.99	0.95	0.90	0.75	0.50	0.25	0.10	0.05	0.01
1	0.000	0.004	0.016	0.102	0.455	1.32	2.71	3.84	6.63
2	0.020	0.103	0.211	0.575	1.386	2.77	4.61	5.99	9.21
3	0.115	0.352	0.584	1.212	2.366	4.11	6.25	7.81	11.34
4	0.297	0.711	1.064	1.923	3.357	5.39	7.78	9.49	13.28
5	0.554	1.145	1.610	2.675	4.351	6.63	9.24	11.07	15.09
6	0.872	1.635	2.204	3.455	5.348	7.84	10.64	12.59	16.81
7	1.239	2.167	2.833	4.255	6.346	9.04	12.02	14.07	18.48
8	1.647	2.733	3.490	5.071	7.344	10.22	13.36	15.51	20.09
9	2.088	3.325	4.168	5.899	8.343	11.39	14.68	16.92	21.67
10	2.558	3.940	4.865	6.737	9.342	12.55	15.99	18.31	23.21
11	3.053	4.575	5.578	7.584	10.341	13.70	17.28	19.68	24.72
12	3.571	5.226	6.304	8.438	11.340	14.85	18.55	21.03	26.22
13	4.107	5.892	7.042	9.299	12.340	15.98	19.81	22.36	27.69
14	4.660	6.571	7.790	10.165	13.339	17.12	21.06	23.68	29.14
15	5.229	7.261	8.547	11.037	14.339	18.25	22.31	25.00	30.58
16	5.812	7.962	9.312	11.912	15.338	19.37	23.54	26.30	32.00
17	6.408	8.672	10.085	12.792	16.338	20.49	24.77	27.59	33.41
18	7.015	9.390	10.865	13.675	17.338	21.60	25.99	28.87	34.80
19	7.633	10.117	11.651	14.562	18.338	22.72	27.20	30.14	36.19
20	8.260	10.851	12.443	15.452	19.337	23.83	28.41	31.41	37.57
22	9.542	12.338	14.041	17.240	21.337	26.04	30.81	33.92	40.29
24	10.856	13.848	15.659	19.037	23.337	28.24	33.20	36.42	42.98
26	12.198	15.379	17.292	20.843	25.336	30.43	35.56	38.89	45.64
28	13.565	16.928	18.939	22.657	27.336	32.62	37.92	41.34	48.28
30	14.953	18.493	20.599	24.478	29.336	34.80	40.26	43.77	50.89
40	22.164	26.509	29.051	33.660	39.335	45.62	51.80	55.76	63.69
50	27.707	34.764	37.689	42.942	49.335	56.33	63.17	67.50	76.15
60	37.485	43.188	46.459	52.294	59.335	66.98	74.40	79.08	88.38

Table of the Student's t-distribution

The table gives the values of $t_{\alpha;\nu}$ where $Pr(T_\nu > t_{\alpha;\nu}) = \alpha$, with ν degrees of freedom

ν \ α	0.1	0.05	0.025	0.01	0.005	0.001	0.0005
1	3.078	6.314	12.076	31.821	63.657	318.310	636.620
2	1.886	2.920	4.303	6.965	9.925	22.326	31.598
3	1.638	2.353	3.182	4.041	5.841	10.213	12.924
4	1.533	2.132	2.776	3.747	4.604	7.173	8.610
5	1.476	2.015	2.571	3.365	4.032	5.893	6.869
6	1.440	1.943	2.447	3.143	3.707	5.208	5.959
7	1.415	1.895	2.365	2.998	3.499	4.785	5.408
8	1.397	1.860	2.306	2.896	3.355	4.501	5.041
9	1.383	1.833	2.262	2.821	3.250	4.297	4.781
10	1.372	1.812	2.228	2.764	3.169	4.144	4.587
11	1.363	1.796	2.201	2.718	3.106	4.025	4.437
12	1.356	1.782	2.179	2.681	3.055	3.930	4.318
13	1.350	1.771	2.160	2.650	3.012	3.852	4.221
14	1.345	1.761	2.145	2.624	2.977	3.787	4.140
15	1.341	1.753	2.131	2.602	2.947	3.733	4.073
16	1.337	1.746	2.120	2.583	2.921	3.686	4.015
17	1.333	1.740	2.110	2.567	2.898	3.646	3.965
18	1.330	1.734	2.101	2.552	2.878	3.610	3.922
19	1.328	1.729	2.093	2.539	2.861	3.579	3.883
20	1.325	1.725	2.086	2.528	2.845	3.552	3.850
21	1.323	1.721	2.080	2.518	2.831	3.527	3.819
22	1.321	1.717	2.074	2.508	2.819	3.505	3.792
23	1.319	1.714	2.069	2.500	2.807	3.485	3.767
24	1.318	1.711	2.064	2.492	2.797	3.467	3.745
25	1.316	1.708	2.060	2.485	2.787	3.450	3.725
26	1.315	1.706	2.056	2.479	2.779	3.435	3.707
27	1.314	1.703	2.052	2.473	2.771	3.421	3.690
28	1.313	1.701	2.048	2.467	2.763	3.408	3.674
29	1.311	1.699	2.045	2.462	2.756	3.396	3.659
30	1.310	1.697	2.042	2.457	2.750	3.385	3.646
40	1.303	1.684	2.021	2.423	2.704	3.307	3.551
60	1.296	1.671	2.000	2.390	2.660	3.232	3.460
120	1.289	1.658	1.980	2.358	2.617	3.160	3.373
∞	1.282	1.645	1.960	2.326	2.576	3.090	3.291

Appendix -III Experimental Result for SS 316 Workpiece

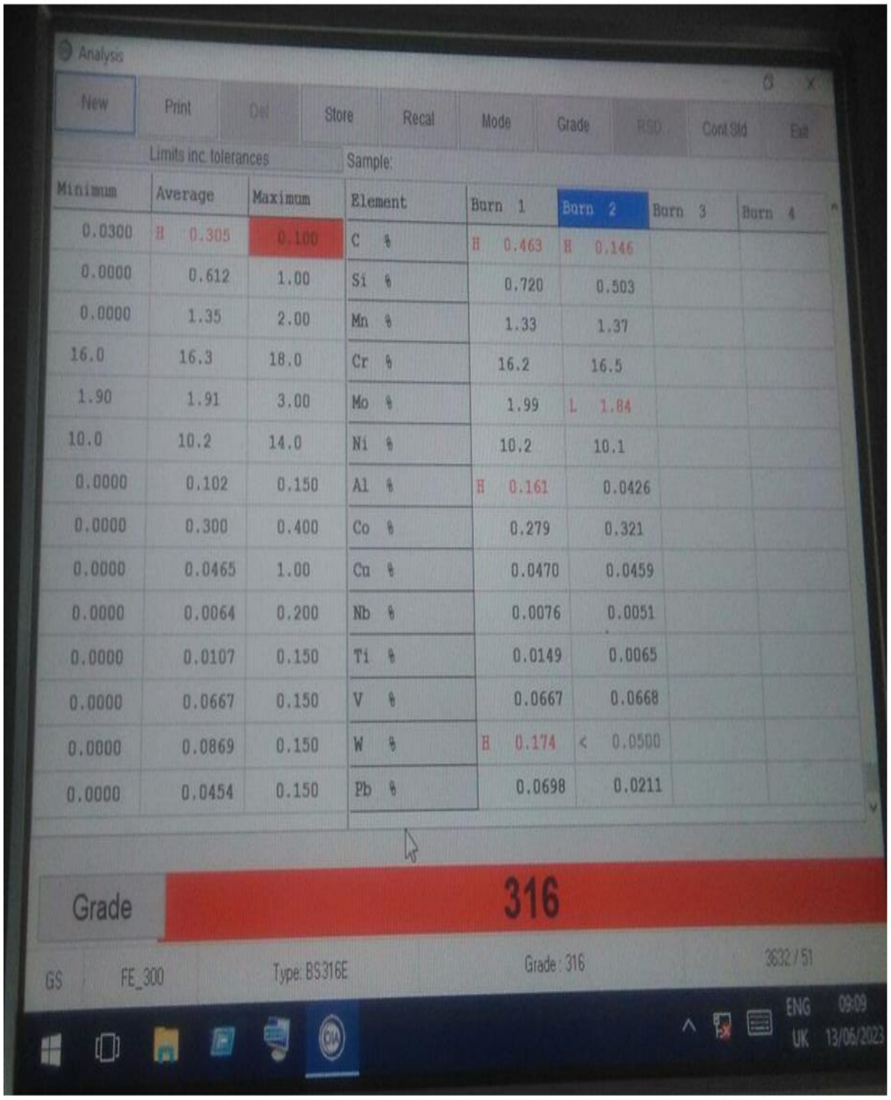

Minimum	Average	Maximum	Element	Burn 1	Burn 2	Burn 3	Burn 4
0.0300	H 0.305	0.100	C %	H 0.463	H 0.146		
0.0000	0.612	1.00	Si %	0.720	0.503		
0.0000	1.35	2.00	Mn %	1.33	1.37		
16.0	16.3	18.0	Cr %	16.2	16.5		
1.90	1.91	3.00	Mo %	1.99	L 1.84		
10.0	10.2	14.0	Ni %	10.2	10.1		
0.0000	0.102	0.150	Al %	H 0.161	0.0426		
0.0000	0.300	0.400	Co %	0.279	0.321		
0.0000	0.0465	1.00	Cu %	0.0470	0.0459		
0.0000	0.0064	0.200	Nb %	0.0076	0.0051		
0.0000	0.0107	0.150	Ti %	0.0149	0.0065		
0.0000	0.0667	0.150	V %	0.0667	0.0668		
0.0000	0.0869	0.150	W %	H 0.174	< 0.0500		
0.0000	0.0454	0.150	Pb %	0.0698	0.0211		

Sample Tested

Appendix IV Experimental Result for ER308L Filler Metal

Analysis

New | Print | Del | Store | Recal | Mode | Grade | RSD | Cont Std | Exit

Limits inc tolerances			Sample				
Minimum	Average	Maximum	Element	Burn 1	Burn 2	Burn 3	Burn 4
	68.8		Fe %	68.8	68.8	68.6	69.1
0.0300	H 0.116	0.100	C %	0.0344	L 0.0231	H 0.375	0.0324
0.0000	0.340	1.00	Si %	0.263	0.304	0.464	0.328
0.0000	1.65	2.00	Mn %	1.68	1.67	1.64	1.61
18.0	19.5	20.0	Cr %	19.8	19.7	19.0	19.5
0.0000	0.183	1.00	Mo %	0.196	0.191	0.169	0.176
8.00	8.95	12.0	Ni %	8.74	8.97	9.26	8.83
0.0000	0.0403	0.100	Al %	< 0.0030	< 0.0030	H 0.161	< 0.0030
0.0000	0.177	0.400	Co %	0.176	0.175	0.176	0.182
0.0000	0.0893	1.00	Cu %	0.0989	0.100	0.0728	0.0855
0.0000	0.0167	0.150	Nb %	0.0356	0.0254	< 0.0050	0.0056
0.0000	< 0.0050	0.150	Ti %	< 0.0050	< 0.0050	0.0070	< 0.0050
0.0000	0.0885	0.150	V %	0.0872	0.0816	0.0957	0.0893
0.0000	< 0.0500	0.150	W %	< 0.0500	< 0.0500	< 0.0500	< 0.0500

Grade 304 H

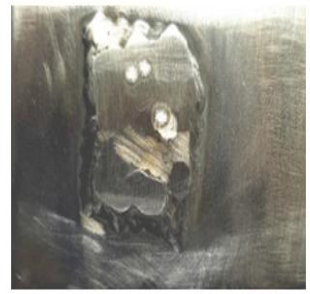

Sample Tested

Appendix V   Preparation of Row Material According to ASTM Standard